AC LOSSES IN HIGH-TEMPERATURE SUPERCONDUCTORS AND THE IMPORTANCE OF THESE LOSSES TO THE FUTURE USE OF HTS IN THE POWER SECTOR

by G.E. Marsh and A.M. Wolsky

Argonne National Laboratory, 9700 South Cass Avenue, Argonne, Illinois 60439
United States of America

May 18, 2000

Work done for and sponsored by the signatories of the International Energy Agency

Implementing Agreement for a Cooperative Programme for Assessing the Impacts of High-Temperature Superconductivity on the Electric Power Sector

TABLE OF CONTENTS

ACKNOWLEDGMENTS ..... *v*

I. PREFACE I-1
- I.1 Content and Purpose I-1
- I.2 Scope I-1
- I.3 Sponsorship I-2
- I.4 Further Sources of Information I-4

II. INTRODUCTION TO ISSUES RAISED BY AC LOSSES II-1
- II.1 Importance of AC Losses II-1
  - II.1.1 Orientation II-1
  - II.1.2 Order of Magnitude of Goals for HTS II-2
  - II.1.3 Power Equipment II-3
    - II.1.3.1 Cables II-3
      - II.1.3.1.1 Cold Dielectric II-4
      - II.1.3.1.2 Warm Dielectric II-5
    - II.1.3.2 Transformers II-5
    - II.1.3.3 Rotating Machines II-7
    - II.1.3.4 SMES II-7
    - II.1.3.5 Flywheels II-7
    - II.1.3.6 Fault Current Limiters II-8
    - II.1.3.7 Summary II-8
  - II.1.4 Self-Contained Refrigeration II-8
    - II.1.4.1 Some Utilities' Desire for Self-Contained Refrigeration II-8
    - II.1.4.2 Cost and Performance of Cryomech's Cryocoolers II-9
    - II.1.4.3 Self-Contained Refrigeration for a Hypothetical 30-MVA HTS Transformer II-9
    - II.1.4.4 Desirable Operating Temperature II-10
- II.2 Varieties of Ceramic Superconductors under Development II-15
  - II.2.1 Bi-2212 ..... II-15
  - II.2.2 Bi-2223 ..... II-15
  - II.2.3 YbaCuO II-16
  - II.2.4 Commonalities among Ceramic Superconductors II-17
- II.3 DC Behavior of Ceramic Superconductors: The E vs. J Curve II-18
  - II.3.1 The ln[E] vs. ln[J] Correlation II-18
  - II.3.2 Definition of Critical Current Density, Voltage Criterion, and n-Value II-19
  - II.3.3 Power Loss II-21
  - II.3.4 Anisotropy II-23
  - II.3.5 Two Different Critical Densities II-23
- II.4 Elementary Theory of AC Loss II-26
  - II.4.1 Hysteresis Loss II-26
    - II.4.1.1 Critical State Model II-29
    - II.4.1.2 Nonlinear Conductor Model II-29

II.4.2 Eddy Current Loss II-30
II.4.3 Relative Importance of Eddy Current to Hysteresis II-31
II.5 Basic Experimental Approaches to Measuring of AC Losses II-32
II.5.1 Calorimetric Method II-32
II.5.2 Thermometric Method II-38
II.5.3 Electrical Method II-38

II.6 From Tape to Cable II-43
II.7 Promising Techniques II-45

III. GROUPS ACTIVE IN THE FIELD III-1
III.1 Contacts in Nonprofit Organizations III-1
III.2 Contacts in For-Profit Organizations III-3
III.3 Individual Investigators III-4

IV. DISCUSSION OF TODAY'S NEEDS AND TODAY'S PERFORMANCE IV-1
IV.1 Figures of Merit IV-1
IV.2 AC Loss Threshold Level and Magnetic Field Requirements for Various Devices IV-2
IV.2.1 Comparison with Copper: Physical Design Trade-Offs for Wire IV-3
IV.2.2 Trade-Offs between AC Losses, Type of Conductor, and Cooling IV-4

V. DIFFICULTIES TO BE SURMOUNTED V-1
V.1 Powder-in-Tube Technology V-1
V.2 Coated Conductor V-2

VI. TODAY'S STRATEGIES FOR LOSS REDUCTION VI-1
VI.1 Hysteresis VI-1
VI.1.1 Increased Critical Current VI-1
VI.1.2 Decreased Filament Diameter VI-1
VI.2 Ohmic Losses in the Normal Matrix VI-2
VI.2.1 Silver Alloy Tubes for BSCCO` VI-2
VI.2.2 Interfilamentary Resistive Barriers VI-4
VI.2.3 Twisted Filaments VI-5
VI.3 Stability and HTSC. VI-9
VI.4 Order-of-Magnitude Costs VI-10
VI.5 The Promise of YbaCuO "Coated Conductor" VI-11
VI.6 Today's Experimental Situation with YbaCuO "Coated Conductor" VI-13

VII. WHAT IS TO BE DONE VII-1
VII.1 Effects of AC Losses on Device Cost and Performance VII-1
VII.2 Performance Goals for AC Losses VII-1
VII.3 Activities Bearing upon AC Losses that Deserve Increased Consideration VII-2
VII.3.1 Relationship between Cost-Performance Goals for AC Losses and for Cryogenics VII-2
VII.3.2 Computer Modeling and Simulation of Coils VII-2

VII.3.3 Localization of AC Losses VII-2
VII.3.4 AC Losses in Coated Conductor VII-2
VII.3.4.1 Measurement of AC Losses in Today's Coated Conductor VII-3
VII.3.4.2 Effect of Coated Conductor Substrate on Losses VII-3
VII.3.4.3 Effect of Induced Currents in the Coated Superconductor .. VII-3
VII.3.5 Precompetitive Cooperation to Reduce AC Losses VII-3

APPENDIX 1. A Critical State Model A1-1
APPENDIX 2. Nonlinear Conductor Model A2-1
APPENDIX 3. Hysteresis Losses Related to the Imaginary Part of the Complex Permeability . A3-1
APPENDIX 4. Measurement of Transport Loss and Lead Configuration A4-1
APPENDIX 5. Benchmark Parameters A5-1
A5.1 Properties of Materials A5-1
A5.1.1 Commercially Available Long Lengths of OPIT Bi-2223 ..... A5-1
A5.1.2 Electrical Resistivity of Materials at Ambient and Cryogenic Temperatures A5-1
A5.1.3 Temperature Dependence of Critical Current Density A5-2
A5.1.4 Mass Densities at 298K A5-2
A5.1.5 Penetration Depth According to the Nonlinear Conductor Model A5-2
A5.I.6 Hysteresis Loss According to the Nonlinear Conductor Model A5-3
A5.2. Prices of Materials and Self-Contained Refrigeration A5-4
A5.2.1 Currency Exchange Rates A5-4
A5.2.2 Price of Metals A5-4
A5.2.3 Today's Approximate "Cost of Materials" for Bi-2223 Tape A5-4
A5.2.4 Cost of Nickel for Substrate of YbaCuO Coated Conductor A5-5
A5.2.5 Price and Performance of Self-Contained Refrigeration A5-6

TABLES

Table IV.2.1 Magnetic Field Environment for Various Electrical Devices IV-2
Table IV.2.2.1 Calculated Conductor Parameters for 50Hz Applications IV-4

FIGURES

Figure II.1.4.3a II-12
Figure II.1.4.3b II-13
Figure II.1.4.3c II-14
Figure II.3.1a II-19
Figure II.3.1b II-21
Figure II.3.4 ..... II-25
Figure II.4.1.1 ..... II-27
Figure II.4.1.2 ..... II-28
Figure II.4.3.1 ..... II-31
Figure II.5.1.1 ..... II-33
Figure II.5.1.2 ..... II-34
Figure II.5.1.3 ..... II-35

Figure II.5.1.4 ..... II-36
Figure II.5.1.5 ..... II-37
Figure II.5.1.6 ..... II-37
Figure II.5.3.1 ..... II-39
Figure II.5.3.2 ..... II-40
Figure II.5.3.3 ..... II-41
Figure II.5.3.4 ..... II-42
Figure II.6.1 ..... II-44
Figure IV.2.1 ..... IV-2
Figure VI.2.1.1 ..... VI-3
Figure VI.2.3.1 ..... VI-5
Figure VI.2.3.2 ..... VI-6
Figure VI.2.3.3 ..... VI-7
Figure VI.2.3.4 ..... VI-8
Figure VI.2.3.5 ..... VI-9
Figure VI.3.1 ..... VI-9
Figure VI.4.1 ..... VI-11
Figure A1.1.1 ..... A1-1
Figure A1.1.2 ..... A1-2
Figure A1.1.3 ..... A1-3
Figure A1.1.4 ..... A1-4
Figure A1.1.5 ..... A1-5
Figure A1.2.1 ..... A1-7
Figure A1.2.2 ..... A1-9
Figure A1.2.3 ..... A1-9
Figure A1.2.4 ..... A1-11
Figure A1.3.1 ..... A1-12
Figure A1.3.2 ..... A1-13
Figure A1.3.3 ..... A1-15
Figure A2.1 ..... A2-7
Figure A2.2 ..... A2-8
Figure A3.1 ..... A3-1
Figure A4.1 ..... A4-1
Figure A4-2 ..... A4.2

ACKNOWLEDGMENTS

This report benefited from our colleagues' contributions and review. The authors are pleased to thank Drs. Steve Ashworth (Brookhaven National Laboratory), Julian Cave (Hydro Québec), John Clem (Iowa State University), Yasunori Mawatari (visiting, Iowa State University), David Driscoll (Rockwell Automation), Amit Goyal (Oak Ridge National Laboratory), Bennie ten Haken (University of Twente), Pradeep Haldar (Intermagnetics), Sven Hornfeldt (ABB-Vasteras), Winston Lue (Oak Ridge National Laboratory), Eddie Leung (MagTec Engineering), Martin Maley (Los Alamos National Laboratory), Ben McConnell (Oak Ridge National Laboratory), Marco Nassi (Pirelli), Heinz-Werner Neumüller (Siemens), Martin Oomen (University of Twente), Dean Peterson (Los Alamos National Laboratory), Bart Riley (ASC), Uday Sinha (Southwire), Kinyoung Tea (Hydro Québec), and Osami Tsukamoto (Yokohama National University) for each reviewing part or all of this or an earlier draft of this report. Their attention was graciously given, and their suggestions were always helpful. Any errors of fact or emphasis that may remain are the responsibility of the authors.

We also appreciate the hospitality extended to us during visits to the University of Twente in the Netherlands, Forschungszentrum Karlsruhe, Siemens Research Laboratory in Erlangen, Vacuumschmelze in Hanau, and Los Alamos National Laboratory, as well as the courtesy shown us during discussions in Fukuoka at ISS'99.

I. PREFACE

I.1 CONTENT AND PURPOSE

This report describes the status of work to reduce AC losses in ceramic superconductors, which were first discovered in 1987. Our discussion is intended for research and development managers in government, electric utilities, private firms, and national laboratories who wish an overview of what is being done and what remains to be done. It is assumed that the reader is acquainted with superconductivity but not necessarily expert in the topics discussed here. Indeed, it is the authors' aim to enable the reader to better understand the experts who may ask for the reader's attention or support. To this end, introductory material, as well as a summary of the status of AC losses in conductors made from high-temperature superconductors, is included. This report may also inform scientists and engineers who, though expert in related areas, wish an introduction to the topic.[1] References to the research literature, although by no means exhaustive, are provided to facilitate further familiarity with the subject.[2]

The topic of AC losses in high-temperature superconductors is a broad one. Here, we emphasize those topics of interest to the electric power industry, including theoretical questions where appropriate; details are often relegated to appendices.

I.2 SCOPE

This study will focus on AC losses in high-temperature superconducting wires and tapes, rather than on the more complex problem of determining losses in cables or the coils needed for practical electrical machinery. This restriction is made because losses at the wire level must be substantially less than losses in normal conductors if superconductors are to be attractive for such applications, and this threshold requirement can be examined without introducing the complexities involved with cables or coils. These latter are constructed from many tapes, which are difficult to model, and although a good deal of effort has been expended in this area, it is often impossible to obtain better than order-of-magnitude predictions for the AC losses. There is a lack of software packages capable of dealing with the anisotropic current-voltage characteristics of the constituent conductors.[3] In addition to the problem of modeling complex configurations of tapes or wire, standardized measurement techniques have not yet been fully developed that would allow validation of the models.

This does not mean that AC losses in cables, transformers, motors, and other applications will not be discussed. Rather, the characteristics of these devices will be used to determine the

---

[1] Technically inclined readers may wish to follow this report by consulting B. Seeber, *Handbook of Applied Superconductivity* (2 vols). Institute of Physics (Bristol, 1999).

[2] A fine compendium of recent work is provided by H.J. ten Kate and B. ten Haken, *Proceedings of the International Cryogenics Materials Conference, Topical Conference on AC Loss and Stability of Low- and High-T_c Superconductors*, North Holland (1998).

[3] Such work is rare, but not universally neglected. An important effort has been undertaken by N. Amemiya et al. See Banno, N., and N. Amemiya, *Numerical Analysis of AC Loss*, IEEE Transactions on Applied Superconductivity, **9**(2)2561-2564 (June 1999).

range of the magnetic field within which the conductor or tape must operate with acceptable losses. Particular problems associated with a given application are also discussed.

Unlike resistive losses due to flux creep (see Section II.4), which are independent of frequency, both hysteretic and eddy current losses increase with frequency. Because this report is intended to be of use primarily to the power industry, the frequency range of interest is generally 50-180 Hz, with the assumption that frequencies above the third harmonic of the power frequency will be severely damped.

The discussion below will also address the question of the applicability of the Critical State Model (which assumes that a critical current density flows in any current-carrying portion of a superconductor) to high-temperature superconductors. (The Critical State Model was developed for low-temperature superconductors, for which it is well suited.)

Technical superconductors (high and low temperature) are Type-II superconductors where, above a critical magnetic field, flux will penetrate the superconductor, forming a mixed state where flux threads an array of normal cores to produce what is called the "flux line lattice." The pinning of this lattice to prevent movement when the superconductor is carrying a current is crucial to obtaining good superconductor performance. Unlike low-temperature superconductors, the flux lines in a high-temperature superconductor are arranged in what has been called a "vortex glass" where there is no regular lattice. The copper oxide layers of a high-temperature superconductor cause the flux in a given layer to form "pancake vortices"; when the coupling between layers is weak compared to thermal energies, these vortices interact strongly within each layer but only weakly with neighboring layers. This makes it difficult to pin the vortex lattice, because pancakes that are free to move in one layer can move relative to pinned pancakes in adjacent layers. Indeed, bismuth compounds (BSCCO) cannot tolerate significant magnetic fields at 77 K because the flux line lattice has "melted," leaving the pancake vortices relatively free to move. Thus, the better the vortex coupling between adjacent copper oxide layers, the better the performance of the superconductor.

Given these differences between high- and low-temperature superconductors, it is important to understand when the Critical State Model, which is used for most AC loss calculations, is applicable. The approach taken here is based on the work of Rhyner[4], which models a high-temperature superconductor as a nonlinear conductor.

I.3 SPONSORSHIP

The preparation of this report was sponsored by institutions in Canada, Denmark, Finland, Germany, Israel, Italy, Japan, Korea, the Netherlands, Norway, Sweden, Switzerland, Turkey, the United Kingdom, and the United States. These institutions are signatories to an International Energy Agency (IEA) Implementing Agreement, entitled *Implementing Agreement for a Co-Operative Programme for Assessing the Impacts of High-Temperature Superconductivity on the Electric Power Sector*.

[4] J. Rhyner, ***Physica C 212***: 292 (1993).

Following are the names and addresses of representatives to the sponsors' Executive Committee for the project from participating countries:

Dr. F.Y. Chu
Manager
Electrical Systems Technology
Ontario Hydro Technologies
800 Kipling Avenue
Toronto, Ontario M8Z5S4
CANADA

Mr. Kinyoung Tea
Manager, Generation Technology
Hydro Québec J3X 1S1
1800, boul Lionel-Boulet
Rez-de-chaussee
Varennes / QuebecHydro-Quebec
J3X151
CANADA

Mr. Mogens Dam Andersen
Chief Engineer
Copenhagen Power and Light
Vognmagergade 8
1149 Copenhagen K,
DENMARK

Dr. Risto Mikkonen
Laboratory of Electromagnetics
Tampere University of Technology
P.O. Box 692
FIN-33101 Tampere
FINLAND

Prof. Dr. Peter Komarek
Director, Institute for Technical Physics
Kernforschungszentrum Karlsruhe
Institut für Technische Physik
Postfach 3640
D-76021 Karlsruhe
GERMANY

Prof. Guy Deutscher
Tel-Aviv University
Ramat-Aviv
Tel Aviv 69978
ISRAEL

Mr. Gabriele Botta
ENEL-CREL
Via Volta 1
20093 Cologno Monzese
Milano
ITALY

Mr. Eiichi Yanagisawa
Director
Energy Conversion & Storage Dept.
New Energy and Industrial Technology
Development Organization
Sunshine 60, 29F,1-1 Higashi-Ikebukuro
Toshima-ku Tokyo 170
JAPAN

Dr. Ok-Bae Hyun, Ph.D.
Center for Advanced Studies in Energy and
Environment
Korea Electric Power Research Institute KEPCO
Power System Laboratory
103-16, Munji-Dong, Yusung-Gu
Taejon, 305-380
REPUBLIC OF KOREA

Dr. Harold E. Dijk
KEMA
P.O. Box 9035
6800 Arnheim
NETHERLANDS

Dr. John Kulsetå s
Research Director
Norwegian Electric Power Research Institute (EFI)
7034 Trondheim
NORWAY

Mr. Kjell Oberger
Elforsk AB
S-101 53 Stockholm
SWEDEN

Dr. Georg Vécsey
Head of the CRPP-Fusion Technology
CRPP-FT
WMHA/C37
CH-5232 Villigen PSI
SWITZERLAND

Dr. Lev Dorosinski, Head
Magnetics and Superconductivity Laboratory
National Metrology Institute
P.O. Box 21 Gebze
41470 Kocaeli
TURKEY

Mr. David Rose
Department of Trade and Industry
151 Buckingham Palace Road
London SW1W9SS
UNITED KINGDOM

Conservation and Renewable Energy
CE-142 5E-036
1000 Independence Ave., SW
Washington, DC 20585
UNITED STATES

Dr. James G. Daley
U.S. Department of Energy

I.4 FURTHER SOURCES OF INFORMATION

Information about specific efforts in the AC loss field can be gained by contacting the researchers engaged in those efforts. Access to them can be facilitated by referring to Chapter III of this report, "Groups Active in the Field."

A related report, *The Status of Progress toward HTS High-Amperage Conductor,* was prepared by Argonne National Laboratory for the participating signatories of the International Energy Agency's *Implementing Agreement for a Co-Operative Programme for Assessing the Impacts of High-Temperature Superconductivity on the Electric Power Sector*. Other Argonne reports that may be of interest are *Superconducting Transmission Cables, Fault-Current Limiters-A Second Look,* and *The Status of Progress toward High-Temperature Superconducting Transformers*.

Copies of these reports can be obtained by requesting them from the member of the sponsors' Executive Committee who represents the country of the requester. The name and address of each member of the Executive Committee are listed in Section I.3.

Also available is a nontechnical, illustrated brochure introducing progress toward power sector applications of ceramic superconductors. That brochure is entitled: *High-Temperature Superconductivity for the Electric Power Sector: Advances toward Power Sector Applications* (January 1997, 20 pages).

Information about the International Energy Agency's *Implementing Agreement for a Co-Operative Programme for Assessing the Impacts of High-Temperature Superconductivity on the Electric Power Sector* and its reports and meetings can be found on the World Wide Web at the following URL:

http://www.iea.org/impagr/imporg/effene/a31htsup.htm

II. INTRODUCTION TO ISSUES RAISED BY AC LOSSES

II.1 IMPORTANCE OF AC LOSSES

II.1.1 Orientation

The power sector's future use of ceramic superconductors depends on the benefits they offer. These include the possibility of much reduced size and weight and much increased power density. Where these are crucial, ceramic superconductors will find a niche. Where conventional technology will suffice, equipment incorporating ceramic superconductors must offer economic benefits to be adopted by the private sector.

It is the promise of this benefit, reduced energy losses with concomitant cost savings, that attracted the initial interest of the public sector and the power sector. This report reviews the status of progress toward increased energy efficiency by reducing "AC losses," which reduction might be enabled by using ceramic superconductors rather than copper to conduct electrical current in the power sector.

As is well known, superconductors carry direct electrical current (DC) with negligible losses. Direct electrical current is rarely used in the power sector because, early in the 20th century, it was realized that losses in conventional cable could be reduced by increasing voltage and reducing current from that available at the generator. This transformation is more easily done with alternating current (AC), and so the grid was built to operate with alternating current. Now, the technical challenge is to fabricate superconductor that operates with negligible "AC loss." Success would reduce operating costs by saving energy.

Another challenge is to fabricate this conductor inexpensively. Success would reduce capital costs. In the long term, new technology will displace conventional technology when the sum of the operating costs and the discounted capital cost for the new technology is perceived to be less than those costs for present practice.

Indeed, simple figures-of-merit for ceramic superconductors are obtained by comparing them to copper.[1] One compares the cost of the capability of carrying one kiloampere of current for one meter by ceramic superconductor with the cost of the capability to do so by copper, all ancillaries included. This creates a goal for the "first cost" or capital cost for ceramic superconductor. To create a goal for the operating cost, one compares it to the operating cost of devices using copper wire. Assuming equal maintenance costs, the relevant engineering parameter is the rate of electrical energy loss (watts) when one kiloampere of current traverses one meter of copper conductor. This report will often describe measured and desired losses in "watts per kiloampere-meter" (denoted by W/kA-m) or in "milliwatts per ampere-meter" (denoted by mW/A-m), two names for the same unit. (Laboratory scientists are inclined to express their results in milliwatts per ampere-meter; power engineers speak of watts per kiloampere-meter.)

[11]A.M. Wolsky, *The Status of Progress toward High-Amperage Conductors Incorporating High-Temperature Superconductors*, for signatories of the IEA Implementing Agreement for a Co-Operative Programme for Assessing the Impacts of High-Temperature Superconductivity on the Electric Power Sector (March 1997), 98 pages. In particular, see Chapter II.

Another aspect of the performance of ceramic superconductors must be considered when discussing losses. This other aspect is the superconductor's operating temperature. It is likely to be in the range 20-77 K (or 85 K, if the cryogen is pressurized), which is far below ambient temperatures (298 K). Thus, ceramic superconductors require refrigeration, and refrigeration requires continuous expenditure of energy. For example, if electrical energy is dissipated to heat, at 77 K, at the rate of one watt, then today's refrigerators must be supplied with approximately 15-25 watts of electrical power to transfer that heat to ambient temperature. (Absent this refrigeration, the superconductor material would warm itself and soon cease to operate as designed.) Thus, for each watt of "AC loss," many more watts must be provided and paid for. The precise number depends on the operating temperature of the superconductor and the efficiency of the refrigerator. This efficiency has a theoretical maximum (i.e.,T_{op}/(298 K-T_{op}), but real refrigerators do not yet approach that maximum.[2] Generally, the bigger the refrigerator, the more efficient it is. Refrigeration also requires investment, which must be paid for. Section II.2.6 returns to this topic.

To summarize, the superconductor's AC loss, at its operating temperature, must be many times smaller than the AC loss of the equivalent amount of copper at ambient temperature.

II.1.2 Order of Magnitude of Goals for HTS

Present practice uses maximum current densities in the range 100 – 400 A/cm^2 in copper conductors. For the sake of definiteness, consider two current densities in copper at ambient temperature, one of 100 A/cm^2 and one of 400 A/cm^2. The resistivity of copper at ambient temperature is 1.7×10^{-6} Ω-cm. For the lower current density, Ohm's Law leads to the conclusion that electrical energy dissipates, Q, at the rate of 17 mW/cm^3 (17 kW/m^3).

$$d/dt\ Q = \rho\ J^2 \times \text{volume} = 1.7 \times 10^{-6}\ \Omega\text{-cm}\ (100\ \text{A/cm}^2)^2 \times \text{volume} \qquad \text{(II.1.2-1a)}$$

$$d/dt\ Q = \rho\ J^2 \times \text{volume} = 1.7 \times 10^{-2}\ (\text{W/cm}^3) \times \text{volume} \qquad \text{(II.1.2-1b)}$$

At this current density, the volume of copper needed to conduct one kiloampere for one meter is 10^3 cm^3. One concludes that the rate of dissipation of electrical energy, $\frac{d}{dt}Q$, is:

$$d/dtQ = 17 \times 10^{-3}\ \text{W/cm}^3 \times 10^3\ \text{cm}^3\text{/kA-m} = 17\ \text{W/kA-m} \qquad \text{(II.1.2-1c)}$$

When the current density is 400 A/cm^2, one finds that the density of dissipated power is 272 mW/cm^3 and the needed volume of copper is 250 cm^3, yielding a loss of 68 W/kA-m. Thus, when the current density increases, one uses less copper (reducing capital cost), but one increases the loss (increasing the operating cost). The balance must be struck between lost earnings from

[2]R.F. Giese, *Refrigeration Options for High-Temperature Superconducting Devices Operating between 20 and 80 K for Use in the Electric Power Sector*, for signatories of the IEA Implementing Agreement for a Co-Operative Programme for Assessing the Impacts of High-Temperature Superconductivity on the Electric Power Sector (Oct. 1994), 51 pages.

lost power and increased annual capital cost, concomitant with ownership of more copper. [3] This balance reflects the designer's and users' guess about future prices.

On March 1, 2000, the commodity price of copper was \$1.73/kg or \$0.015/cm^3. The price of electrical copper to the wire factory might be 50% higher. The result is a cost of copper in the range between \$5.60/kA-m (for 400 A/cm^2) and \$22.40/kA-m (for 100 A/cm^2). Further, the design operating current density in conventional equipment depends on the device itself. Underground and underwater cable tend to operate with current densities near 100 A/cm^2.[4] Transformer designs tend to operate at 400 A/cm^2.[5] This range shows the importance of reducing today's capital cost of ceramic superconductor and of finding other capital cost savings, most likely from increased power density, such as might be had from increasing the capacity of existing underground tunnels or existing substations.

As discussed in more detail in Section II.3, if one had a refrigerator with a coefficient of performance (COP) of 15, one would want the AC loss in the ceramic superconductor to be at least one-fifteenth of the loss in copper. In that case, one might want the ceramic superconductor to have AC losses of not more than 1 W/kA-m. When the refrigerator is less efficient, one wants lower losses. A benchmark for the cost of refrigeration is presented in Section II.2.6.2.

In practice, the power sector would want the promise of less loss to compensate for the risk of new technology and the possibility of higher capital cost of the new technology (i.e., conductor with refrigeration). For the sake of definiteness, one might set the goal

$$0.25 \text{ mW/A-m} = 0.25 \text{ W/kA-m} \qquad \text{(II.1.2-2)}$$

for AC losses at 77 K under steady-state conditions. (If higher current is put through the same conductor, losses will rise steeply and nonlinearly. [See Section II.3])

As stated above, this goal, 0.25 W/kA-m, is nominal and should be adjusted to reflect "device-specific" and "refrigeration-specific" considerations, if and when they differ from our nominal assumptions. These nominal assumptions do not account for the capital cost of refrigeration, something that cannot be neglected if self-contained refrigeration is desired.

II.1.3 Power Equipment

When trying to put AC losses[6] in perspective, it is necessary to recall other sources of heat that must be removed by refrigeration. These sources include heat generated in the

---

[3]Here we bracket present practice by considering its upper and lower current densities. Other authors have taken a single middling number — for example, 250 A/cm^2. Such an estimate is presented in G. Ries et al. *Physica C* **310**:283 (1998).

[4]Order of magnitude was kindly provided by S. Hornfeldt (March 2000). For an overview of common practice during the 1970s, as well as an excellent introduction to its subject, see B.M. Weedy, *Underground Transmission of Electric Power*, Wiley (Chichester, 1980).

[5]Order of magnitude was kindly provided by S. Hornfeldt (March 2000).

[6]Scientists are trained to think in terms of the instantaneous values of power, current, and voltage. Here, we follow the practice of the power sector which is to consider the average power per cycle and thus the root mean square current and root mean square voltage. The power conveyed by a 3 phase circuit is $V_{rms}I_{rms}\sqrt{3}$, where V_{rms} and I_{rms} are related to the maximum values in each phase as follows: $V_{rms} = V_m/\sqrt{2}$ and $I_{rms} = I_m/\sqrt{2}$.

dielectric, heat from the environment that flows through the thermal insulation to the cold region, and heat that flows to the cold region from the electrical leads that are at ambient temperature. In the case of rotating machines, one must also consider the heat that flows down the shaft (aka torque tube). Below, we sketch the orders-of-magnitude.

To put AC losses in perspective, it is also necessary to consider the cost of refrigeration, which affects both capital and operating cost.

II.1.3.1 Cables

Today's underground or underwater cable is often designed to operate with a current density of approximately 100 A/cm^2. At that current density, its loss is approximately 20 W/kA-m because its operating temperature is a bit above the ambient level.

Unlike other HTS devices, cables have a very large surface-to-volume ratio. One must pay attention to the heat flow from the environment to the cold region. HTS cables can be designed in two ways: (a) with dielectric at ambient temperature (warm dielectric) and (b) with dielectric at the superconductor's operating temperature (cold dielectric). One expects the warm dielectric design to have the largest thermal load. Of course, thermal loads can be dealt with by a mixture of refrigeration (with capital and operating cost) or thermal insulation (capital cost).[7] While the heat flow through the thermal insulation (aka cryostat) depends on that mixture, we think it is informative to note the contributions of each source to today's prototypes. These contributions are discussed below.

II.1.3.1.1 Cold Dielectric

Southwire is working to demonstrate an AC cable with cold dielectric. Southwire has graciously shared the following information about its prototype, for the readers of this report. The cable is 30 m long; it is designed to carry a maximum operating current of 1250 A at a voltage of 12.5 kV. It has three rigid cryostats, each thermally insulating a single phase. The total heat load on each cryostat is one watt per meter per phase. Southwire estimates that an additional 0.6 W/kA-m must be removed because it is generated by AC losses. (One might consider an alternative design with three flexible cryostats. In that case, the heat load is estimated to be three watts per meter per phase.)

Roughly speaking, the Southwire prototype with three rigid cryostats has a heat load of approximately 3 W/kA-m, and an additional 0.6 W/kA-m, due to AC loss, must also be removed.

For the sake of projecting into the future, not for any project now under way, Southwire considered a one-kilometer, 2-kA (rms) cable with three flexible cryostats. They estimate the heat load on the cryostat from the environment to be 9 kW and the heat load from AC losses to be 3.6 kW. The heat load from the terminations (i.e., the connections to the rest of the electrical grid) is estimated to be 300-350 W per phase per termination. Because there are two terminations per phase and there are three phases, the total termination load is in the range 1.8 –

[7]For a discussion of design, see R. Wesche et al., *Design of Superconducting Power Cables, Cryogenics* **39**:767-775 (1999).

2.1 kW. Thus, the total heat load on the cable would be approximately 15 kW at operating temperature, which would be somewhere in the range 67-77 K.

Pirelli is also actively pursuing AC cable development and has graciously shared its estimates of the expected ranges of losses for the readers of this report. Setting aside the heat losses from the terminations, Pirelli finds that it must consider heat flow from the environment to the cold region in the range 1 – 10 W/m. Pirelli notes that the additional heat generated by the viscous flow of the cryogenic fluid can be in the range 0.1-3.0 W/m. Besides these losses, one must also consider the losses within the cold dielectric; they are in the range 0.5–4.5 W/m. As discussed in Section II.3, the superconductor's AC losses depend very much on the current; they are in the range 0.5–8.0 W/m. Besides its operating current, AC losses are also determined by the cable's critical current, which depends on both the operating temperature and the fault current that the cable is designed to survive. Thus, AC losses will depend on many things, including load and weather. AC losses can be expected to contribute anywhere from 25 to 50% of the total refrigeration requirement for the cable.

In general, cable designers are giving their attention to cables carrying 2 kA-m (rms) per phase at 77 K under normal operating conditions. For such a cable, AC losses might amount to 1 W/m of cable per phase.

Although AC losses are important, the loss caused by removing heat that had flowed from the environment to the cold region is substantially bigger.

When considering how to reduce the refrigeration cost (capital and operating), one must choose the least-cost approach. That may well be to reduce AC losses. However, that approach cannot eliminate the whole refrigerator load, or even most of it; better insulation and/or better refrigeration must also be considered.

II.1.3.1.2 Warm Dielectric

The authors expect that the heat flow from ambient temperature to the cold region will be greater in the warm dielectric cable than in the comparable cold dielectric cable. A warm dielectric cable made by Pirelli, with support from the U.S. Department of Energy and from EPRI, is being tested at Detroit Edison's Frisbie Substation.

II.1.3.2 Transformers

Several groups have considered HTS transformers.[8,9] ABB demonstrated a transformer test-bed in Geneva that was cooled by LN_2. It was constructed and operated to gain experience, not to prove commercial feasibility. Its BSSCO conductor was not optimized for AC; indeed, its AC loss was approximately 3 W/kA-m, twelve times larger than the nominal goal presented above. However, the results have so encouraged the participants (ABB, EdF, and ASC) that they

[8]Many of these considerations remain unpublished. An informative exception is J.K. Sykulski, C. Beduz, R.L. Stoll, M.R. Harris, K.F. Goddard, and Y. Yang, *Prospects for large high-power transformers: conclusions from a design study*, IEEE Proc.-Electric. Power Appl., **146**, (1) (Jan. 1999).

[9]K. Funaki and M. Iwakuma, "Recent activities for applications to HTS transformers in Japan," Supercond. Sci. Technol. **13**:60-67 (2000). K. Funaki, M. Iwakuma, et al., *Development of a 500 kVA-class oxide superconducting power transformer…*, Cryogenics Vol. 38 (1998).

are building a prototype HTS transformer in Europe. Furthermore, both Waukesha Electric[10] and ABB-USA are each partnering with USDOE to build different prototypes in the United States. These transformers may be operated at lower temperatures (e.g., 30-45 K). In such cases, the coolant could be a noble gas that is recycled through a refrigerator (aka cryocooler) located nearby. This cryocooler would be most efficient if it were big, raising the thought that one finally wants many HTS transformers at the same substation, where each could be served by a common cryocooler. Because transformers are relatively compact, AC losses and lead losses become more important than heat flow through the thermal insulation.

When considering the goals and performance of HTS transformers, we should recall the characteristics of conventional transformers. They operate above ambient temperature (e.g., 85 C = 388 K). At that temperature, copper has a greater resistivity (i.e., approximately 2×10^{-6} Ω-cm), and so conventional losses are higher (i.e., approximately 80 W/kA-m at 400 A/cm^2). Also, a conventional 10-MVA transformer has approximately 3,750 kA-m with coil losses of approximately 30 kW (0.3% of the throughput power).

Let us consider a hypothetical HTS 10-MVA transformer. More specifically, consider a three-phase 10-MVA transformer having 100 A (rms) and 60 kV (rms) on the high-voltage side (system side) and 600 A (rms) and 10 kV (rms) on the low-voltage side (distribution side). (N.B. 100 A x 60 kV x 3 = 10 MVA.) The six terminations (two per phase and three phases) would carry a total current of 2.1 kA, which would result in approximately 94.5 W entering the cold region. Heat would flow from the environment through the cryostat into the cold region at the rate of approximately 1 W/m^2. Assuming 20-30 m^2 of surface (e.g., a box that is 2 m × 2 m × 1 m), the environmental contribution to heat flow into the cold region would be 20-30 W. Thus, one would have to remove approximately 115-125 W in addition to the AC loss. If the transformer had 3,750 kA-m of conductor dissipating electrical energy at the rate of 0.25 W/kA-m, the coils would generate heat at the rate of approximately 900 W.[11] One sees that this transformer's refrigeration requirement would be dominated by AC losses in the coil. (This would remain true, even if the transformer used only half the assumed conductor.[12])

The nominal goal of 0.25 W/kA-m for AC losses was presented, after assuming a 15:1 energy loss from refrigeration. That combination of refrigeration and coil performance would reduce coil losses to approximately 5% of today's losses in copper [i.e., (15 x 0.25 W/kA-m) / (80 W/kA-m)= 0.047]. If the electrical energy consumed by refrigeration is 30:1, the coil losses would be reduced to 9% of today's coil losses. In fact, one transformer designer states that it is desirable to reduce coil losses from 30 kW at ambient to 300 W at 77K or 150 W at 45K. This performance would certainly accommodate inefficient refrigeration. It would also reduce the AC losses to the point where one might consider whether improved current leads or thermal insulation would be cost-effective.

---

[10]The Waukesha team continues to scale up. Past work is reported in S.W. Schwenterly et al., "Performance of a 1–MVA HTS Demonstration Transformer," *IEEE Transactions on Applied Superconductivity* **9**(2):680-684 (June 1999).

[11]Here we use the same number of kiloampere-meters as in a transformer with copper coils. We think this reasonable for two reasons: (1) the new transformer must have the same voltages and currents as the old one it is to replace, and (2) the interior dimensions must take account of electrical insulation between turns and between coils of the same voltage as the old one. We expect that there will be differences here (for a review, see *Cryogenics*, **38**(11), Nov. 1998), but not order-of-magnitude differences in size. Same current and similar size suggest a similar number of kiloampere-meters. Of course, as long as ceramic superconductor is more expensive than copper, which is more expensive than electrical steel, electrical engineers will have an incentive to reduce the amount of conductor (e.g., by trying to compensate with increased use of electrical steel in the yokes).

[12]M.S. Walker estimates that a 30-MVA transformer could be built with approximately 5,000 kA-m of conductor (Feb. 2000).

The market for "transmission" transformers is believed to center in the 40-60 MVA range. For each such transformer, there are several smaller "distribution" transformers. In fact, their total value is larger than the total value of "transmission" transformers. Nonetheless, the market for HTS transformers will certainly be for transformers greater than 10 MVA.[13] Thus, it is important to know how the AC losses scale with increased power rating. When one compares two geometrically similar transformers of different size, one concludes that (a) current and voltage scale with the second power of a linear dimension, (b) core and coil losses with the third power of a linear dimension, (c) capital cost scales with the third power of a linear dimension, and finally (d) power (MVA) scales with the fourth power of a linear dimension. The same results can be expressed in a different way by using the throughput power, instead of a linear dimension, as the scaling variable. In this way, one concludes that (a) current and voltage scale with the square root of the throughput power ($MVA^{0.50}$), (b) core and coil losses with the cube of the fourth root of the throughput power (i.e., $MVA^{0.75}$), and finally (c) capital cost scales with the cube of the fourth root of the throughput power (i.e., $MVA^{0.75}$). Regarding these rules as a rough guide to practical scaling, one finds that AC losses would remain the principal source of the refrigeration load, when prototypes are scaled up to future commercial HTS transformers.

II.1.3.3 Rotating Machines

The HTS motor and LTS generator projects for the power sector confine the use of superconductor to the machine's field coils. They carry DC, and each machine is designed to minimize the time-dependence of fields that react back on the field coil. It is the armature coils that see a time-dependent magnetic field; that field induces the currents in the armature. These coils are made from conventional conductor.[14] Many years ago, Siemens worked on an all-superconducting generator made from NbTi. That machine was not completed after the retirement of key staff. AC losses in HTS conductors are not an impediment to rotating machines with HTS field coils and conventional armatures.

Rockwell has graciously shared the order of magnitude of the losses in its 770-kWe (1,000-hp) HTS motor and its 3,850-kWe (5,000-hp) HTS motor. Roughly speaking, the current leads and the torque tube each allows approximately 10 W to flow into the cold region. Since any rotating machine must have a nonnegligible magnetic field, it is reasonable to assume that any rotating machine using Bi-2223 would operate in the range 25–35 K. At that temperature, radiation from ambient temperature would convey some heat into the cold region, but the rate would be somewhat less than 10 W. Again, because of the coil's operating temperature, one should take account of DC losses; they are likely to be approximately 5 W. Steady state AC losses are negligible compared to the sources just mentioned. Of course, during fault conditions with rapidly changing currents, the field coil will see some magnetic field, but these conditions are by nature exceptional and do not affect our general statement: AC losses are not an impediment to rotating machines with conventional armatures and HTS field coils.

II.1.3.4 SMES

[13]As of July 23, 1997, N. Aversa (Chmn. Emeritus,Waukesha) estimated that the U.S. market for transformers consists of 874 transformers in the range 10-100 MVA (total 33,000 MVA) and 78 transformers above 100 MVA (total 26,000 MVA) and that the rest of the world's market is three to four times larger and growing twice as fast as the U.S. market.

[14]Were the military, particularly the Air Force, to use HTS rotating machines, they would prize light weight and small volume, stimulating the development of an all HTS machine in which AC losses would be a critical issue for energy efficiency. However, the military is more often concerned with performance than with energy efficiency.

Today, there is a commercial micro-SMES, incorporating NbTi. Any SMES sees time-dependent magnetic fields when it discharges and recharges; thus, AC losses affect its performance. However, the losses are small compared with those in the AC-DC converters.

II.1.3.5 Flywheels

Flywheels can use HTS in their bearings. These are a combination of ferromagnets, rigidly attached to the rotor, and HTS, rigidly attached to the stationary containment. Any inhomogeneity in the field, the source of which is the rotating magnets, will appear as a time-dependent magnetic field to the stationary superconductor. That time-dependent field will drive hysteresis in the superconductor with a consequent dissipation of energy. The importance of this effect depends on the purpose of the flywheel. Flywheels meant for power quality have high-power motor-generators, the idling losses of which can swamp bearing loss. Flywheels meant for energy storage over many hours must take account of bearing loss. To date, HTS bearings and other flywheel components have been demonstrated, which together could provide storage over 24 hours with 90% round-trip efficiency.

II.1.3.6 Fault Current Limiters

Many designs have been proposed for fault current limiters, and a substantial number of projects have been undertaken to explore them. Here, we report on the AC losses for a current-controller-limiter (General Atomics), inductive limiter (e.g., Israel), and resistive limiter (Siemens).

General Atomics' current controller-limiter incorporates three HTS coils, one for each phase, through which direct current flows when the grid has no faults to be controlled or limited. Because the HTS coils see negligible AC in this condition, AC losses do not arise. Indeed, it is reported that the heat load of one coil was measured to be 3 W at 25 K (without current) and 7.67 W at 32 K (at a full current of 2000 A dc).[15]

Both Hydro-Québec and Israel have investigated the possibility of using bulk superconductor to shield an inductor from the normal current flowing in a power line. Were this current to grow greatly because of a fault, the unusually large current would generate a magnetic field that could not be shielded from the inductor. Instead, power would be transferred to an otherwise dormant circuit. The AC losses would occur in the superconducting shield, where superconducting AC eddy currents would be generated by the oscillating magnetic current of the normal AC current flowing in the power line. A recent report from Israel suggests that the losses would be roughly 15 W/kg of Bi-2212 shielding material.[16] Such losses do not appear to present an insuperable barrier to operation. However, an evaluation should wait until the whole design is available for consideration.

Siemens' resistive fault current limiter always has AC flowing through a serpentine film of YBaCuO that coats a plate. Siemens has kindly made available the following information for this report: Siemens splits the current (e.g., 3 kA) into many parallel currents, each of approximately 100 A and each with its own plate. The result is negligible AC loss. The

[15]E. Leung et al., "Design & Development of a 15 kV, 20 kA HTS Fault Current Limiter," IEEE Transactions on Applied Superconductivity, **10**(1):832-835 (March 2000).

[16] H. Castro, A. Gerber, and A. Milner, "Calorimetric study of ac-field losses in superconducting BSCCO tubes," *Physica* C **331**:141-149 (2000).

cryogenic load due to the current leads is on the order of 45 W/kA for uncooled leads and 24 W/kA for gas-cooled leads.

II.1.3.7 Summary

While the economics of almost all devices would benefit from reduced AC losses, the economics of transformers would benefit most. Recalling that a single 30-MVA transformer incorporates approximately 5,000–8,500 kA-m of conductor, it appears that transformers offer the largest potential market for ceramic superconductors in the electric power sector.

II.1.4 Self-Contained Refrigeration

II.1.4.1 Some Utilities' Desire for Self-Contained Refrigeration

AC loss itself causes foregone revenue. To this cost must be added one that is many times greater — the cost of removing heat from the cold region and transferring it to the environment. One method is to cool a liquid cryogen (liquid nitrogen, aka LN_2) at a remote location and then transport it to the electric utility where it can be boiled off, recollected, and then cooled again for subsequent use. This may be the least-cost solution for some devices (e.g., cable), and it deserves to be considered for all devices.

However, some electric utility staff have strongly emphasized their wish for self-contained refrigeration systems that can operate without utility employees being present and that do not require non-utility personnel to be in utility facilities.[17] Today, this is technically feasible. Here, we present today's cost for two such commercial machines. We offer this information because we suppose that other machines will have approximately the same performance and price; in other words, this information should be taken as a benchmark, not a recommendation for purchase.

II.1.4.2 Cost and Performance of Cryomech's Cryocoolers

Both machines are manufactured by Cryomech, Inc.[18] One, designated AL300, requires 7.4 kW of electricity and 5L/min of cooling water. The unit weighs 118 kg, and its dimensions are 58 cm × 53 cm × 66 cm. The unit's cooling capacity depends on the cold temperature. Cryomech states that at 70 K, the AL300 can remove 300 W; at 60 K, it can remove 265 W; at 50 K, 225 W; at 40 K, 160 W; and finally, at 30 K, the AL300 can remove 90 W. The price of the AL300 is $27,440.

The other Cryomech unit, designated AL330, is a variant of the first, but now optimized for operation below 50 K. The AL330 requires 7.0 kW of electrical input power. Cryomech states that at 50 K, the AL330 can remove 200 W; at 40 K, it can remove 150 W; at 30 K, 100

[17] Statements from the floor at IEA Workshop on Impact of HTS on System and Customer Reliability, sponsored by USDOE (Santa Fe, N.M., Oct. 5-6 1999). It is recognized that some substations may allow delivery of LN_2 without internal access to the station.

[18] Cryomech, Inc, does business at 113 Falso Drive, Syracuse NY, 13211, USA, phone 1 (315) 455-2555, fax 1 (315) 455-2544, URL http://www.Cryomech.com/.

W; at 20 K, 50 W; and finally, at 10 K, the AL330 can remove 25 W. The price of the AL330 is $33,400.

II.1.4.3 Self-Contained Refrigeration for a Hypothetical 30-MVA HTS Transformer

Let us consider the goals discussed in Sections II.1.2 and II.1.3.2 in light of the cost and performance just described. We focus on the transformer because AC losses provide most of its refrigeration load.

A hypothetical 10-MVA transformer, wound with ceramic superconductor and having AC losses of 0.25 W/kA-m, would require 900 W of cooling at its operating temperature. If this were 70 K, the transformer would require three AL300 cryocoolers. These units would draw 22.2 kW, which is 0.21% of the throughput power. The total investment in these units (i.e., "first cost") would be $82,320.

If the hypothetical transformer is scaled up from 10 MVA to 30 MVA, its losses increase by a factor of $3^{0.75} = 2.28$, while the throughput power increases by 3; thus, the ratio of the losses to the throughput decreases. This is an incentive to scale up to 30 MVA, instead of building three 10–MVA transformers. If the hypothetical 30–MVA machine operated at 70 K, it would require 51 kW for its cooling and an investment of $188,000 for its AL300 cryocoolers. Recalling the importance many buyers attach to first cost, one sees why a transformer builder would prefer AC losses of 0.08 W/kA-m to the nominal goal of 0.25 W/kA-m, at 70 K; also, recall that a conventional 30-MVA transformer costs about $250,000–$300,000.[19] It is also important to consider the possibility of economies of scale arising from building a large refrigeration system that would cool many transformers at the same substation. One rule of thumb for scaling similar refrigeration units is that cost increases with the 0.56 power of capacity.[20] Therefore, doubling the capacity would increase the cost by 1.47. Another possibility deserves consideration, when circumstances are favorable: pipelining liquid nitrogen to a substation. We note that liquid oxygen pipelines are in place near some regions with steel plants.

II.1.4.4 Desirable Operating Temperature

Let us now consider the potential benefit from operating a coil of ceramic superconductor at temperatures less than 70 K. These considerations will be indicative, not definitive. (The latter would require a full cost analysis, which is not the subject of this report.) Our approach is to express the annual cost of the superconducting coil, with refrigeration, as a function of operating temperature. We then identify the temperature that requires the least annual cost. That temperature will depend on the comparison of capital costs for conductor and for refrigeration, as well as the operating cost of the refrigeration. We incorporate both by calculating annual cost per kiloampere-meter of coil. Because transformers are the biggest potential application of

[19]Purchase of a new conventional transformer entails an additional cost of approximately $150,000 for oil containment and fire suppression, which would not be needed by an HTS transformer. B. McConnell and M.S. Walker, *HTS Transformers*, 1997 Annual Peer Review, U.S. Department of Energy, July 21-23, 1997.

[20] H. Quack, "Refrigerators," appearing in B. Seeber, *Handbook of Applied Superconductivity* Vol.1, Institute of Physics (Bristol, 1998).

ceramic superconductors, we neglect sources of heat other than AC losses. (See Section II.3 for a discussion of DC losses.)

We begin by recalling that for every monetary investment in equipment, each year a certain fraction must be returned to the investors (profits and dividends), government (taxes), insurance company (insurance), and management to be set aside for a future replacement (depreciation), as well as for salaries (overhead). The sum of all these charges is called the "fixed charge rate," denoted by FCR. Its numerical value varies with each utility. For the sake of definiteness, we will use the following value:

$$FCR = 0.2 \text{ per year.} \qquad \text{(II.1.4.3-1)}$$

The size of the investment reflects the cost of the coil, K_{coil}, and the cost of the concomitant cryogenics, $K_{cryogenics}$. The annual operating cost of the cryogenics will depend on the amount of electric power, S_{cryo}, required and on the price, p_e, that the utility charges for it. The annual operating cost should also include labor and maintenance, but these costs will be neglected here. Thus, the annual cost can be expressed as

$$\text{Annual cost per kiloampere-meter} = FCR \{K_{coil} + K_{cryogenics}\} + p_e S_{cryo} \qquad \text{(II.1.4.3-2)}$$

Except for the fixed charge rate and the price of electricity, these quantities depend on the temperature. For a demonstration transformer made with Bi-2223, we might take K_{coil} to be 300 \$/kA-m, if that coil were operated at 77 K at low field. However, the critical current density increases as the temperature declines, so less material is needed at lower temperatures. We express the cost of the coil per kiloampere-meter as follows:

$$K_{coil}[T] = K_{coil}[77] \, (J[77] / J[T]) \qquad \text{(II.1.4.3-3)}$$

We know that the performance of refrigeration depends on temperature; that is, the ratio of watts of input shaft power to heat removed, $\Omega[T]$, from the cold region increases as temperature declines. We write this as

$$S_{cryo} = \Omega[T] \, (d/dtQ_{AC}[T] + \text{const} \times (1 - (T/298K)^4), \qquad \text{(II.1.4.3-4)}$$

where $d/dtQ_{AC}[T]$ is the AC power loss per kiloampere-meter at the indicated temperature. Finally, we know that the investment in cryogenics depends strongly on the amount of input electrical power required. For the sake of simplicity, we assume the investment is essentially proportional to the input power. (N.B.: Later, we neglect the cost of the cryostat compared to the cost of conductor.) We express this by

$$K_{cryogenics} = k_{cryo} \, S_{cryo} + K_{cryostat} \, , \qquad \text{(II.1.4.3-5)}$$

where k_{cryo} is measured in money per electric power (kWe) input to the cryogenics of a self-contained system. (If the unit is scaled up, rather than replicated, k_{cryo}, might increase as the 0.56 power of the electric power.)

Our purpose is to understand the importance of reducing AC losses. We will consider three possible technical performance specifications and look at how the cost varies with the specification.

$$d/dtQ_{AC}[T] = \{0.08 \text{ W/kA-m or } 0.25 \text{ W/kA-m or } 0.5 \text{ W/kA-m}\} \qquad \text{(II.1.4.3-6)}$$

All of the above discussion can be expressed as follows:

Annual cost per kiloampere-meter = FCR { $K_{coil}[77]$ (J[77] / J[T])

$$+ k_{cryo}\ \Omega[T]\ d/dtQ_{AC} + K_{cryostat}\}$$

$$+ p_e\Omega[T]\ (d/dtQ_{AC} + \text{const x } (1 - (T/298K)^4)\ )$$

(II.1.4.3-7)

The annual cost at any operating temperature depends on the temperature through the current density and through the efficiency of the refrigeration, as well as through the heat leaks.

It has been found that the current density of Bi-2223 increases as the temperature declines from 77 K to 4.2 K.[21]

$$J[T] = J[0]\ (1 - T/107K)^{1.4} \qquad \text{(II.1.4.3-8a)}$$

$$J[77] = J[4.2] / 5.5 \qquad \text{(II.1.4.3-8b)}$$

For the sake of definiteness, we assume the efficiency of the cryogenics is similar to that of the AL300 cryocooler, as expressed by the formula

$$\Omega[T] = 7.3\ \Omega_{carnot}[T] = 7.3\ \{(298 - T) / T\} \qquad \text{(II.1.4.3-9)}$$

Figure II.1.4.3a presents a graph of this ratio of input shaft power to output "cold power."

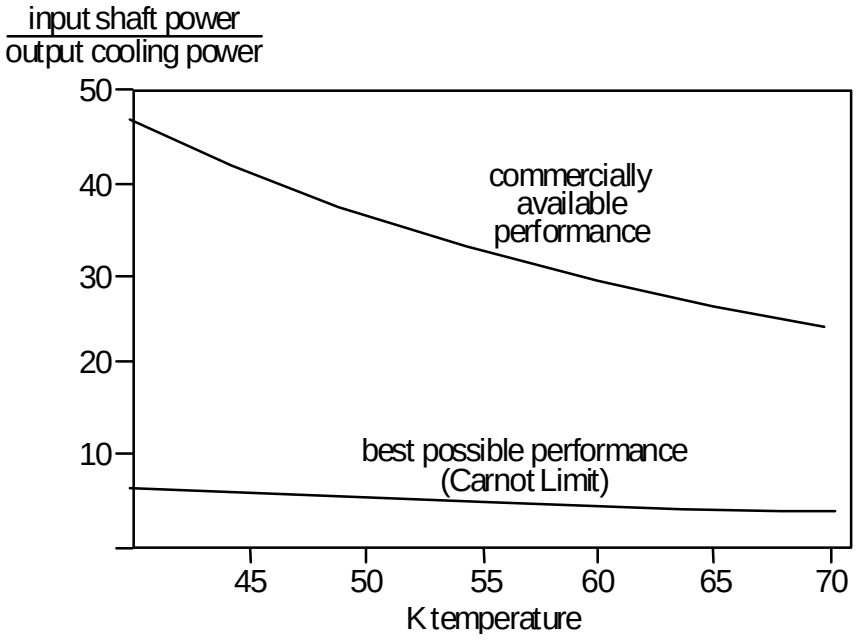

Figure II.1.4.3a. Upper curve is ratio of input shaft power to output cooling power at various temperatures for a cryocooler that is 7.3 times worse than a Carnot cryocooler, the performance of which is shown in the lower curve. The performance of Cryomech's AL300, with an input of 7.4 kWe and a price of $27,400, is similar to that shown in the upper curve.

[21]The authors are grateful to both B. Riley and R. Wesche for timely information on this subject, and to R. Wesche for providing Eq. II.1.4.3-8a, via personal communications, March 2000.

As above, we use numbers appropriate to today's demonstration technology. The price of the coil is \$300/kA-m. The price of self-contained refrigeration equipment is (\$27,400/7.4)/kWe, and the price of electricity is \$0.1/kWhe. Furthermore, we consider the effect of reducing the cost of Bi-2223 to \$50/kA[22] and AC losses in the range 0.08–0.50 W/kA-m at 77 K. The results are shown in Figure II.1.4.3b.

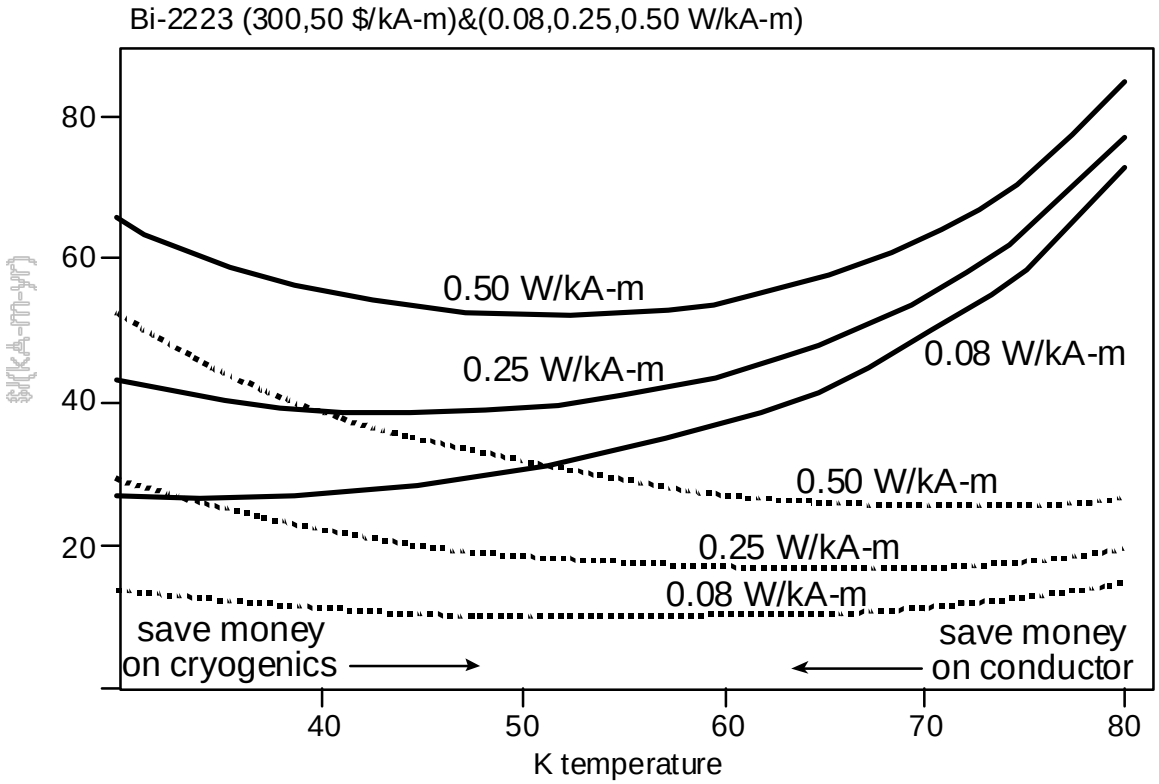

Figure II.1.4.3b. Upper three curves indicate how annual cost per kiloampere-meter depends on temperature when today's cost parameters are used and the AC loss is assumed to be 0.5, 0.25, and 0.08 W/kA-m, respectively. Lower three curves indicate how annual cost would depend on temperature, if the cost of ceramic superconductor fell from \$300/kA-m to \$50/kA-m and AC loss varied as above, while all other prices and performance remained fixed. The price of electricity was taken to be \$0.10/kWh. (Each reader should adjust the result to reflect his or her electricity price.)

The curves in Figure II.1.4.3b show that at 77 K, the principal cost is capital cost for the Bi-2223 tape. By comparison, the cost of cryogenics is a correction. As temperature declines, the current density increases and so one needs less and less conductor. At 30 K, the cost differences due to different AC losses are just as important as different conductor prices.

One sees that the more expensive conductor is best operated at lower temperatures than those used for less expensive conductor.

[22]L. Masur et al., *Long Length Manufacturing of BSCCO-2223 Wire for Motor and Cable Applications*, 1999 CEC/ICMC, Montreal, Canada, July 13-16, 1999.

Next, we consider the importance of AC loss, assuming YBaCuO coated conductor becomes as inexpensive as is hoped. For YaBaCuO on RABiTS, the dependence of current density on temperature is[23]

$$J[T] = J[0]\,(1 - T/88K)^{1.2} \qquad \text{(II.1.4.3-10)}$$

The results are presented in Figure II.4.3c.

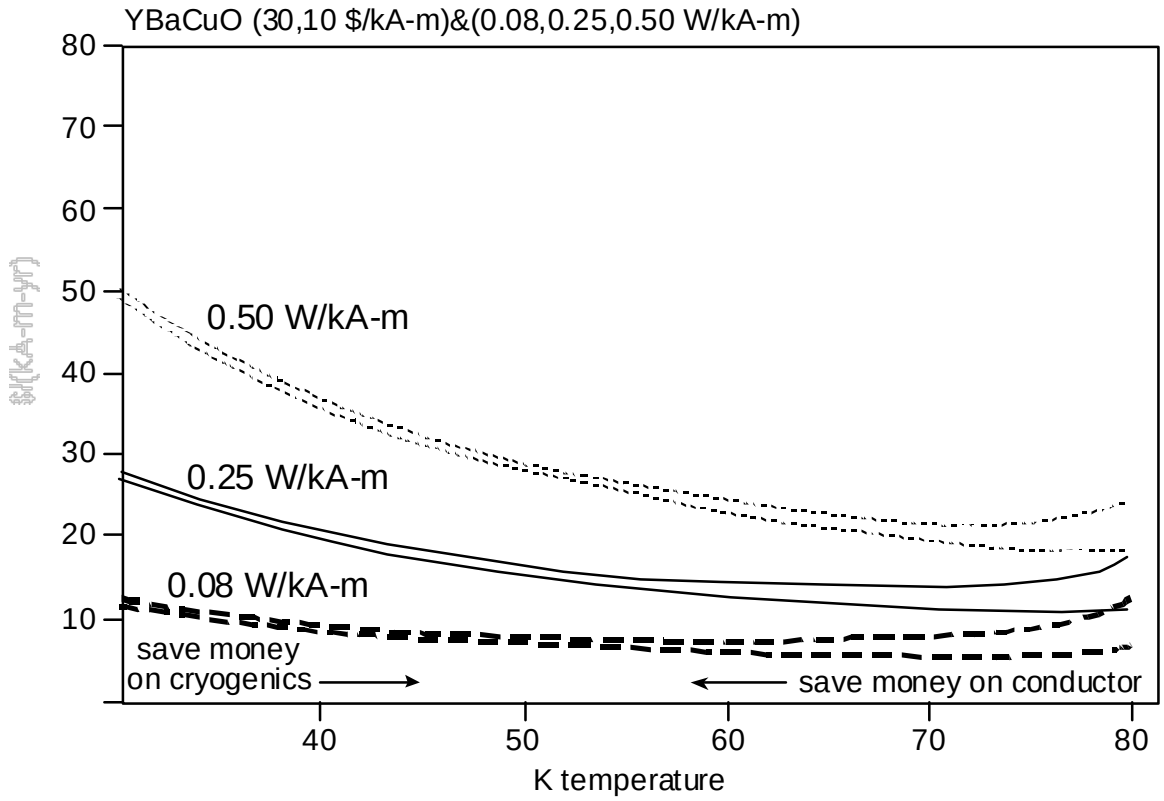

Figure II.1.4.3c. Upper three curves indicate how annual cost per kiloampere-meter depends on temperature, assuming the not yet achieved price of $30/kA-m and AC losses of 0.5, 0.25, and 0.08 W/kA-m, respectively. Lower curves indicate how annual cost would depend on temperature, if the cost of ceramic superconductor were 10 $/kA-m and AC loss varied as above, while all other prices and performance remained the same. The price of electricity was taken to be 0.10 $/kWh. (Each reader should adjust the result to reflect his or her electricity price.)

The curves in Figure II.1.4.3c show that at 77 K, the difference between $30/kA-m and $10/kA-m capital cost of YBaCuO tape would still be important. As temperature declines, the current density increases and so one needs less and less conductor, until the cost of cryogenics dominates the cost of conductor and begins to climb. However, at all temperatures, the cost differences due to different AC losses are the most important influence on annual cost. The AC loss also determines the needed capacity of the cryocoolers, which affects the capital cost and thus, the first cost to the customer.

[23]The authors are grateful to R. Wesche for providing Eq.II.1.4.3-10, personal communication, March 2000.

In general, as the temperature drops the conductor becomes less and less expensive, driving down the total cost until the worsening efficiency of the refrigeration drives the refrigeration cost so high that it negates the decline in conductor cost. For today's prices, this does not occur until the temperature is near 50 K. However, if the cost of ceramic superconductor were reduced from $300/kA-m to $10/kA-m, the most economical operating temperature would rise to the 65–75 K range. One also sees that the cost becomes insensitive to operating temperature, because the capital cost of the conductor has fallen to near the cost of refrigeration, and as the one declines the other increases. Finally, one sees that at all temperatures, the decline in AC losses from 0.5 W/kA-m (comparable to today's performance) to 0.08 W/kA-m would greatly reduce the annual cost of the coil.

II.2 VARIETIES OF CERAMIC SUPERCONDUCTORS UNDER DEVELOPMENT

Since Bednorz and Mueller's discovery, in 1986, that LaSrCuO becomes a superconductor at 40 K, many other copper oxides have been found to be superconducting.[24] However, only three materials have received substantial, sustained attention, arising from the hope that they could become the basis for practical high-amperage conductor: Bi-2212, Bi-2223, and YBaCuO. The status of progress with these materials was reviewed in 1997,[25] so we confine ourselves here to recalling their salient features and noting recent progress.

II.2.1 Bi-2212

Bi-2212 has the lowest transition temperature, approximately 80 K, and thus its practical application would entail operating temperatures below the boiling point of liquid nitrogen (77 K). Indeed, it has been used in a prototype cable cooled by liquid neon[26] and in some prototype transformer coils, made by IGC for Waukesha, that were meant to operate in the region 20–30 K. Others have considered using Bi-2212 at liquid helium temperatures because its performance in high magnetic fields, at those temperatures, surpasses that of Nb_3Sn. Potential applications include NMR magnet inserts (i.e., coils that could be inserted in an existing NMR to increase its field), high-energy physics, and fusion magnets. Bi-2212 is appealing because it is less expensive to fabricate conductor from it (perhaps $100/kA-m) than from the other two materials and because it can be made to have less anisotropic response to magnetic field than conductor made from Bi-2223. Like Bi-2223, Bi-2212 is made into conductor either (1) by putting it into tubes of silver or silver alloy, a method known variously as Powder-In-Tube (PIT) or Oxide Powder-in-Tube (OPIT), with subsequent bundling and drawing; or (2) by coating silver or silver alloy tapes with Bi-2212 (first by "Dip Coating," and subsequently by various electrophoretic techniques).

II.2.2 Bi-2223

Of the three "practical" materials, Bi-2223 has the highest transition temperature, approximately 110 K. Thus, hope and substantial effort have been focused upon developing a conductor that would be practical at the boiling point of liquid nitrogen. Indeed, Bi-2223 has been used in several prototype cables that were cooled by liquid nitrogen and in some test-bed transformer coils, made by ASC for ABB in Geneva, Switzerland, that were operated at 77 K. Others have considered using Bi-2223 at lower temperatures because its performance in

[24]A convenient guide to 26 types of structure is provided by H. Shaked et al., *Crystal Structures of High-Tc Superconducting Copper-Oxides*, Elsevier (Amsterdam, 1994).

[25]A.M. Wolsky, *The Status of Progress toward High-Amperage Conductors Incorporating High-Temperature Superconductors*, for signatories of the IEA Implementing Agreement for a Co-Operative Programme for Assessing the Impacts of High-Temperature Superconductivity on the Electric Power Sector (March 1997), 98 pages.

[26]G. Vecsey, report to ExCo Meeting on Oct. 4, 1999.

magnetic fields improves substantially at lower temperatures (e.g. 65 K and 45 K) without incurring a greatly increased cooling penalty. (See Section II.1.4.3.) Potential applications include transformer coils and fault-current-limiter coils, as well as cable. (Prototype coils for rotating machines have also been made.) Bi-2223 is made into conductor by putting it into tubes of silver or silver alloy, with subsequent bundling, drawing, and heat treatments. In fact, during these treatments, Bi-2212 is converted to Bi-2223. Unfortunately, the heat treatments require long times and excellent temperature control, making the production process slower and more capital-intensive than the process for Bi-2212. Today, one firm (ASC) publicly offers to sell Bi-2223 for $300 /kA-m at 77 K in self-field and holds out the hope that the price could fall to $50/kA-m, if and when there is a large demand. Despite today's price, Bi-2223 will continue to be offered by competing firms, and we expect it to continue to be used in prototype HTS equipment. Indeed, ASC reports that its Bi-2223 tape has improved long length characteristics both electrically and mechanically. The company reports having achieved an average engineering current density of 14,000 A/cm^2 and a concomitant average critical current density of 35,000 A/cm^2. In addition, ASC says it has the ability to add a steel lamination that strengthens its tape. [27]

II.2.3 YBaCuO

The third material is YBaCuO, also called 123. It was discovered in 1987, but it has only been within the past five years that serious hopes have been raised for a practical method to make high-amperage conductor from this material.[28] Such a method is now being sought in Japan, the United States, and Europe (particularly in Germany) for two reasons. First, YBaCuO offers much better performance in magnetic fields than the two bismuth conductors introduced above. The current density is greater, and the anisotropy in a magnetic field is less. The second reason is the possibility that conductor fabricated from films of YBaCuO would be much less expensive than those made from either bismuth-based conductor. This possibility is plausible to 3M, which is investigating it. 3M specializes in products made from films laid upon substrates (called webs by 3M). Furthermore, ASC reports that its YBaCuO films (0.4 μm in thickness, with critical current density of 2 MA/cm^2 at 77 K in self-field) have achieved "performance parity" with its Bi-2223 tapes.[29] Also, Intermagnetics (IGC) recently announced that it is "…convinced that this is the technology that we and many electric utilities have been waiting for to enable commercial exploitation of the energy-saving characteristics and increased reliability of HTS devices. Our [IGC] mission now is to turn this from promise to reality." IGC's president estimates that it will take at least two years to develop a manufacturing process that can turn out superconducting tape at an acceptable cost-performance threshold.[30] Others think it will take longer.

Within the past five years, several groups have shown how to make short lengths of YBaCuO tapes by depositing it on nickel tapes, the surface of which has been prepared with layers of other material. In part because nickel is much less expensive than silver, this work has raised hopes for less expensive tapes. Because nickel is not so good a conductor as silver, eddy currents and concomitant problems should be suppressed. However, nickel is a ferromagnet. Thus, it is possible that hysteresis within the nickel may generate losses and problems. Some experimental work has been done, without disclosing the anticipated difficulties.[31] However, this

---

[27] B. Riley (ASC) to A.M. Wolsky, March 17, 2000.

[28] D.K. Finnemore et al., "Coated conductor development: an assessment," *Physica* C **320**:1-8 (1999).

[29] B. Riley (ASC) to A.M. Wolsky, March 17, 2000.

[30] IGC press release, March 13, 2000.

[31] H.R., Kerchner et al., "Alternating current losses in biaxially textured $YBa_2Cu_3O_7$ 2 d films deposited on Ni tapes," *Appl. Phys. Lett*. **71**:2029 (1997).

desirable outcome is not yet definitive because the tests were done in self-field, which is small because only small samples of tape are available.[32] (Tests in fields of 0.1-0.5 T would be desirable.) Indeed, ORNL has continued to seek a non-ferromagnetic alloy and, recently, ORNL announced progress with nickel-13% chrome.[33] Similarly, ASC continues to seek a non-ferromagnetic alloy.[34]

II.2.4 Commonalities among Ceramic Superconductors

The critical current density of each of the ceramic superconductors increases as its temperature declines. For example, the critical current density of Bi-2223 grows approximately linearly with declining temperature, increasing by a factor of 5.5 as the temperature falls from 77 K to 4.2 K.

Furthermore, each of the three ceramic superconductors can be described to engineering accuracy by the same kind of phenomenological E vs. J curve. The only difference is in the values of the relevant parameters, each being particular to whatever material is under consideration. Together, the phenomenological E vs. J curve and the principles of electricity and magnetism lead us to expect hysteresis, the irreversible dissipation of electrical energy, in a cyclic process, of which AC is the most prominent example. This hysteresis is the principal contributor to AC losses.

Unlike copper or aluminum, ceramic superconductors cannot stand by themselves; they must be embodied within a matrix or laid down upon a substrate. To date, the only matrix materials known to have suitable properties are the noble metals, of which silver is the least expensive. Unfortunately, even silver is not cheap, and it is also an excellent conductor. The conductivity of silver would raise no problem if the current were DC. However, when AC is conveyed, the silver is exposed to time-dependent magnetic fields, and silver's excellent conductivity allows non-negligible currents to be induced. These eddy currents dissipate electrical energy, something the use of superconductors is meant to avoid, and generate heat, which must be removed to maintain the operating temperature of the superconductor. This issue is reminiscent of the problems raised by the possibility of induced eddy currents in the laminations of transformers.

Three approaches to reducing eddy currents have been explored. They will be mentioned here and described in subsequent sections. (See Section VI.2). The first approach is to find a silver alloy that has all the needed physical and chemical properties and is much more resistive than pure silver. Silver doped with gold is such a material, but it is too expensive to be of commercial interest. The second approach is to insert electrically insulating material around the superconducting filament and silver jacket. Pioneered at the University of Geneva, this approach

---

H.R. Kerchner et al., "Alternating transport-current flow in superconductve films: The role of a geometrical barrier to vortex motion," *Phys. Rev. B*, **60**(9):6878 (Sept. 1999).

[32]Cables operate near 0.1 T, and transformers would operate in the range 0.1-0.5 T.

[33]A. Goyal, Proceedings of the DOE Wire Development Workshop 2000, held in St. Petersburg, Fla., USA, Feb. 9, 2000 (forthcoming).

[34]B. Riley (ASC) to A.M. Wolsky, March 17, 2000.

is now being explored by several other groups (e.g., ASC and FZK).[35,36] It is not clear how effective or how expensive such insulation is. The third approach is to twist the superconducting filaments. This reduces the current in the superconductor that is devoted to shorting the induced currents; that current reduces the effective transport critical current density in the superconductor. Many groups have made prototype twisted tape (e.g., ASC, IGC, Vacuumschmelze).

All of these approaches are made necessary by the wish to reduce eddy currents in the silver or silver alloy matrix used in the OPIT approach. For many years, some groups attempted to make conductor from films of YBaCuO deposited on a silver substrate. Precisely the same issues would have been raised by such an approach.

In summary, while there are three kinds of ceramic superconductor under development and each has different properties, all share a common set of important issues.

II.3 DC BEHAVIOR OF CERAMIC SUPERCONDUCTORS: THE E VS. J CURVE

II.3.1 The ln[E] vs. ln[J] Correlation

Measured values of the electric field and concomitant current density are often reasonably well fitted with straight lines on log-log graph paper, as can be judged from Figure II.3.1a. These correlations have the form shown in Equation II.1:

$$\ln E = n \ln J - \text{constant} \qquad \text{(II.3.1-1a)}$$

where n is substantially greater than 1. This description is mathematically equivalent to the following:

$$E = E_0 \left(\frac{J}{J_c} \right)^n \quad \text{where} \quad n \ln J_c - \ln E_o = \text{constant} \qquad \text{(II.3.1-1b)}$$

This behavior is different from that of normal conductors, which is described by Ohm's Law:

$$E = \rho J \qquad \text{(II.3.1-2)}$$

Although the form of the correlation shown in Eq. II.3.1 is simple, no derivation from an underlying theory has been found. In general, the relation between current density and electric field is expected to depend on the temperature and the applied magnetic field. The correlation shown in Eq. II.3.1 is commonly used because it is simple and because it fits the data reasonably well in the region of technological interest. Figure II.3.1a presents data taken in the laboratory in

[35]K. Kwasnitza, S. Clerc, R. Flükiger, et al., "Reduction of alternating magnetic field losses in high-Tc multifilament Bi(2223)/Ag tapes by high resistive barriers," *Cryogenics* **39**(10):829-841 (Oct. 1999).

[36]W. Goldacker, M. Quilitz, B. Obst, et al., "Novel resistive interfilamentary carbonate barriers in multifilamentary low AC loss Bi(2223)-tapes," *IEEE Trans. Appl. Supercon.* **9**(2):2155-2158, Part 2 (June 1999).

H. Eckelmann, M. Quilitz, C. Schmidt, et al., "AC losses in multifilamentary low AC loss Bi(2223) tapes with novel interfilamentary resistive carbonate barriers," *IEEE Trans. Appl. Supercon.* **9**(2):762-765, Part 1 (June 1999).

a logE-logJ plot, and Figure II.3.1b presents a graph of the E vs. J curve for several values of n according to Eq.II.3.1-1b. (N.B.: The plot shows E vs. J, not log[E] vs. log[J].)

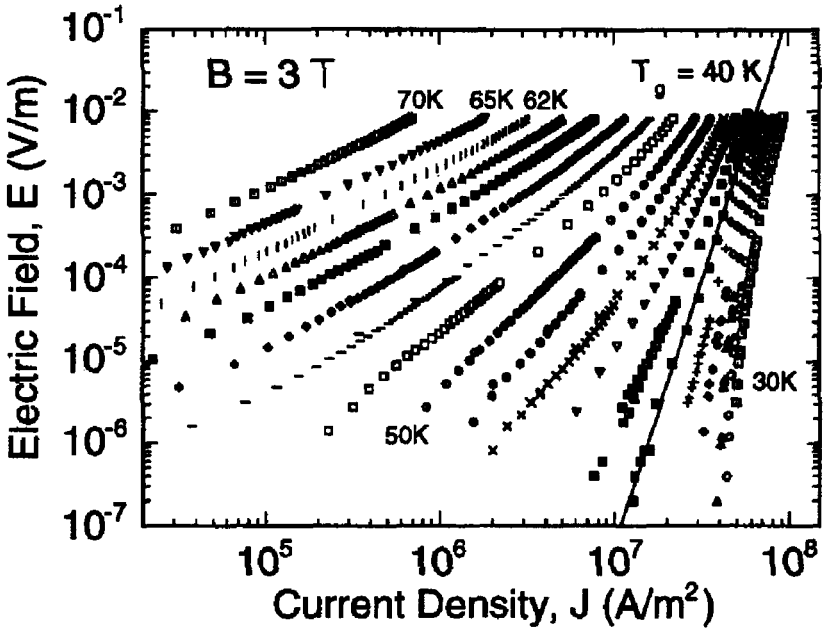

Figure II.3.1a. Electric field, *E*, vs transport current density, *J*, at *B* = 3 T for 70 K to 30 K, in intervals of 2 K. Source: R. Flükiger et al., "Current Densities at 77 K and 4.2 K of Bi(2223) Tapes Prepared by Cold and Hot Deformation," *IEEE Trans. on App. Supercond.* **5**:1150 (1995).

II.3.2 Definition of Critical Current Density, Voltage Criterion, and n-Value

Considering this correlation, one sees that the exponent n is significant in its own right, but neither J_c nor E_o has any significance apart from the other. Put another way, the same correlation can be described by many different pairs, E_o and J_c. The parameter, E_o, is called the "voltage criterion," although it has the dimensions of electric field. The parameter, J_c, is called the "critical current density." To avoid needless confusion, most observations, at 77 K, are reported with the parameter E_o chosen to be 1×10^{-6} V/cm; this value may be assumed, unless the contrary is stated. However, some groups report observations at 4 K, with the parameter E_o chosen to be ten times smaller, 0.1×10^{-6} V/cm. Although many parameter pairs describe the same correlation, the one chosen generally reflects the smallest electric field at which the current density can be reliably measured.

A few authors define the critical current density to be a slightly different quantity. From the point (E_o, J_c), these authors follow the tangent to the E-J curve until the tangent intersects the J axis. The point of intersection is called the "critical current density defined by the off-set criterion"; it is smaller than the critical current density defined above. In fact, when Eq. II.3.1 describes the superconductor, the two definitions are simply related as shown:

$$J_{c\ \text{off-set}} = (1 - n^{-1})J_c \qquad \text{(II.3.2-1)}$$

When n is large, there is only a small numerical difference between these two quantities, J_c and $J_{c\ \text{off-set}}$.

A different, but closely related, way to describe the current-carrying capacity of a superconductor is sometimes used. Instead of plotting E vs. J (or ln[E] vs. ln[J]), one plots the ratio E/J vs. J (or ln[E/J] vs. ln[J]). If the E vs. J correlation is well-described by the form discussed above, Eq. II.1, then E/J will be correlated with J as follows:

$$\frac{E}{J} = \left(\frac{E_0}{J_c}\right)\left(\frac{J}{J_c}\right)^{a-1} \qquad \text{(II.3.2-2a)}$$

or

$$\ln\left[\frac{E}{J}\right] = \ln\left[\frac{E_0}{J_c}\right] + (n\text{-}1)\ln\left[\frac{J}{J_c}\right] \qquad \text{(II.3.2-2b)}$$

As already emphasized, this behavior is very different from that of a normal conductor. For a normal conductor (i.e., one that is described by Ohm's law), the ratio E/J depends on temperature but is independent of J. The ratio is called the resistivity and is denoted by ρ, as already shown in Section II.3.1.□

At 77 K, the resistivity of silver is 2.9×10^{-9} Ω–m, while silver's resistivity declines to 5.0×10^{-12} Ω–m at 4.2 K. Some authors define a superconductor's critical current density to be the value of J for which the observed resistivity is 10^{-13} Ω–m. This resistivity is one-fiftieth (0.02) of silver's resistivity at 4.2 K and less than one ten-thousandth (0.0001) of silver's resistivity at 77 K.

When n is large, the value of the critical current density becomes insensitive to which definition (electric field or resistivity) is used. The ratio of the two different definitions of critical current density for the same material is shown below:

$$\frac{J_{c-electric}}{J_{c-resistivity}} = \left(\frac{E}{\rho_0 J_{c-electric}}\right)^{\frac{1}{n-1}} \qquad \text{(II.3.2-3)}$$

For example, when n equals 15 and $J_{c\text{-electric}}$ equals 10^4 A/cm^2, the ratio of the two different definitions of the critical current density is 1.17, which illustrates the insensitivity.

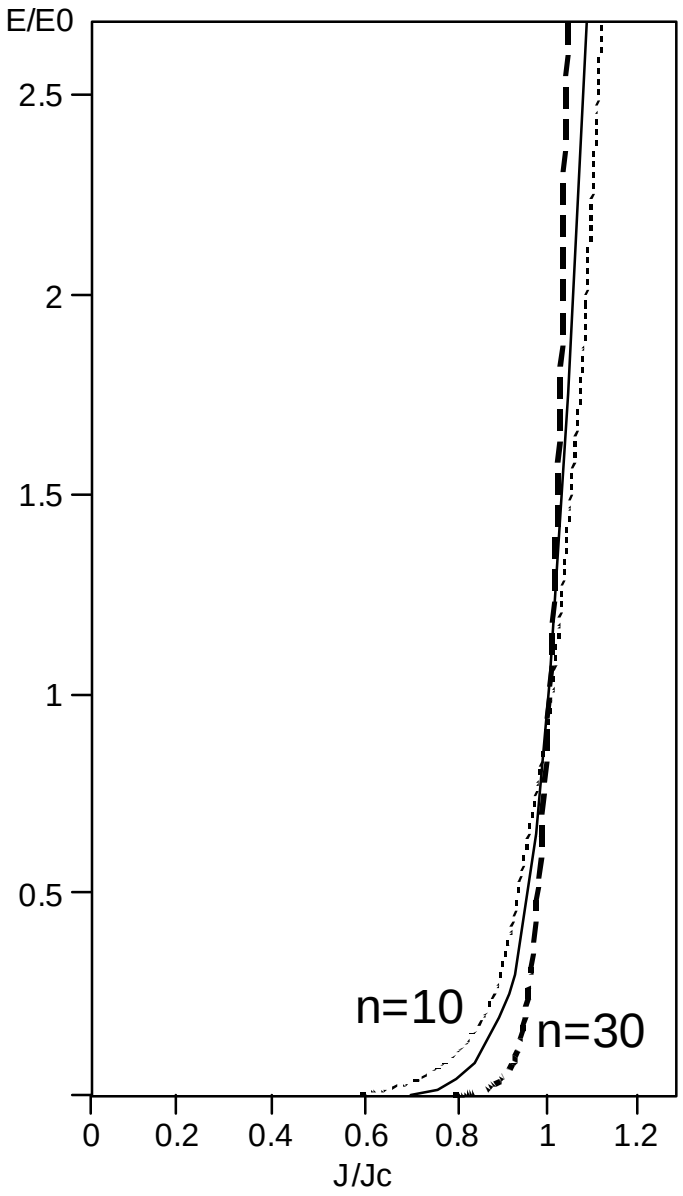

Figure II.3.1b. This figure shows the relation between current density, J, and applied electric field, E, when they are related by the equation $(E/E_o) = (J/J_c)^n$, where n = 10, 15, and 30. The n-value of today's ceramic superconductors is in the range 10-15. A typical n-value for NbTi is 30, although much higher values have been obtained. Note that a negligible electric field causes the current density to be close to the critical current density, J_c, and that much larger fields cannot increase the current density much above J_c.

II.3.3 Power Loss

In general, the average rate of electrical energy loss within the volume V is given by the following:

$$P = T^{-1} \int_0^T dt \int_V J' \, E dV \qquad \text{(II.3.3-1)}$$

This is also the rate at which heat is generated in the same volume. In many applications, the volume has a constant cross-section and variable length, and so one speaks of watts per meter. When the cross-section is scaled to the current density, one speaks of watts per kiloampere meter. Recalling that one watt equals one joule per second and that there are 50 or 60 cycles in a second, one can also speak of joules per cycle per kiloampere-meter.

Equations II.1 and II.3.3.1 yield a quantitative prediction for the electric power dissipated within the superconductor:

$$\text{electric power loss per volume} = EJ = E_0 J_c \left(\frac{J}{J_c} \right)^{n+1} \qquad \text{(II.3.3-2)}$$

For niobium-based superconductors (LTS), a typical n-value is 30, although much higher values have been attained. For such values, the power loss is much less than $E_o J_c$ when J is even slightly less than J_c, and it is much greater when J is even slightly greater than J_c. In small magnetic fields, the value of n is in the range 10-15 for the best ceramic superconductors. For these superconductors, n declines as the magnetic field increases.□

Equation II.6 describes the rate at which heat is generated in the superconductor. Since the superconductor operates below ambient temperatures, this heat must be transferred from the superconductor and rejected to the environment, which is at approximately 298K or 25°C. Refrigeration requires shaft power, which occasions additional loss to the power system. As in Section II.1, we express the total power loss as the product of the heat generated, the Carnot Coefficient of Performance (COP) of the ideal refrigerator, and the ratio of real COP to Carnot COP:

$$\text{total power loss per volume} = \left\{ E_0 J_c \left(\frac{J}{J_c} \right)^{n+1} \left(\frac{T_{ambient} - T_{cold}}{T_{cold}} \right) \right\} \times \left\{ \frac{COP_{carnot}}{COP_{real}} \right\} \qquad \text{(II.3.3-3)}\square$$

In addition to the power loss per volume, it is also informative to normalize the power loss by the volume of conductor needed to carry one ampere for one meter; this volume is called an ampere-meter. For the sake of definiteness, we choose the current density as the critical current density of the HTS. This quantity, power loss per ampere-meter of HTS, facilitates comparison between different conductors:

$$\text{electric power loss per ampere-meter} = \frac{EJ}{J_c} = E_0 \left(\frac{J}{J_c} \right)^{n=1} \qquad \text{(II.3.3-4)}$$

$$\text{total power loss per ampere-meter} = \left\{ E_0 \left(\frac{J}{J_c} \right)^{n+1} \left(\frac{T_{ambient} - Tcold}{T_{cold}} \right) \right\} \times \left\{ \frac{COP_{carnot}}{COP_{real}} \right\} \qquad \text{(II.3.3-5)}\square$$

These formulas provide the foundation for loss estimates within the superconductor. When direct current flows, their application is straightforward. When alternating current flows through the superconductor, their application requires sophisticated analysis because the electric field is related to the time variation of the magnetic field and to its strength. Also, when alternating current flows, there is an additional loss mechanism–eddy currents, in nearby normal conductors.

II.3.4 Anisotropy

High-amperage ceramic superconductor is anisotropic for two reasons: (1) the crystals of the superconductor are anisotropic and (2) the tape is made to preserve this anisotropy instead of randomly orienting different crystals, which would make the macroscopic sample isotropic. In practice, Bi-2223 and YBaCuO are made in the form of tapes with large aspect ratios. The manufacturing goal is to put the a and b axes of the crystals in the plane of the tape and have the crystals' c-axis perpendicular to that plane. A further manufacturing goal is to align the a-axis and b-axis of each crystal with all others. The critical current density is largest in the a-b plane of each crystal. This is the plane in which the current is intended to flow when the tape is fabricated. Another, different dependence affects applications. The critical current in the a-b plane is reduced by the presence of an external magnetic field. The amount of reduction depends very much on the orientation of the field with respect to the crystal. Fields parallel to the a-b plane have least effect; fields parallel to the c-axis (perpendicular to the a-b plane) have the most detrimental effect. This effect is shown in Figure II.3.4. Anisotropy is most pronounced in Bi-2223. In all materials, the anisotropy declines as the temperature declines.

II.3.5 Two Different Critical Current Densities

As emphasized in Section II.3.1, the description given here of the relation between current density and electric field is a phenomenological, two-parameter fit. The two parameters are the critical current density, J_c, and the n-value, n. Each depends (more or less) on direction, local temperature, and local magnetic field. Transport current data are usually gathered by measuring the total voltage drop through a measured distance and the total current in the conductor. One then estimates the cross-sectional area of the superconductor and divides by the same to obtain a quantity having dimensions of current density. Similarly, one divides voltage drop by distance to get a quantity having dimensions of electric field. This approach does not call attention to the possibility of more complex electrical behavior. However, the use of magneto-optical techniques (which has resolved the difference in magnetic field at nearby locations) by a group at Argonne National Laboratory has shown a variation in magnetic field that is not projected by the Bean model. The Argonne group interpret their data as showing the simultaneous presence of two different critical current densities.[37] The group points out that this is plausible because the tubes of magnetic flux can arrange themselves either with crystal-like

[37]V.K. Vlasko-Vlasov et al., "Peak effect in Bi and Tl cuprates- a disorder driven phase transition in the FLL," Workshop on Vortex Physics in High-Temperature Superconductors (Hachimantai, Japan, June 21-26, 1998).
V.K. Vlasko-Vlasov, G.W. Crabtree, U. Welp, and V.I. Nikitenko, "Magneto-Optical Studies of Magnetization Processes in High-Tc Superconductors," R. Kossowsky et al. (eds.), *Physics and Materials Science of Vortex States, Flux Pinning and Dynamics* (Kluwer Academic Publishers, Dordrecht, Boston, London, 1999), pp.205-237.

regularity or in a tangled, glass-like array.[38] Each such arrangement will have its own critical current. The state of the flux tubes at any location and time is expected to depend on history (e.g., kinetics), as well as on temperature and average local field. Thus, two different locations within the superconductor can each have their own relation between current density and electric field (current and voltage). The Argonne group varied the applied field very slowly (quasistatic conditions), which could not reveal current-voltage characteristics. The group obtained successive images at different fields. This work is significant to those interested in AC losses because the existence of different critical currents in different phases of the flux tubes suggests different hysteresis in different parts of the conductor or different hysteresis at different times, and thus different dissipation of electrical energy and generation of heat. Related work is described in Section II.7.

[38]A. Koshelov and V. Vinakour, *Phys.Rev B*, **57**:8026-8033 (1998).

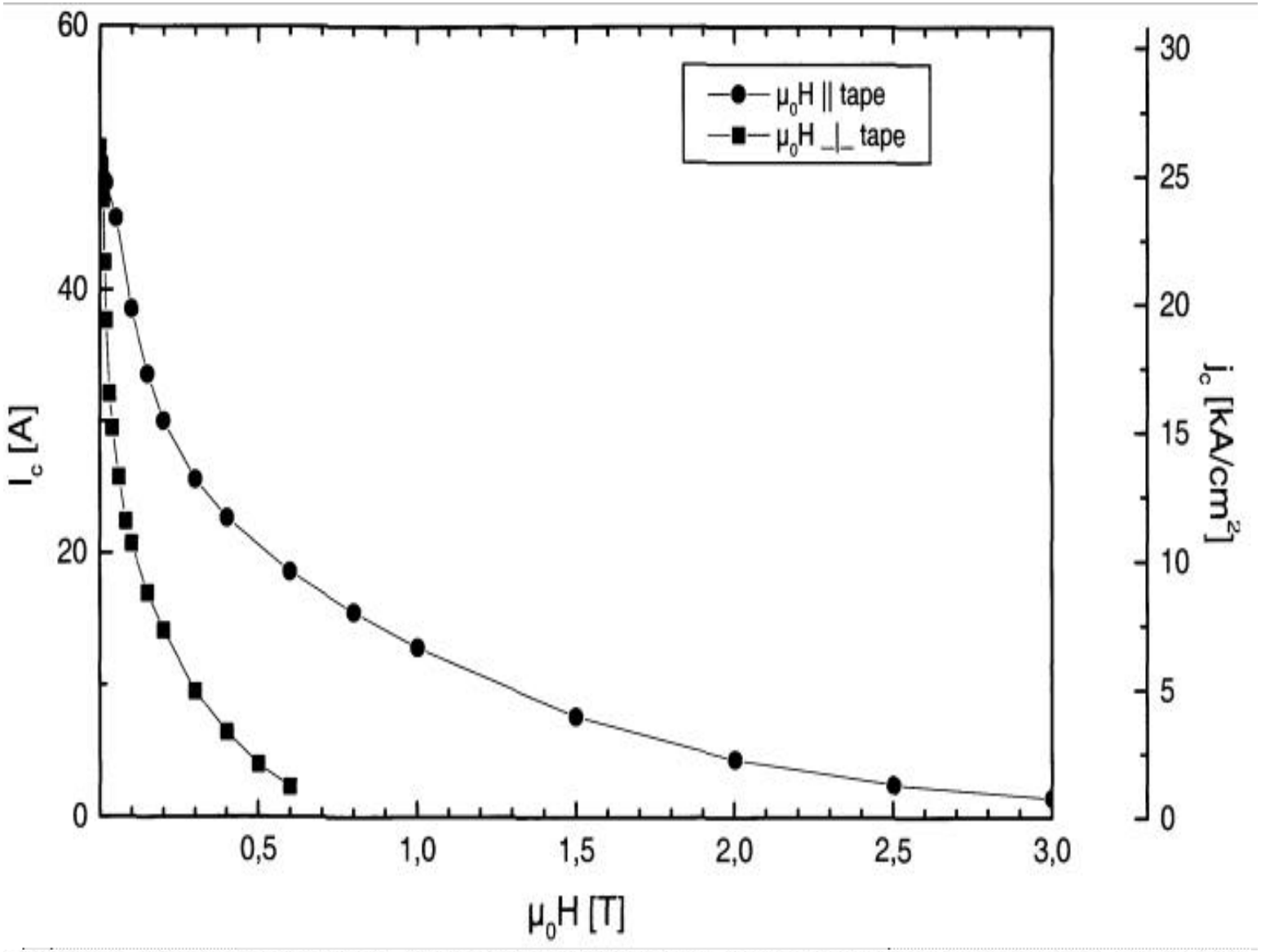

Figure II.3.4. Dependence of the critical current on the magnetic field at 77 K. Source: Presentation at Vacuumschmelze, April 23, 1999.

II.4 Elementary Theory of AC Loss

There are three basic types of losses to be considered: *hysteresis losses*, in which dissipated electrical power is linearly proportional to the frequency; *eddy current losses*, which are proportional to the square of the frequency; and any *resistive losses* attributed to flux creep, which are independent of frequency and appear at high currents. If no transport currents are flowing, hysteresis losses per cycle in HTS are proportional to the area of the hysteresis loop and in the critical state model are not frequency-dependent. Eddy current losses, which are generated in the normal metal portion of a composite superconductor, are well understood.

Hysteresis losses, in the context of the critical state model are treated in detail in Appendix 1, and eddy current losses are treated in Section VI. The frequency dependence of these different AC losses has been measured over a large frequency range by Stavrev and Dutoit.[39]

II.4.1 Hysteresis Loss

Hysteresis losses are the result of magnetic flux moving in and out of a superconductor. When this occurs, an electric field is generated that does work on any flowing currents. These could be either shielding currents due to a time-varying external field or a transport current. They are called hysteresis losses because the flux that entered the superconductor does not leave in precisely the same manner by which it entered. If one plots the magnetic induction, *B*, versus the magnetic intensity, *H*, an hysteresis loop, which is traversed once per cycle, is obtained. The electrical energy loss per cycle is proportional to the area of this loop, provided that no transport currents are flowing. Such hysteresis losses are dissipated as heat.

In a superconductor, current flows in a surface layer, which in the critical state model (discussed in Section II.4.1.1 and Appendix 1) has the current density equal to the critical current density. If the conductor is carrying an AC current, the current distribution at peak AC current is the same as it would be for the same value of DC current. The thickness of this current-carrying sheath varies during an AC cycle (this is true for both transport and shielding currents). When the transport current or external field producing the shielding currents is large enough, the current sheath reaches the center of the superconductor for most of the cycle. This is called "full penetration." Losses differ below and above full penetration, and for applied fields perpendicular to the current, the loss density above full penetration is proportional to the thickness of the superconductor.

For the case of the magnetic field perpendicular to a tape, the loss density is always proportional to the thickness of the tape and is proportional to the width of the tape at field values in excess of that needed for full penetration. As pointed out by Dresner,[40] and earlier by Rhyner, however, a power law superconductor like Ag/BSCCO does not have a sharp superconducting-to-normal transition, and this can affect the magnitude of hysteresis losses as well as their frequency dependence. The thickness of the current-carrying sheath for AC

[39]S. Stavrev and B. Dutoit, *Physica C* **310**:86 (1998).

[40]L. Dresner, *Physica C* **310**:213 (1998).

currents in a power law superconductor is governed by the nonlinear diffusion equation; the relation of this equation to the critical state model is discussed in Section II.4.1.2 and in Appendix 2.

As noted in Section II.3.4, HTS tapes have the *c*-axis of the superconducting crystals aligned perpendicular to the tape. In such tapes, losses are not isotropic.[41] There is a large difference in the losses for a time-varying magnetic field perpendicular or parallel to the tape. The calculated effects of this anisotropy can be seen in Figure II.4.1.1.

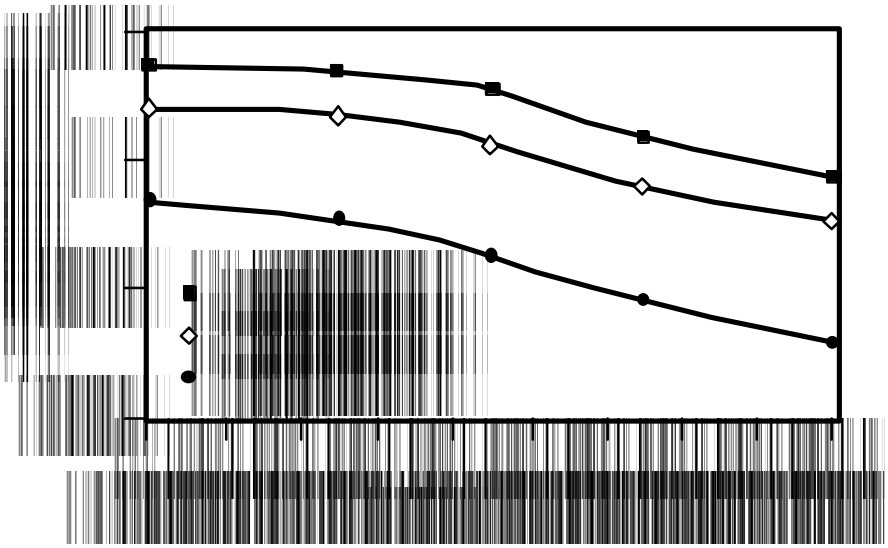

Figure II.4.1.1. Calculated angular dependence of AC loss due to an external magnetic field. Source: J. Rhyner, *Physica C* **310**:42 (1998).

Measured losses as a function of angle and field strength can be modeled by the simple expression

$$\begin{aligned} Q_u &= Q_\perp B_a \sin\alpha + Q_\parallel B_a \cos\alpha \\ Q_l &= Q_\perp B_a \sin\alpha , \end{aligned} \qquad \text{(II. .14)}$$

where α is the angle between the direction of the applied magnetic field B_a and the surface of the tape, $Q_\perp$ and $Q_\parallel$ are the losses with the field perpendicular and parallel to the tape, and Q_u and Q_l are the upper and lower loss limits. The closeness of the fit can be seen in Figure II.4.1.2.

[41] M. Ciszek et al., *IEEE Trans. on Appl. Supercond.* **9**:817 (1999).

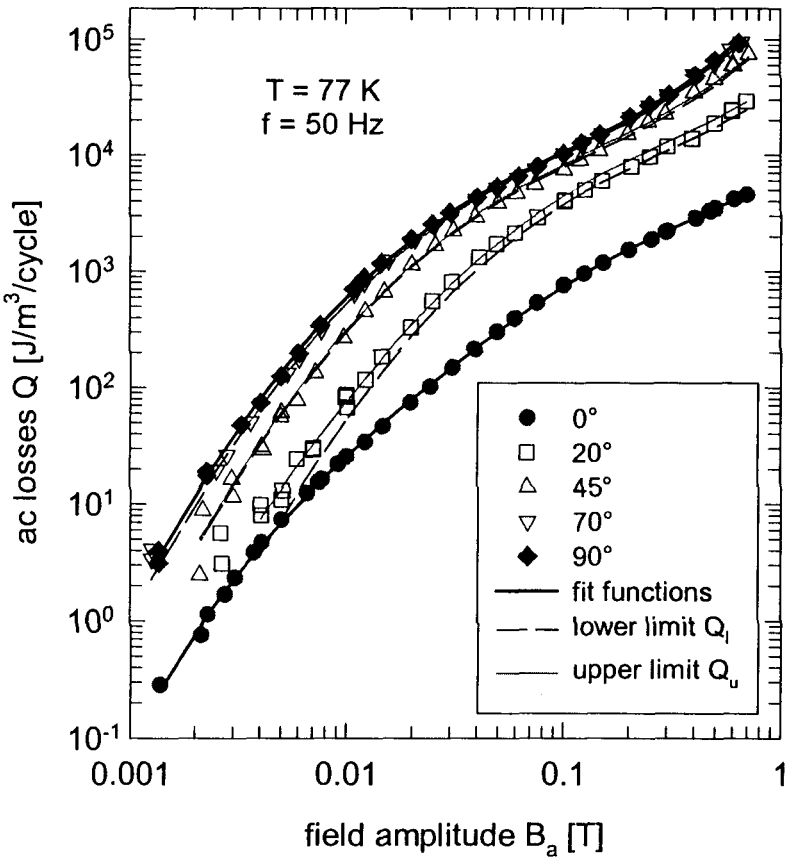

Figure II.4.1.2. Angular dependence of AC losses. Source: M. Oomen et al., *APL* **70**:3038 (1997); presented by M. Leghissa at the Workshop on AC Losses, April 8-9, 1999, Palo Alto, Calif.

The anisotropic losses of HTS tapes become especially important when winding coils for practical devices.[42] The problem occurs at the ends of a coil where the perpendicular field (along the *c*-axis of the BSCCO crystals) can be almost half of the maximum parallel component. One can use iron or other high permeability materials to minimize such end effect losses, but these materials are useful only in the range of field strengths where they do not saturate. The feasibility and desirability of putting the iron in the cryostat must also be considered.

In addition to AC losses, the critical current of a multifilamentary tape also depends on whether the applied magnetic field is parallel or perpendicular to the tape. This can be seen in Figure II.3.4.

[42]T. Honjo et al., *IEEE Trans. on Appl. Supercond.* **9**:829 (1999).

II.4.1.1 Critical State Model

In the critical state model,[43] developed for LTS, it is assumed that the critical current density J_c flows in any current-carrying portion of a superconductor. The magnetization curve for any type-II superconductor has two critical fields, H_{c1} and H_{c2} . The first critical field corresponds to the field strength where flux enters the superconductor, forming what is known as the "mixed state" (where the magnetic field forms a fluxon lattice composed of an array of normal cores containing flux, each of which has encircling supercurrent vortices); and the second corresponds to the maximum field for which the mixed state can persist. Below H_{c1}, the superconductor is a perfect diamagnet with a surface current flowing to the penetration depth so as to shield the interior. Above H_{c1}, a bulk current density flows in addition to the surface current. In the critical state model, this bulk current density is set equal to the critical current density and determines the depth of penetration by the field. For Bi-2223 compounds at 77 K, the flux line lattice has already "melted" so that H_{c1} is essentially zero for these compounds. The critical state model is discussed in greater detail in Appendix 1.

II.4.1.2 Nonlinear Conductor Model

The critical state model, having been developed for LTS, describes superconductors having a very steep *J-E* characteristic or, expressing the same thing in another way, a very large n-value (see Section II.3). But for HTS, n is not always large. When thermally activated flux creep and macroscopic inhomogeneities are present, the critical state model is not quantitatively reliable. Martinez et al.[44] have measured AC losses in textured polycrystalline thin rods of BSCCO-2212 and compared the results with numerical calculations.[45] Martinez et al.[46] have measured AC losses in textured polycrystalline thin rods of BSCCO-2212 and compared the results with numerical calculations.[47] For $n \sim 8$, they found that the results do not differ much from the critical state model.

An alternative to the critical state model is to model a HTS with a power law current-voltage characteristic as a nonlinear conductor (as discussed in Section II.3; also see Appendix 2 for a complete discussion). In this model, $n = 1$ corresponds to a normal ohmic conductor and $n =$ to the critical state model. The power law current -voltage characteristic interpolates between the ohmic linear case, where the skin effect is important, and the critical state case, where hysteresis effects dominate. Results show that $n \sim 8$ corresponds closely to the critical state model, justifying its use for many calculations. This can be seen in Figure A2.1 of Appendix 2. A diffusion model has also been used by Paasi and Lahtinen for numerical calculations of AC losses in HTS composite conductors.[48]

---

[43]C.P. Bean, *Phys. Rev. Lett.* **8**:250 (1962); *Rev. Mod. Phys.* **36**:31 (1964). To a large extent, the presentation in this appendix follows that of M. N. Wilson, *Superconducting Magnets* (Clarendon Press, Oxford, 1986).

[44]E. Martinez et al., *IEEE Trans. on Appl. Supercond.* **9**:805 (1999).

[45]E.H. Brandt, *Phys. Rev. B* **54**:4246 (1996); T. Yazawa et al., *Physica C*, in press.

[46]E. Martinez et al., *IEEE Trans. on Appl. Supercond.* **9:**805 (1999).

[47]E.H. Brandt, *Phys. Rev. B* **54**:4246 (1996); T. Yazawa et al., *Physica C*, in press.

[48]J. Paasi and M. Lahtinen, *IEEE Trans. on Appl. Superconductivity* **7:**322 (1997).

The applicability of the critical state model depends not only on n-value, but also on the geometry of the sample. Meerovich et al.[49] have measured the AC losses of a hollow melt-cast BSCCO 2212 cylinder carrying a current induced by an external 50 Hz magnetic field. The cylinder constituted the one turn secondary of a transformer. Above full penetration, they found that the AC losses depended on the sample shape and differed significantly from those predicted by the critical state model. The BSCCO cylinder used had an *n* value of 7, very close to the value where the nonlinear conductor model predicts the critical state model should apply.

II.4.2 Eddy Current Loss

When an external time-varying magnetic field penetrates into a normal conductor, it induces a changing electric field, which in turn causes currents to flow. These are known as eddy currents. The depth of penetration of the field is determined by the skin depth, which is defined as

$$\delta = \left(\frac{2\rho}{\mu_0 \omega} \right)^{1/2} \qquad \text{(II.4.2.1)}$$

where ρ is the resistivity, and ω the frequency. At 77 K, the resistivity of silver is 2.9×10^{-9} Ω-m, and so the skin depth is 4 mm. Recalling that a tape is roughly 3 mm and 0.15 mm thick, one sees that the textbook expression for loss may not be applicable.[50] Instead, we estimate[51] that the electrical power dissipated in the normal conductor would be roughly

$$d/dt\ Q = J \times E \times \text{volume} = (E^2 / \rho)\text{volume} = ((\text{length}\ \omega B / 2)^2 / \rho)\ \text{volume} \qquad \text{(II.4.2-2)}$$

One sees that the eddy current loss is proportional to the square of the frequency and inversely proportional to the resistivity. This is the reason that investigators have sought alloys with higher resistivity than pure silver. Supposing an individual tape, 0.15 mm thick, is subjected to an oscillating magnetic field of 0.1 T, the loss due to eddy currents within the pure silver matrix

---

[49]V. Meerovich et al., *Physica C* **319**:238 (1999).

[50]Textbooks usually discuss skin depth and related losses for the case in which skin depth is much less than any geometrical length in the problem. This is often appropriate for microwaves and their wave-guides, but not for power frequencies of 50-60 Hz. In fact, if one uses the textbook result for the Poynting Vector, $S = (\Omega/2)d(B^2/2m_0)$, one finds that S = 0.25 W/cm^2 for bulk silver at 77 K facing a magnetic field of 0.1 T. This is so big as to be intolerable, as can be seen by thinking of a three-phase transformer as three pairs of concentric coils, each pair being 1 m high and 0.5 m in diameter. The total surface area would be 3 m^2 and so the total loss from eddy currents would be 3×2.5 kW at cryogenic temperatures, far too big for economic operation. In fact, the silver is subdivided into distinct tapes, and the interfacial resistance cannot be and is not negligible. Another way to see the importance of not allowing the silver to be an electrical monolith is to assume an engineering current density of 10^4 A/cm^2; this leads to a loss of 5 W/kA-m.

[51]Maxwell's equation curl[E] = -∂/∂t B suggests ΔE/length ≈ ω B where ΔE is the change in E over a characteristic length, such as the thickness of the tape. Assuming ΔE is smaller or comparable to the average value of 2xE, one finds E ≈ length Ω B / 2.

will be 1.9×10^{-3} W/cm^3 or 1.2×10^{-2} W/kA-m at 80 K and six times greater at 40 K because the resistivity falls by a sixth. Thus, at 40 K, the loss from the eddy current alone would be 0.08 W/kA-m, which is the goal for the total loss that a transformer designer might set. These estimates are just estimates, not precise calculations. The situation might be worse because of coupling currents that flow between superconducting filaments and because a detailed calculation would involve both 0.15 mm thickness and the 3-mm width of the tape, giving a greater effective length than 0.15 mm. However, these estimates do suggest why attention is given to reducing eddy currents below what they would be in pure silver.

As will be seen in Section VI, eddy current losses associated with coupling of the filaments can be reduced by twisting the filaments and thereby reducing the area to be integrated over in Equation II.4.2.3. These types of coupling losses are sometimes termed eddy current losses and are discussed in detail in Appendix 1, Section A1.2. Eddy current losses in regions away from the superconducting filaments depend on the conductivity of the matrix material and the frequency and magnitude of the applied field, as discussed above.

II.4.3 Relative Importance of Eddy Currents to Hysteresis

It is important to realize that, at 50 Hz, hysteresis losses are bigger than eddy current losses, as seen in Figure II.4.3.1 for negligible fields, but they grow as the field increases.

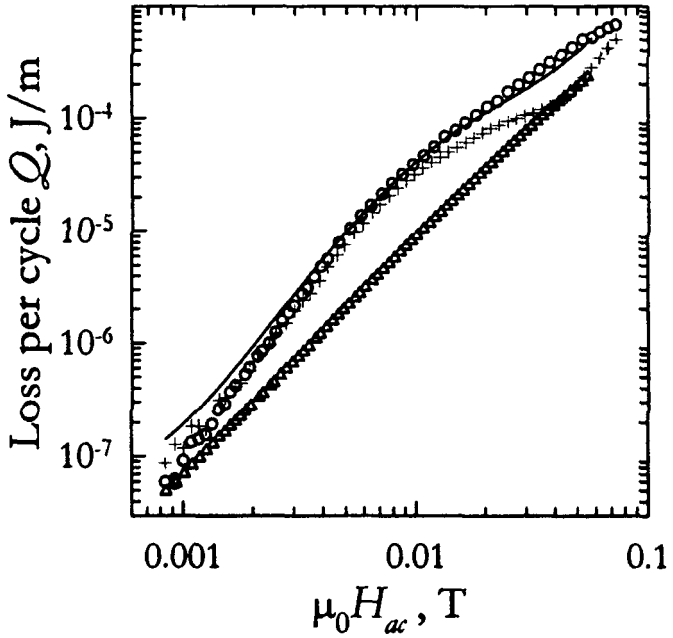

Figure II.4.3.1. Losses in twisted tape at 43 *Hz*, 77 K. The total losses are indicated by m, the hysteresis by +, and the eddy current or coupling loss by ; the solid line is the sum of the coupling and hysteresis losses. The pitch length was 10 *mm*. Source: Y. Yang et al., *Physica C* **310**:147 (1998).

Figure II.4.3.1 shows that for this twisted filament tape, the sum of the hysteresis loss and coupling loss coincides well with the measured total loss except at very low fields. Below 40

mT, where the filaments are uncoupled, the hysteresis losses significantly exceed the coupling losses, and at 0.01 T this difference is a factor of about 3.5. The eddy current and hysteresis losses per cycle become comparable at 0.04 T, where the filaments are no longer uncoupled.

II.5 BASIC EXPERIMENTAL APPROACHES TO MEASURING AC LOSSES

There are three basic techniques that are commonly used for measuring AC losses: calorimetric, thermometric, and electrical. Of these, the calorimetric and electrical methods are most often used. In general, different applications will require different techniques:

Example	Technique
Quick measurement of losses in tape	Electrical
Measurement in limited areas (e.g., thin-film YBCO)	Thermometric (thermocouples)
Cable; magnet windings	Calorimetric

The following subsections will describe each of the different techniques.

It should be noted that, based on a series of electrical AC loss measurements made on Bi-2223 tape under the aegis of the Brite EuRam Research program SACPA, C. Beduz et al.[52] believe the electrical technique has been validated and lays the basis for a measurement standard for HTS tapes and wires. Coletta et al.[53] have used three techniques to measure power frequency AC losses of a 1.5-*m* sample of four-layer multistranded cable. Two of these techniques are calorimetric (boil-off and temperature difference), while the third is electrical. The three approaches yielded similar results.

While the electrical, thermometric, and calorimetric techniques are the most often used methods of measuring AC losses, there is a new approach (which could be subsumed under the category of electrical) that does not rely on the assumption of any particular model for the magnetic field distribution within a superconductor. Instead, Ashworth and Suenaga[54] measure the energy supplied by the power supplies used to drive the magnetic field and transport current (in the case where an external field and transport current is applied to a superconducting tape or other magnetically active material).

To demonstrate the feasibility of this approach in the case of AC currents and magnetic fields, the signal-to-noise ratio was optimized by taking data only for the magnetic field normal to the tape (in this configuration, the losses are about an order of magnitude larger than when the field is parallel to the tape). At the current stage of development, it is difficult to compare this approach with the ones discussed below.

II.5.1 Calorimetric Method

---

[52]C. Beduz et al., *Physica C* **310**:67 (1998).

[53]G. Coletta et al., *IEEE Trans. on Appl. Supercond.* **9**:1053 (1999).

[54]S.P. Ashworth and M. Suenaga, *Physica C* **313**:175 (1999); *IEEE Trans. on Appl. Supercon.* **9**:1061 (1999).

The calorimetric approach to measuring AC losses usually relies on measuring the boil-off of the cooling medium. A clear presentation of this, given by Wilson,[55] is shown in Figure II.5.1.1.

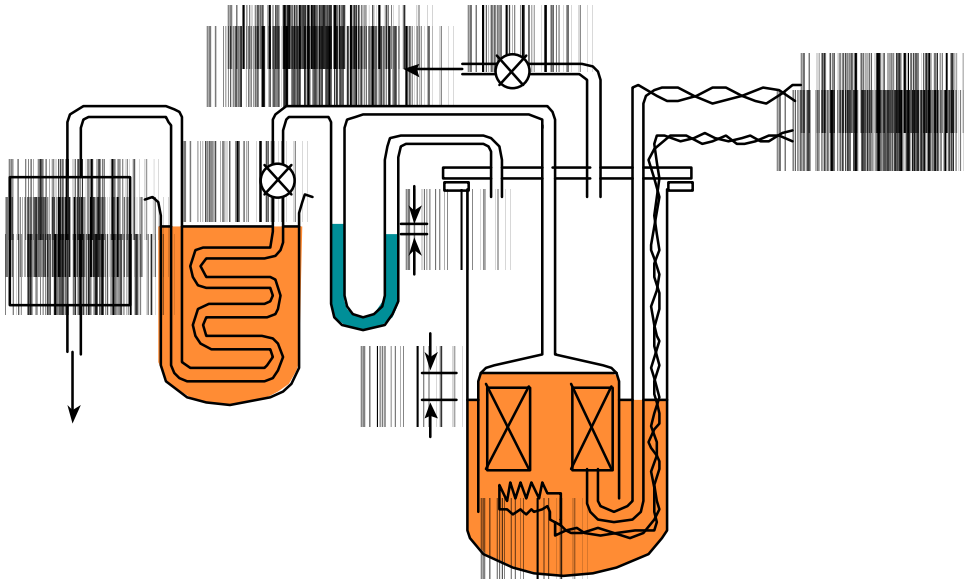

Figure II.5.1.1. Calorimetric measurement of AC loss by measuring the rate of evolved coolant. Adapted from: M. N. Wilson, *Superconducting Magnets* (Clarendon Press, Oxford, 1986), Ch. 10.

In the figure, the gas flow through the valve V1 measures boil-off due to cryostat heat leaks, current leads, etc., and the flow through V2 measures the boil-off due to losses; pressure in and outside the bell jar are kept equal by minimizing the level difference *h* by adjusting the valves V1 and V2 (the relation between the levels *h* and *H* depends on the specific gravity of the fluid used for cooling — helium in this case — and the fluid used in the manometer). The purpose of the bath after the valve V2 is to bring the boil-off gas to room temperature. Measurement of the volume of gas boiled off by AC-loss heat and knowledge of the latent heat of vaporization of the coolant gives the power loss. This method, which only gives the total loss, is associated with a large thermal time constant, so it takes a significant amount of time for the system to come to thermal equilibrium.

In the case of HTS tapes, a rather elegant calorimetric technique has recently been developed for measuring losses due to both time-varying transport currents and external magnetic fields.[56] The time for the tape to reach thermal equilibrium is about 5 to 10 seconds, and the sensitivity is 0.01 *W/m*.

---

[55]M.N. Wilson, *Superconducting Magnets* (Clarendon Press, Oxford, 1986).

[56]S.P. Ashworth and M. Suenaga, *Physica C* **315**:79 (1999).

The technique can measure losses of any combination of external AC field and current, which may have any relative phase. While the approach will not provide the sensitivity or range of electrical measurements, it can be of use in the high-current region relevant for HTS tape applications in electrical machinery. The capability of measuring losses in external fields that are out of phase with the transport current is important, for example, in transformer applications.

The basic calorimeter is shown in Figure II.5.1.2.

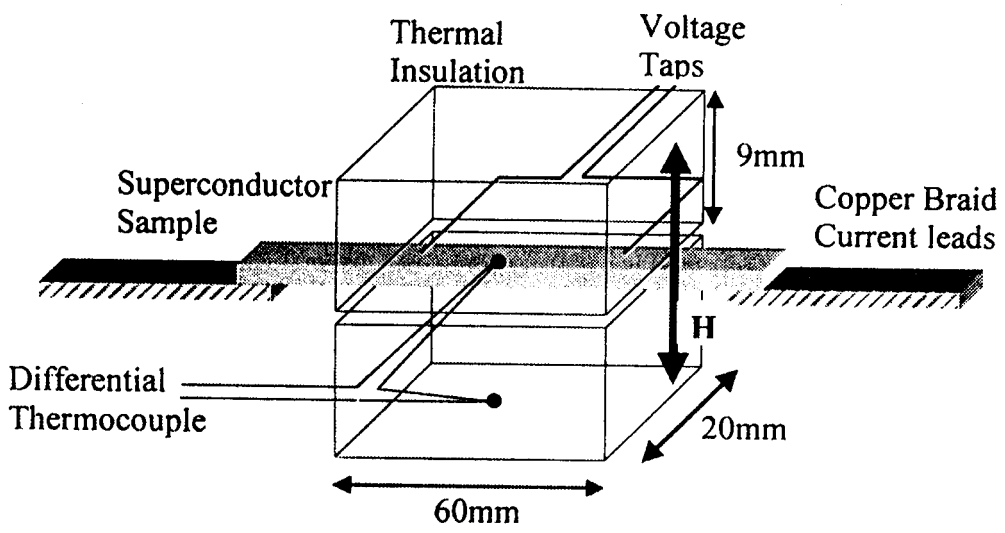

Figure II.5.1.2. A simple calorimeter for measuring AC losses in HTS tape carrying a transport current in an external magnetic field. Both the transport current and external field are time-varying and may have any relative phase. [From S. P. Ashworth and M. Suenaga, *Physica C* **315**:79 (1999).]

The calorimeter shown above uses styrofoam for thermal insulation and a silicone rubber sealant for the gap between the styrofoam blocks. The calorimiter is immersed in liquid nitrogen. Cooling of the test section of HTS tape is by thermal conduction along the tape to the region outside the insulation.

The effect on AC losses of a variation between the phase of the external magnetic field and the transport current is shown below.

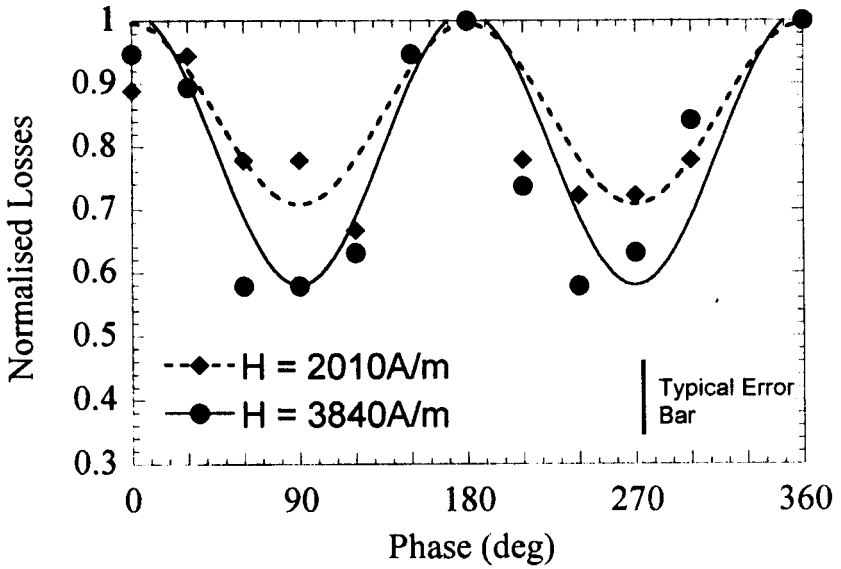

Figure II.5.1.3. AC losses as a function of phase angle. The 100 *Hz* external magnetic field is perpendicular to the tape, and the transport current has a peak value equal to the critical current. The data have been normalized to unity at a phase angle of 180°. [Source: S. P. Ashworth and M. Suenaga, *Physica C* **315**:79 (1999).

Calorimetric methods have also been used by Hardono et al.[57] on short (6-*cm*) samples of 37-multifilamentary tape to measure AC losses to an accuracy of milliwatts per centimeter. Measurements were taken for both parallel and perpendicular applied magnetic fields.

A temperature-difference calorimeter, with a sensitivity of less than 1 *mW/m*, has been developed by Daney et al.[58] at Los Alamos for measuring AC losses in one-meter-long samples of multistrand cables. The calorimeter can also measure three-phase losses by virtue of having two additional copper conductors parallel to the cable sample and arranged in an adjustable equilateral triangle. These can be used to closely approximate the magnetic field that would be produced by the presence of the two additional phases. The temperature profile along the sample is measured at six axial positions and fitted to a parabolic temperature profile. Such a profile is the solution to the steady state heat conduction equation for a rod or cable with axially uniform heat generation. The technique has been used to measure losses in cables manufactured by Pirelli and Southwire.

The Los Alamos temperature-difference calorimeter has been used to measure the AC losses in a four-layer prototype multistrand conductor intended for use in the DOE-Pirelli-Detroit Edison superconducting power transmission line demonstration project.[59] The single-phase losses for the PMC 4LA cable are shown in Figure II.5.1.4. This cable had a critical current of

---

[57]T. Hardono et al., *IEEE Trans. on Appl. Supercond.* **9**:813 (1999).

[58]D.E. Daney et al., *Cryogenics* **39**:225 (1999); *Advances in Cryogenic Engineering* (*Materials*) **44**:791 (1998); *Physica C* **310**:236 (1998).

[59]D.E. Daney et al., Paper IBB-2 of the *Cryogenic Engineering Conference/International Cryogenic Materials Conference*, Montréal, Québec, Canada, July 13-16, 1999. To appear in *Advances in Cryogenic Engineering*.

about 6000 A at 77.3 K with the 1-μV/cm criterion. Note that the *n*-value in the figure should not be confused with the exponent of the current-voltage relation of the superconducting tape or cable, but rather corresponds to the exponent of a power law fit to the data.

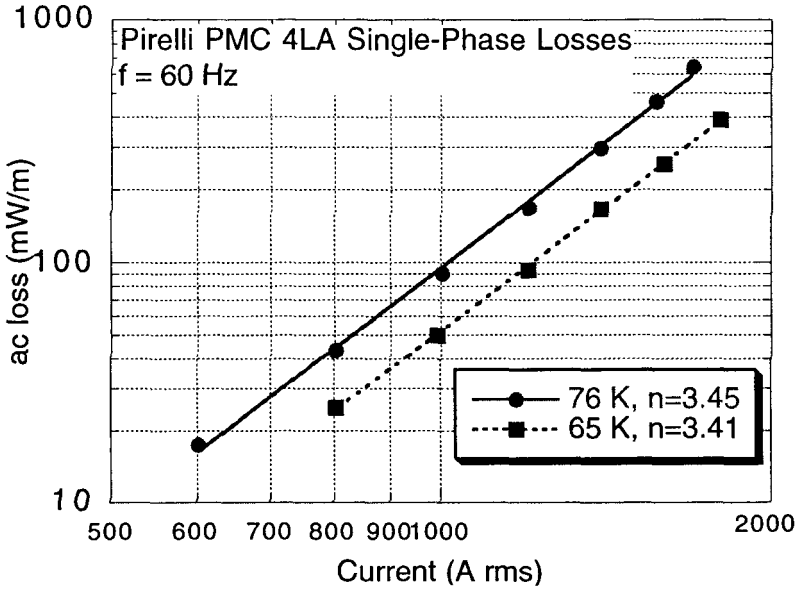

Figure II.5.1.4. Single-phase AC losses at 60 Hz for the Pirelli PMC 4LA cable at 76 K and 65 K. *n* is the exponent of a power law fit to the data.

These results have also been compared with a two-layer cable,[60] designated PMC 3, constructed at American Superconductor Corporation. This cable had a critical current of 2800 A at 75.3 K with the 1 *mV/cm* criterion. As can be seen in Figure II.5.1.5, the losses were measured up to 1200 A for PMC 3 and 1700 A for PMC 4LA. Because losses increase as the transport current approaches the critical current, a linear extrapolation of the PMC 3 losses may underestimate their true value. For reasons that are not clear, single-phase losses show a much larger variation in *n* values than do either the two- or three-phase losses.

[60]J.O. Willis et al., *Single and Multiphase Losses in HTS Prototype Conductors*, Proceedings of the Applied Superconductivity Conference, Palm Springs, Calif., Sept. 14-19, 1998.

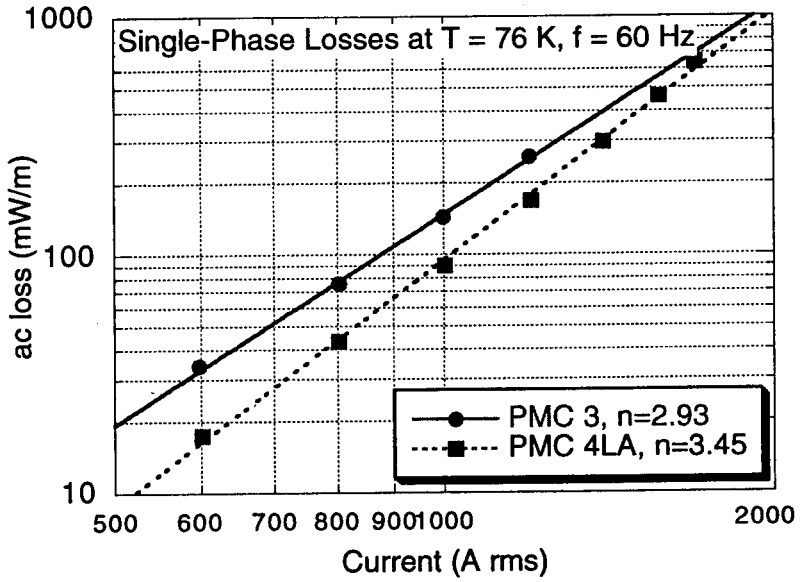

Figure II.5.1.5. Comparison of single-phase AC losses at 60 Hz for the two-layer cable PMC 3 and the four-layer cable PMC 4LA. *n* is the exponent of a power law fit to the data.

The two-phase AC losses for PMC 4LA are shown in Figure II.5.1.6.[61]

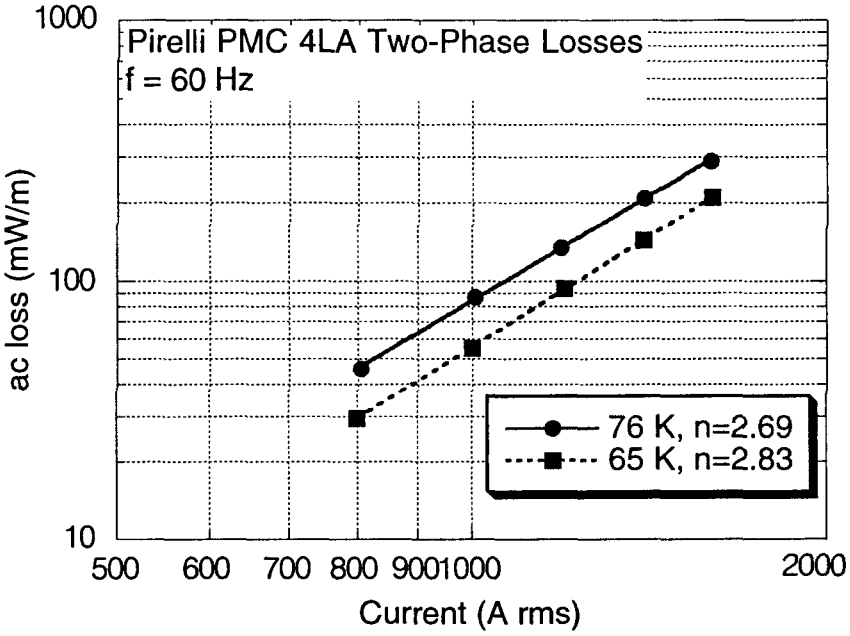

Figure II.5.1.6. Two-phase AC losses for PMC 4LA as a function of 60-Hz current flowing in the two normal conductors of the temperature-difference calorimeter. *n* is the exponent of a power law fit to the data.

[61]J.O. Willis et al., Paper IBB-3 of the *Cryogenic Engineering Conference/International Cryogenic Materials Conference*, Montréal, Québec, Canada, July 13-16, 1999. To appear in *Advances in Cryogenic Engineering*.

Note that there is no current flowing in the superconducting cable itself; the losses are shown as a function of current in the two normal copper conductors of the calorimeter.

A null calorimetric technique, where the heat generated by a superconductor and a reference conductor of the same size and shape are compared, has been developed by Dolez et al.[62] The superconductor and reference conductor are alternately powered by approximately 5-sec AC and DC pulses, respectively. The DC current in the reference is adjusted to minimize temperature oscillations at the pulse frequency. An increase in sensitivity can be obtained by using the amplitude of the Fourier transform corresponding to the pulse frequency, rather than the thermocouple signal itself.

The null calorimetric method, when compared with the electrical method, gave comparable results except at lower transport currents, where longer measurement times would be needed to reduce noise by averaging over more numerous data. The null calorimetric technique, like other calorimetric approaches, may have an advantage in complex electromagnetic and geometrical environments where it may be difficult to implement other methods.

II.5.2 Thermometric Method

The thermometric technique of measuring AC losses, which can be subsumed under the calorimetric rubric, is useful for measuring losses in conductors where the coupling loss is dominant. It is generally not used to measure transport current losses.

A sample is either subjected to a pulsed magnetic field and the temperature rise measured directly, or it is connected via a thermal resistance to the coolant bath and subjected to a continuously varying magnetic field. In both cases, thermocouples are used to measure temperature differences.

In the pulsed case, one has

$$Q_{TOT} = \int_{T_{INIT}}^{T_{FIN}} C(T)dT = H(T_{FIN} - T_{INIT}) \quad , \qquad \text{(II.5.2.1)}$$

where *H* is the enthalpy; whereas in the case where a thermal resistance is used,

$$P_{TOT} = \frac{(T_{SAMPLE} - T_{BATH})}{R_{TH}} . \qquad \text{(II.5.2.2)}$$

II.5.3 Electrical Method

The electrical method of measuring AC losses is by far the most sensitive, but it involves considerable complexity compared with the calorimetric or thermometric techniques.[63] There are several electrical measurements that are important for determining hysteresis loss, transport loss, and coupling loss. The relevant voltage measurements are defined for a tape with twisted superconducting filaments in Figure II.5.3.1 below–the figure is conceptual, the actual placement of coils and taps may vary so as to minimize measurement errors.

---

[62]P. Dolez et al., *Supercond. Sci. Technol*. **9**:374 (1996); *Cryogenics* **38**:429 (1998); *Supercond. Sci. Technol.* **11**:1386 (1998).

[63]O. Magnusson, S. Hornfeldt, J.J. Rabbers, B. ten Haken, and H.H.J. ten Kate, "Comparison between calorimetric and electromagnetic total ac loss measurement results on a BSCCO/Ag tape," *Supercond. Sci. Technolo*. **13**:1-4 (2000).

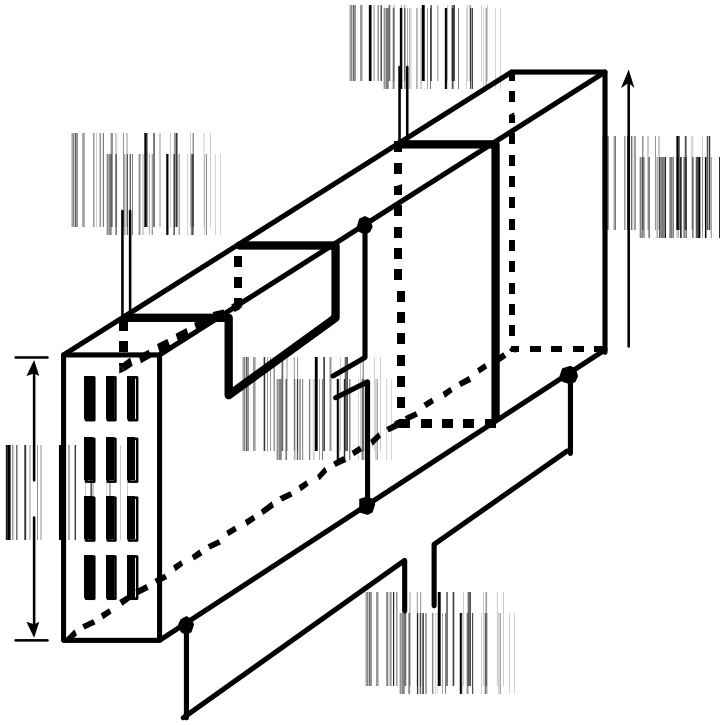

Figure II.5.3.1. Conceptual pickup coils and taps for measuring various losses of a superconducting tape. [Adapted from Y. Yang et al., *Physica C* **310**:147 (1998).]

The component of the voltage V_s picked up by the saddle coil, which is in phase with the applied field, measures the hysteresis loss. The applied field H_{ac} is along the *a*,*b*-axes of the HTS in the tape. It is shown in Appendix 3 that the hysteresis losses are proportional to the area of the hysteresis loop, A_H, which in turn is proportional to the imaginary part μ'' of the complex permeability. From the discussion given there, the loss per unit volume per cycle is

$$W_V = \frac{A_H}{\mu_0} = \frac{\pi b_0^2}{\mu_0}\mu'', \qquad \text{(II.5.3.1)}$$

where the area of the hysteresis loop is

$$A_H = \mu''\pi b_0^2 \qquad \text{(II.5.3.2)}$$

and b_0 is the magnitude of the time-dependent component of the external field.

There are some subtleties that should be discussed at this point. Because the hysteresis loop represents a nonlinear response of the superconductor to the external field, the voltage picked up by V_S will contain not only the fundamental frequency, but also higher harmonics. Bean[64] has shown that the voltage of all the harmonics, including the fundamental, may be written in terms of the voltage of the third harmonic. But this is true only for the superconductor.

[64]C.P. Bean, *Rev. Mod. Phys.* **36**:31 (1964).

In fact, V_3 - V_1 will be a function of the applied field if there are coupling losses. The total loss due to the sum of coupling losses and hysteresis losses is then proportional to the first harmonic and the hysteresis losses to the third harmonic.[65]

It is shown in Appendix 1, Section A1.2, that coupling currents in a twisted composite tape produce an electric field that appears along paths parallel to the external time-varying magnetic field. The electric field in turn produces the voltage labeled V_T in Figure II.5.3.1 above, given by

$$V_T = \dot{B}_i \left(\frac{L}{2\pi} \right) w \quad , \qquad \text{(II.5.3.3)}$$

where B_i is the field inside the tape and L is the pitch length of the twisted filaments. The power dissipated *per unit volume* is then

$$P = \dot{B}_i^2 \left(\frac{L}{2\pi} \right)^2 \frac{1}{\rho_{et}} \quad , \qquad \text{(II.5.3.4)}$$

where r_{et} is the effective transverse resistivity, discussed in Section VI.2.3.1.

When current flows along the twisted superconducting filaments, it creates a magnetic field directed along the tape, as shown in Figure II.5.3.2.

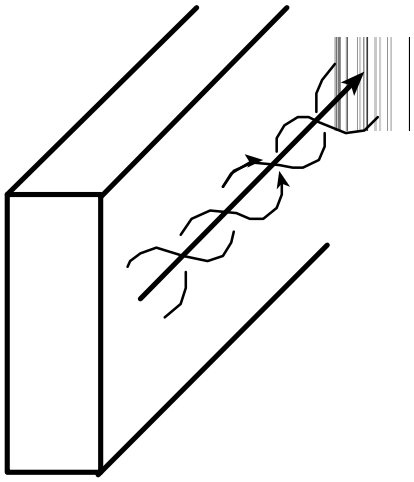

Figure II.5.3.2. Current flowing along twisted filaments creates a magnetic field.

This magnetic field will change in time if the tape is carrying an AC current, and this in turn will induce the voltage labeled V_H in Figure II.5.3.1. The point of detecting this field is that above a certain value, current flows through the matrix longitudinally, rather than along the helical superconducting filaments. This can be seen in Figure II.5.3.3.

---

[65] Y. Yang et al., *Physica C* **310**:147 (1998).

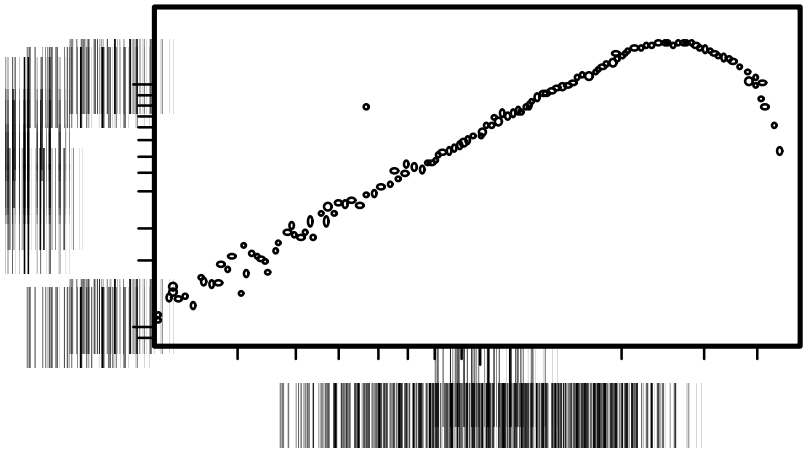

Figure II.5.3.3. Above a critical value (here about 25 A corresponding to the peak of the curve), current flows through the matrix rather than along the superconducting filaments. [Source: Y. Yang et al., *Physica C* **310**:147 (1998).]

Conceptually, measurement of transport loss is straightforward. One simply measures the in-phase (with respect to the current source) voltage drop along the tape, labeled V_L in Figure II.5.3.1, and computes the time-averaged power dissipation $P = \langle I(t)V_L(t) \rangle$. In practice, this is somewhat difficult because the changing magnetic fields due to the transport current may couple to the leads and induce, due to hysteresis, an in-phase error voltage.[66] The large out-of-phase voltage induced in the voltage-measuring circuit by the field due to the transport current is often compensated for by variable mutual inductances (Rogowski coils) between the voltage-measuring and transport current circuits. Approaches to minimizing the induced voltage due to the coupling of changing external magnetic fields in transport current loss measurements are discussed in Appendix 4. A good example of transport current losses for different magnetic fields is shown in Figure II.5.3.4.

[66]M. Ciszek et al., *Physica C* **233**:203 (1994); J.R. Clem et al., "Voltage-Probe-Position Dependence and Magnetic-Flux Contribution to the Measured Voltage in ac Transport Measurements: Which Measuring Circuit Determines the Real Losses?" in *Recent Developments in High Temperature Superconductivity*, Proceedings of the 1st Polish-U.S. Conference held in Wroctaw and Duszniki Zdrój, Poland, Sept. 11-15, 1995, edited by J. Klamut et al. (Springer-Verlag, Berlin, 1996), *Lecture Notes in Physics* No. 475, pp. 253-264.

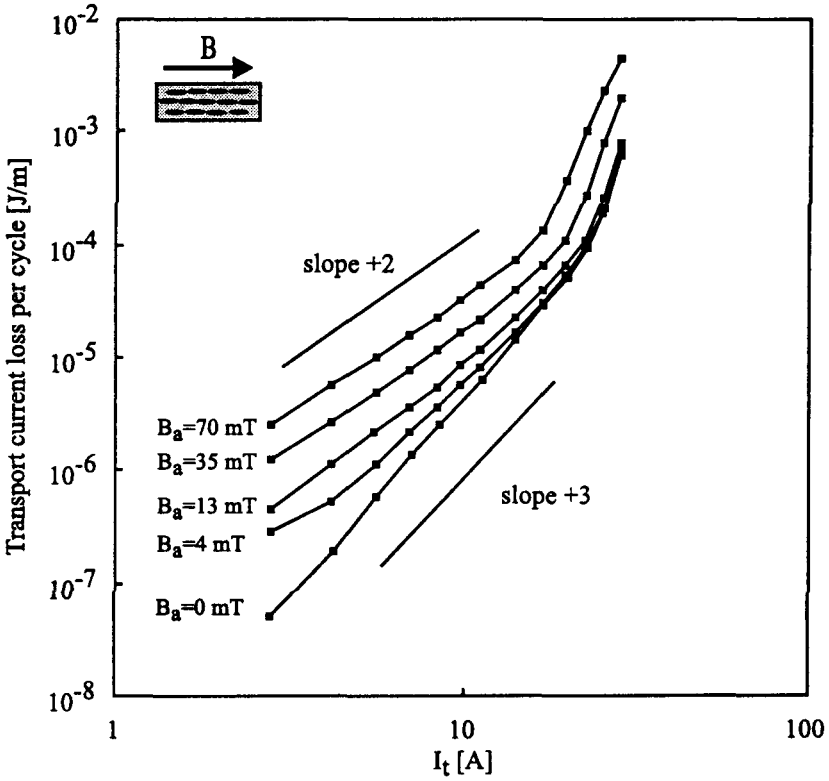

Figure II.5.3.4. Transport current loss in an external alternating magnetic field parallel to the tape conductor (T = 77 K, f = 35 *Hz*). Source: J. J. Rabbers et al., Paper LLB-13, presented at ASC '98, Palm Desert, Calif., USA.

Here, the transport current loss shows a slope of between three and four for zero applied external field, which abruptly changes due to the appearance of flux flow resistance when the critical current is exceeded. It is interesting to compare these slope values with the limiting slopes for elliptical and rectangular cross-section conductors as calculated by Norris.[67] Conductors having elliptical cross sections have losses proportional to I_t^3 (slope = 2), while conductors with rectangular cross sections have losses proportional to I_t^4 (slope = 3). Whether the loss due to a transport current dominates that due to an external AC magnetic field clearly depends on their relative magnitudes.[68]

When the external field is nonzero, the loss curves have a slope of two below the field-dependent critical current, which again increases above the critical current due to flux flow. The slope of two is indicative of a "resistive" loss mechanism and has therefore been termed dynamic resistance (see the end of Section VI.2.3.1). This resistance is related to the interaction between the transport current and the shielding currents due to the external, transverse, time-dependent magnetic field.[69]

---

[67]W.T. Norris, *J. Phys D* **3**:489 (1970).

[68]J.J. Rabbers et al., *IEEE Trans. on Appl. Superconductivity* **9**:1185 (1999).

[69]J.J. Rabbers et al., *Physica C* **310:**101 (1998); W.J. Carr, Jr., *AC Loss and Macroscopic Theory of Superconductors* (Gordon and Breach, New York, 1983).

II.6 FROM TAPE TO CABLE

Ultimately, one wants to know the losses in a device that is made from many tapes. The extrapolation from the performance of laboratory samples of tape to cables or transformers raises questions that are difficult, but not insuperable. Foremost among these questions is how the current will distribute itself among different tapes. It has been suggested that this distribution depends on the character of the joints between normal cable and a superconducting cable.[70] If so, this issue will affect all AC devices embedded in an existing grid.

J. Clem has tried to answer the question: "If the current were equalized in each layer, how would the losses be affected?" He found that:

- In multilayer cables carrying equal currents in each layer, the AC losses at *low* currents are *higher* than they would be if the current penetrated into the inner layers only after the outer layers reached their critical currents;

- But, AC losses at *high* currents are *lower* than they would be if the current penetrated into the inner layers only after the outer layers reached their critical currents;

- Each layer of the cable should be inductively equivalent and inductive means should be used to equalize the current in each layer.

These results can be seen in Figure II.6.1.

---

[70]S. Olsen, S. Kruger, C. Traeholt, A. Kule, O. Tonnesen, M. Daumling, J. Ostergard, "Loss and Inductance Investigations in a 4 layer Superconducting Prototype Cable Conductor," *IEEE Trans. on Appl. Supercon.* **9**(2), (June 1999).

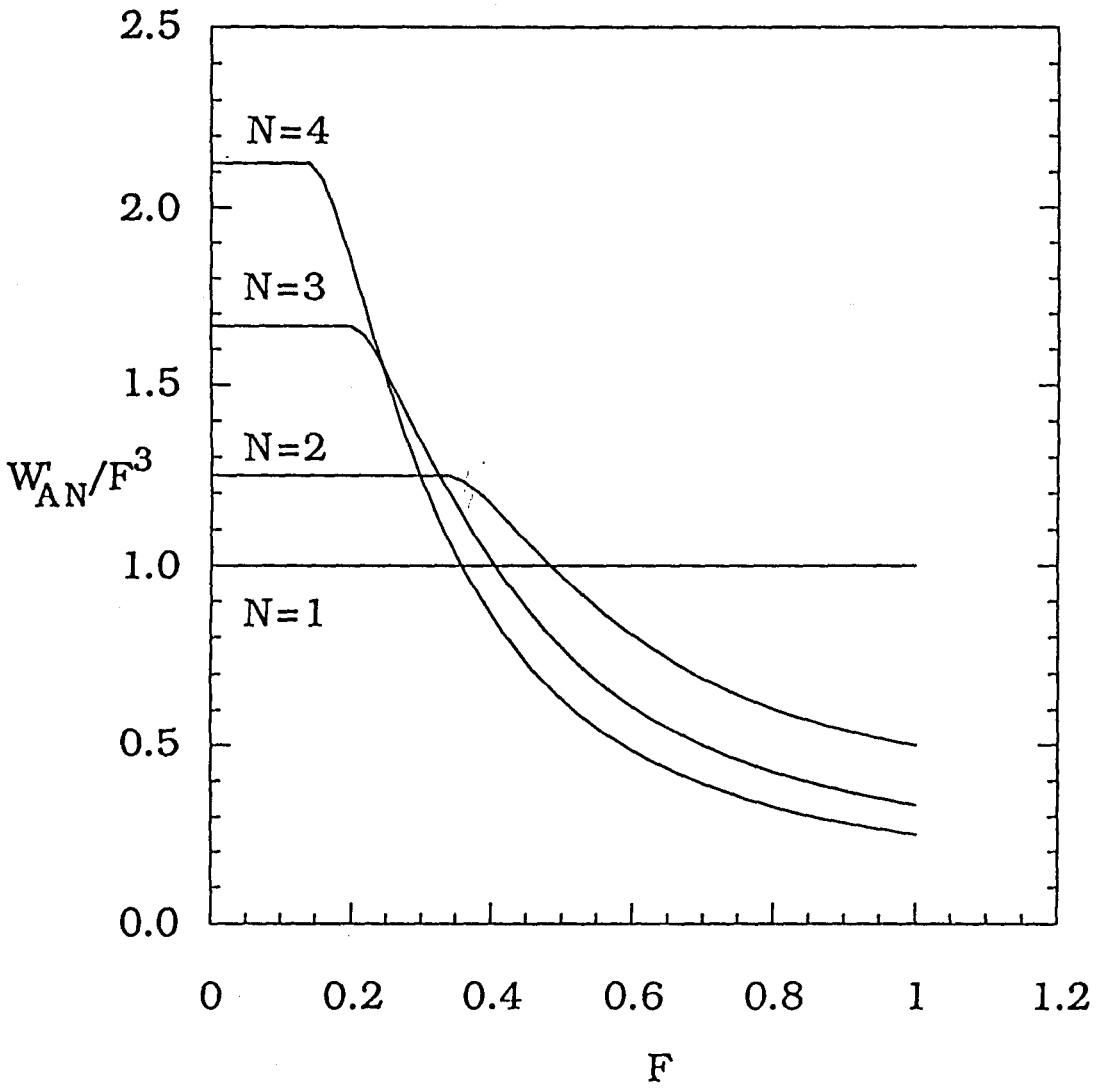

Figure II.6.1. AC losses with equal current in N layers normalized to one-layer losses at the same F. Here $F = I_0/I_c$ where $I = I_0 \cos wt$ and W_A is the loss per cycle per unit of external surface area (The prime on W_{AN} indicates the normalization so that $W'_{A1}/F^3 = 1$). Source: J. R. Clem, *Calculations of Hysteretic AC Losses in Power Transmission Cables Consisting of Multiple Layers*, presented to the Workshop on AC Losses, EPRI, Palo Alto, California, April 8, 1999.

Equal currents in multilayered cables have been achieved by Rieger et al.[71] using "transformatoric coupling," and they were able to quantitatively describe their experimental results obtained with a 10-meter cable. This required taking account of the HTS nonlinear current-voltage characteristic. Helical windings with varying pitch have also been used by

[71]J. Rieger et al., "AC Losses in a Flexible 10-m long Conductor Model for a HTS Power Transmission Cable," preprint, May 8, 1998.

Mukoyama et al,[72] to obtain equal currents in each layer. They found that the pitch angles required were such as to cause no reduction of the critical currents of the tapes and that the current distribution in the various layers depended on the total current being carried.

It should be noted that the twisting of the tapes on a given cylinder will produce a longitudinal field,[73] which will combine with the field of an internal concentric layer to cause a field line to spiral about the internal layer rather than describing a circle. Ries et al.[74] have used a "zero-flux condition," combined with adjusting the pitch angle of different concentric layers to inductively equalize transport current among layers, to ensure that no self-field crosses the outer layers. A 10-*m* model was made and current was shared nearly equally by the four layers of the cable, with measured AC losses at 50 *Hz* of 0.8 *W/m* at 2 kA_{rms}[75]

The measurement of AC losses in cables is difficult and has been addressed by a variety of authors. Variations between the electrical and calorimetric techniques are not insignificant and can amount to almost a factor of two.[76] In the case of the electrical technique, details on the voltage lead position, phase errors, inductive compensation, and location of current return leads have been discussed by Krüger, Olsen, et al.[77]

II.7 PROMISING TECHNIQUES

Two scientific techniques that might illuminate AC loss have been little used, to date, for the investigation of AC loss. One is experimental and the other is computational.

The experimental technique involves the use of magneto-optical imaging to record time-dependent behavior in the superconductor. Several groups use magneto-optics to study time-independent behavior (i.e., dc properties). However, to the author's knowledge, only the group at Bar-Ilan University has used magneto-optics to study time-dependent fields and currents. The Bar-Ilan group reports a break in the slope of the magnetic induction as it penetrates their sample. As discussed elsewhere in this report, the Bean model has a single critical current density, to which the slope of the magnetic induction is proportional. Like the Argonne group (see Section II.3.5), the Bar-Ilan group interpret their data as showing the presence of two critical current densities, each in a different part of the sample and each manifesting a different ordering (crystal-like and glass-like) or thermodynamic phase of the flux tubes within that part of the sample.[78] One might expect that each cycle of a strong enough time-dependent field would be

---

[72]S. Mukoyama et al., "Uniform Current Distribution Conductor of HTS Power Cable with Variable Tape-Winding Pitches," ISS '98, Fukuoka, Nov. 16, 1998.
[73]J. Lee et al., *IEEE Trans. on Appl. Supercond.* **9**:750 (1999); S. Fukui et al., *IEEE Trans. on Appl. Supercond.* **9**:825 (1999).
[74]G. Ries et al., *Physica* C **310**:283 (1998).
[75]J. Rieger et al., *Physica* C **310**:225 (1998).
[76]J.W. Lue et al., "AC Loss of a 5-m HTS Transmission Cable," 1999 HTS Wire Development Workshop, Cocoa Beach, Fla. (Jan. 12-13, 1999).
[77]S. Krüger, G. Olsen, et al., *Supercond. Sci. Technol.* **12**:360 (1999).
[78]D. Giller, A. Shaulov, T. Tamegi, and Y. Yeshurun, "Transient Vortex States in $Bi_2Sr_2CaCu_2O_{8+d}$ Crystals," *Phys. Rev. Letters* **84**(16):3698-3701 (April 17, 2000).

marked by two critical currents, and the calculation of AC losses would require taking account of both.

As suggested by its name, the computational technique would use computers to calculate AC loss by incorporating both anisotropy and the nonlinear current voltage characteristic or by incorporating anisotropy, local defects, and the time-dependent Ginzburg–Landau equations. The results could be presented by tables and curves or by computer-driven animations.[79] Only a few groups have pursued this approach to date.

[79]K. Demachi, Y. Yoshida, H. Asakura, and K. Miya, "Numerical Analysis of Magnetization Processes in Type II Superconductors based on Ginzburg-Landau Theory," *IEEE Transactions on Magnetics*, **32**(3) (May 1996).

N. Banno and N. Amemiya, "Numerical Analysis of AC Loss," *IEEE Transactions on Applied Superconductivity,* **9**(2):2561-2564 (June 1999).

G.W. Crabtree, D.O. Gunter, H.G. Kaper, A.E. Koshelev, G.K. Leaf, and V.M. Vinokur, "Numerical Solution of Driven Vortex Systems," *Phys. Rev*. **B**(61):1446-1455 (2000).

III. GROUPS ACTIVE IN THE FIELD

Many excellent groups are investigating AC losses, with the goal of reducing them. This work will continue as long as interest persists in ceramic superconductors. To facilitate the reader's ability to keep abreast of future progress, we present contact information for a representative sample (not an exhaustive list) of today's active groups and individual investigators. Their research is done individually and collaboratively. An outstanding example of the latter is the European collaboration, now under way. [1]

III.1 CONTACTS IN NONPROFIT ORGANIZATIONS

Following is contact information for lead members of several active groups engaged in nonprofit research on AC losses or otherwise dealing with the effects of AC losses. The contact persons named below are either engaged in work concerning AC losses or can put the reader in touch with those persons within their organizations who are so engaged.

Ole Tønnesen
Professor of Experimental Electric Power Engineering
Institut for Elteknik
Department of Electric Power Engineering
Technical University of Denmark
DTU, Building 325
DK-2800 Lyngby
DENMARK
Phone: 45-45-25-35-11
Fax: 45-45-88-61-11
E-mail: ot@eltek.dtu.dk

Yosi Yeshurun
Department of Physics
Bar Ilan University
52900 Ramat-Gan
ISRAEL
Phone: 972 (0)3-531-8369 (office)
Fax: 972 (0)3-535-3298
E-mail: F67069@BARILVM

Osami Tsukamoto
Director
Cooperative Research and Development Center
Faculty of Engineering
Yokohama National University
79-5 Tokiwadai
Hodogaya-ku Yokohama
JAPAN
Phone: +81-45-339-4121
Fax: +81-45-338-1157
E-mail: osami@tsukalab.dnj.ynu.ac.jp

[1] C. M. Friend et al., *IEEE Trans. on Appl. Supercond.* **9**: 1165 (1999).

Kazuo Funaki
Research Institute of Superconductivity
Faculty of Engineering
Kyushu University
6-10-1 Hakozaki, Higashi-Ku
Fukuoka 812-81
JAPAN
Phone: +81-92-642-4016
Fax: +81-92-632-2438
E-mail: funaki@sc.kyushu-u.ac.jp

Bennie ten Haken
University of Twente
Enschede
Xavier Obradors I Berenguer
Consejo Superior de Investigaciones Cientificas
Institut de Ciencia de Materials de Barcelona
Campus de la UAB, E-08193-Bellaterra, Espana
SPAIN
Phone: 34-(9)-3 580 18 53
Fax: 34-(9)-3 580 57 29
E-mail: xavier.obradors@icmab.es

Sven P. Hörnfeldt
Adjunct Professor
Department of Electric Power Engineering
Electrotechnical Design
Royal Institute of Technology
Kungl Tekniska Högskolan
Teknikringen 33
SE-100 44 Stockholm
SWEDEN
Phone: 46 8 790 76 19
Fax: 46 21 323 264
E-mail: Sven.Hornfeldt@secrc.abb.se

René Flükiger
Applied Superconductors
Department de Physique de la Matiere Condensée
University of Genéve
24, quai Ernest-Ansermet
CH-1211 Geneve 4
SWITZERLAND
Phone: (41+22) 702-62-40
Fax: (41+22) 781-21-92
E-mail: Rene.Flukiger@Physics.UNIGE.ch

Georg Vécsey
Head of CRPP - Fusion Technology Division
Federal Institute of Technology Lausanne
Centre de Recherches en Physique des Plasmas
CRP-Technologie de la Fusion
Bld. WMHA/C37
CH-5232 Villigen PSI,
SWITZERLAND
Phone: (41)-56 310 32 72

THE NETHERLANDS
Phone: 31 - 53 489 3190
Fax: 31 - 53 489 1099
E-mail: B.tenHaken@TN.UTwente.NL

Wilfried Goldacker
Superconducting Materials Division
Institut für Technische Physik
Forschungszentrum Karlsruhe GmbH
Postfach 3640
D-76021 KarlsruheGERMANY
Phone: 49 -(0)7247/824 179
Fax: 49 -(0)7247/822 849
E-mail: wilfried.goldacker@itp.fzk.de
Fax: (41)-56 310 37 29
E-mail: vecsey@psi.ch

Mas Suenaga
Senior Metallurgist
Department of Applied Science
Brookhaven National Laboratory
Building 480
Upton, New York 11973-5000
USA
Phone: 1 (631) 344-3518
Fax: 1 (631) 344-4071
E-mail: mas@sun2.bnl.gov

Martin Maley
Los Alamos National Laboratory
MST-STC Mail Stop: K763
Los Alamos, New Mexico 87545
USA
Phone: 1 (505) 665-3030
Fax: 1 (505) 665-3164
E-mail: dpeterson@lanl.gov

Winston Lue
Superconductivity Program
Oak Ridge National Laboratory
Post Office Box 2008
Oak Ridge, Tennessee 37831-6195
USA
Phone: 1 (423) 574-8057
Fax: 1 (423) 574-6073
E-mail: hawseyra@ornl.gov

Archie M. Campbell
IRC in Superconductivity
University of Cambridge
Madingley Road
Cambridge CB3 0HE
UNITED KINGDOM
Phone: +44 1223 337076
Fax: +44 1223 337074
E-mail: amcl@cam.ac.uk

I. Hlasnik
Institute of Electrical Engineering SAS
Dúbravská cesta 9,
842 39 Bratislava
SLOVAK REPUBLIC
Phone:
Fax:
E-mail:

Naoyuki Amemiya
Yokohama National University
Division of Electrical and Computer Engineering
79-5, Tokiwadai, Hodogaya
Yokohama, 240-8501
JAPAN
Phone: 81.45.339.4119
Fax: 81.45.338.1157
E-mail: ame@rain.dnj.ynu.ac.jp

III.2 CONTACTS IN FOR-PROFIT ORGANIZATIONS

The following organizations were established to make a profit. They are engaged in conductor development and have either considered or are actively pursuing AC conductor. The contact persons named below are either engaged in work concerning AC losses or can put the reader in touch with those persons within their organizations who are so engaged.

Miles Apperley
MM Cables - HTSC Development Facility
Australian Technology Park
Eveleigh NSW 1430
AUSTRALIA
Phone: 61-2-9209-4221
Fax: 61-2-9209-4222
E-mail: milesa@ozemail.com.au

Juan Farré
Managing Director
Nordic Superconductor Technologies A/S
Priorparken 878
DK-2605 Brandby
DENMARK
Phone: +45 43 48 25 05
Fax: +45 43 48 25 01
E-mail: j.farre@nst.com

Hans Krauth
Vacuumschmelze GmbH
Grüner Weg 37
D-63450 Hanau
GERMANY
Phone:
Fax:
E-mail:

Takeshi Fukui
General Manager
Electric Power System
Technology Research Laboratories
Sumitomo Electric Industries, Ltd.
Osaka Works
1-1-3, Shimaya, Konohana-ku
Osaka, 554
JAPAN
Phone: 06-466-5776
Fax: 06-466-6583
E-mail: fukui@okk.sei.co.jp

C.M. Friend
BICC Cables Ltd
Wrexham Technology Centre
Wrexham
Clwyd
LL13 9XP
UNITED KINGDOM
Phone: 44 1978 662 612
Fax: 44 1978 662 464
E-mail: cfriend@bicc.co.uk

Steven Fleschler
American Superconductor Corporation
Two Technology Drive
Westborough, MA 01581
USA
Phone: 1 (508) 836-4200
Fax: 1 (508) 836-4248
E-mail: sfleshl@asc.mhs.compuserve.com

Michael S. Walker
Senior Staff Scientist
Advanced Devices & Systems Group
Intermagnetics General Corporation (IGC)
450 Old Niskayuna Road
PO Box 461
Latham, NY 12110-0461
USA
Phone: 1 (518) 782-1122 Ext. 3016
Fax: 1 (518) 783-2615
E-mail: mwalker@igc.com

III.3 INDIVIDUAL INVESTIGATORS

Many of the persons listed below are now employed by or provide consulting services to the organizations named in the previous sections; however, some do not do so, and others may change their affiliations after this report is published. To facilitate future professional contact, we list the participants, with contact information, in two recent meetings of technical experts.

Participants in the 1999 Workshop on AC Losses held on April 8-9, 1999, at EPRI in Palo Alto, California

Dr. S. P. Ashworth (Steve)
Brookhaven National Laboratory
Box 5000
Upton New York 11973-5000
USA
Phone: 631-344-5413
Fax: 631-344-4071
E-mail: ashworth@bnl.gov

Dr. R. G. Buckley (Bob)
Industrial Research
PO Box 31310
Lower Hutt, New Zealand
Phone: +64 4 569-0288
Fax: +64 4 569-0117
E-mail: R.Buckley@irl.cri.nz

Dr. Julian Cave
Pavillon Lionel Boulet
Institut de Recherche d'Hydro-Québec
1800 boul. Lionel-Boulet, Varennes
Québec, Canada, J3X 1S1
Phone: +1 450 652-8946
Fax: +1 450 652-8905
E-mail: cave.julian@ireq.ca

Dr. Toshimi Chiba
Department of Materials Science and Technology
Faculty of Engineering
Iwate University
Ueda 4-3-5 Morioka 020-8551
Japan
Phone: 81-19-621-6494
Fax: 81-19-621-6373
E-mail: 5196008@iwate-u.ac.jp

Dr. Marian Ciszek
Yokohama National University
Faculty of Engineering
Division of Electrical and Computer Engineering
79-5 Tokiwadai, Hodogaya-ku
Yokohama 240 8501
Japan
Phone: +81 45 338 3187
Fax: +81 45 338 1157
E-mail: ciszek@tsukalab.dnj.ynu.ac.jp

Prof. John R. Clem
A517 Physics
Iowa State University
Ames, IA 50011-3160
USA
Phone: 515-294-4223
Fax: 515-294-0689
E-mail: clem@ameslab.gov

Dr. Giacomo Coletta
Pirelli Cavi & Sistemi
Viale Sarca 222
20126 Milano
Italy
Phone: +39 02 64429409
Fax: +39 02 64429431
E-mail: giacomo.coletta@pirelli.com

Prof. E. W. Collings (Ted)
MSE
477 Watts Hall, 2041 College Rd.
Ohio State University
Columbus, OH 43210
USA
Phone: 614-688-3607
Fax: 614-688-3677
E-mail: Ted+@osu.edu

Dr. Frank Darmann
MM Cables High Temperature Superconducting
Development Facility
Australian Technology Park
Eveleigh NSW 1430
Australia
Phone: +61 2 9209 4220
Fax: +61 2 9209 4222
E-mail: htscdev@ozemail.com.au

Dr. Lawrence Dresner (Larry)
111 Stanton Lane
Oak Ridge, TN 37830-8408
USA
Phone:
Fax:
E-mail: LDresner@AOL.COM

Dr. Juan Farré
President and CEO
NST - Nordic Superconductor Technologies
Priorparken 878 - DK 2605 Broendby
Denmark
Phone: +45 43 48 25 00
Fax: +45 43 48 25 01
E-mail: j.farre@nst.com
http://www.nst.com

Dr. Steven Fleshler (Steve)
American Superconductor Corporation
Two Technology Drive
Westborough, MA 01581
USA
Phone: (508) 836-4200 Ext. 218
Fax: (508) 836-4248
E-mail: sfleshler@amsuper.com

Dr. Chris M. Friend
Senior Research Engineer
BICC Superconductors
Oak Road, Wrexham LL13 9XP
United Kingdom
Phone: +44 1978 662612
Fax: +44 1978 662464
E-mail: cfriend@bicc.co.uk

Prof. John S. Hurley
Clark Atlanta University
Department of Engineering (Electrical)
223 James P. Brawley Drive SW
Atlanta, Georgia 30314
USA
Phone: 404-880-6831
Fax: 404-880-6983
E-mail: jhurley@cau.edu

Dr. H. R. Kerchner (Rich)
M.S. 6061, Bldg. 3115
Oak Ridge National Laboratory
P.O. Box 2008
Oak Ridge, TN 37831-6061
USA
Phone: 423-574-6270
Fax: 423-574-6263
E-mail: kerchnerhr@ornl.gov

Dr. Martino Leghissa
Project Manager
Siemens Corporate Technology
P.O. Box 3220
91050 Erlangen, Germany
Phone: +49 - 9131 - 7 32634
Fax: +49 - 9131 - 7 33323
E-mail: martino.leghissa@erls.siemens.de

Dr. J. W. Lue (Winston)
Oak Ridge National Laboratory
P. O. Box 2009
Oak Ridge, TN 37831-8071
USA
Phone: (423) 574-1461
Fax: (423) 574-0584
E-mail: LueJW@ornl.gov

Dr. Milan Majoros
IRC in Superconductivity
University of Cambridge
Madingley Road
Cambridge CB3 OHE
United Kingdom
Phone: +44 1223 337441
Fax: +44 1223 337074
E-mail: mm293@cus.cam.ac.uk

Dr. Elena Martinez
Institute of Cryogenics
University of Southampton
University Road
Southampton S017 1BJ
United Kingdom
Phone: 44 1703 592872
Fax: : 44 1703 593230
E-mail: emf@soton.ac.uk

Dr. Renata Mele
Pirelli Cavi & Sistemi
Viale Sarca 222
20126 Milano
Italy
Phone: 39 02 64429410
Fax: 39 02 64429431
E-mail: renata.mele@pirelli.com

Dr. Koshichi Noto
Department of Materials Science and Technology
Faculty of Engineering
Iwate University
Ueda 4-3-5 Morioka 020-8551
Japan
Phone: 81-19-621-6357
Fax: 81-19-621-6373
E-mail: noto@iwate-u.ac.jp

Prof. Dr. Johan J. Smit
Delft University of Technology
Fac. ITS-ET/HT
High Voltage Laboratory
P.O. Box 5031
600 GA Delft
The Netherlands
Phone: +31 15 278 4231
Fax: +31 15 278 8382
E-mail: j.j.smit@its.tudelft.nl

Dr. Michael Staines
Industrial Research Ltd
P O Box 31-310
Lower Hutt
New Zealand
Phone: +64-4-5690291
Fax: +64-4-5690117
E-mail: M.Staines@irl.cri.nz

Dr. Masaki Suenaga
Brookhaven National Laboratory
Upton, NY 11973-5000
USA
Office: 516-344-3518
Fax: 516-344-4071
E-mail: mas@sun2.bnl.gov

Ms. Chandra Trautwein
Intermagnetics General Corporation (IGC)
450 Old Niskayuna Rd.
P.O. Box 461
Latham, NY 12110-0461
USA
Phone: 518-782-1122
Fax: 518-783-2615
E-mail: ctrautwein@igc.com

Prof. Osami Tsukamoto
Faculty of Engineering
Yokohama National University
79-5 Tokiwadai, Hodogaya-Ku
Yokohama, 240-8501
Japan
Phone: +81-45-339-4121
Fax: +81-45-338-1157
E-mail: osami@tsukalab.dnj.ynu.ac.jp

Dr. Michael S. Walker
Intermagnetics General Corporation (IGC)
450 Old Niskayuna Rd.
P.O. Box 461
Latham, NY 12110-0461
USA
Phone: 518-782-1122, Ext. 3016
Fax: 518-783-2615
E-mail: mwalker@igc.com

Dr. Jeffrey O. Willis
Los Alamos National Laboratory
Mail Stop K763; MST-STC
Los Alamos, NM 87545
USA
Phone: 1-505-665-1320
Fax: 1-505-665-3164
E-mail: jwillis@lanl.gov

Dr. Dingan Yu
American Superconductor Corporation
Two Technology Drive
Westborough, MA 01581
USA
Phone: (508) 836-4200 Ext. 125
Fax: (508) 836-4248
E-mail: dyu@amsuper.com

Participants in the Topical Conference on AC Loss and Stability of Low- and High-T_c Superconductors

Akhmetov, Alexander
IVT
Russian Academy of Science
Ozorskaya 13/19
Moscow 127412
RUSSIA
Phone:
Fax: +7095362-55-64
E-mail: akhmetov@ivt.ac.orbita.ru

Amemiya, Naoyuki
Yokohama National University
Division of Electrical and Computer Engineering
79-5, Tokiwadai, Hodogaya
Yokohama, 240-8501
JAPAN
Phone: 81.45.339.4119
Fax: 81.45.338.1157
E-mail: ame@rain.dnj.ynu.ac.jp

Arndt, Thomas J.
Vacuumschmelze GmbH
Dept. HT-SE
Grüner Weg 37
D-63450 Hanau, Hessen
GERMANY
Phone: +49 6181 38 3148
Fax: +49 6181 38 3159
E-mail: thomas.arndt@hau.siemens.de

Ashworth, Steve
Brookhaven National Laboratory
Bldg. 902-A
Upton, NY 11973-5000
USA
Phone: 631.344.5413
Fax: 631.344.4071
E-mail: ashworth@bnl.gov

Beduz, Carlo
University of Southampton
Dept. of Mechanical Engineering
SO17 1BJ
Southampton, Hampshire
UNITED KINGDOM
Phone: +44 1703 594760
Fax: +44 1703 593230
E-mail: Cb3@soton.ac.uk

Bodin, Peter
Nordic Superconductor Technologies a/s
Priorparken 878
DK-2605 Brøndby
DENMARK
Phone: +45 4348 3543
Fax: +45 4348 2501
E-mail: p.bodin@nst.com

Bonito Oliva, Alessandro
Oxford Instruments
Research Instruments Group
Old Station Way
Eynsham, OX8 12TL
UNITED KINGDOM
Phone: 44 1865 393 298
Fax: 44 1865 393 333
E-mail:

Bottura, Luca
CERN
Division LHC
CG-1211
Geneva, 23
SWITZERLAND
Phone: 41.22.767.3729
Fax: 41.22.767.6230
E-mail: Luca.Bottura@cern.ch

Bruzek, Christian-Eric
GEC Alsthom, DEA/FIL-Bat. 52
Groupes Machines Electriques
3 Avenue des Trois Chenes
90018 Belfort Cedex
FRANCE
Phone: +33 384 55 13 45
Fax: +33 384 55 70 93
E-mail: Christian-eric.bruzek@wanadoo.fr

Bruzzone, Pierluigi
EPFL-CRPP
Technolgie de la Fusion
PSI/Villingen 5232
SWITZERLAND
Phone: 41-56-310-4363
Fax: 41-56-310-3729
E-mail: bruzzone@psi.ch

Campbell, Archie M.
University of Cambridge
IRC in Superconductivity
Madingley Road
Cambridge CB3 OHE
UNITED KINGDOM
Phone: +44 1223 337076
Fax: +44 1223 337074
E-mail: amcl@cam.ac.uk

Caplin, David
Imperial College
Blackett Laboratory
Prince Consort Road
SW7 2BZ London
UNITED KINGDOM
Phone: +44 171 594 7608
Fax: +44 171 594 7580
E-mail: d.caplin@ic.ac.uk

Carr, W.J., Jr.
(private address)
1460 Jefferson Heights
Pittsburgh, PA 15235
USA
Phone: +1 412-824-3456
Fax: +1 412-824-3456
E-mail: wjamescarrjr@worldnet.att.net

Cereda, Ezio
CISE SpA
Via Reggio Emila 39
20090 Segrate (Milano)
Milano, ITALY
Phone:
Fax:
E-mail:

Ciotto, Marco
ENEA (ERG-FUS-TECN-SP)
Sezione Superconduttivita
Via E. Fermi 45
P.O. Box 65
00044 Frascati (Roma)
ITALY
Phone: +39 6 9400 5767
Fax: +39 6 9400 5734
E-mail: Ciotti@frascati.enea.it

Coletta, Giacomo
Pirelli Cavi SpA-c.2714
DRS/RSA
Viale le Sarca 222
20126 Milano
ITALY
Phone: +39 2 6442 9409
Fax: +39 2 6442 9431
E-mail: giacomo.coletta@pirelli.com

Collings, Edward W.
Ohio State University
Dept. of Materials Science and Engineering
2041 College Rd, 477 Watts Hall
Columbus, OH 43210
USA
Phone: (614) 688-3607
Fax: (614) 688-3677
E-mail: ted+@osu.edu

Daney, David E.
Los Alamos National Laboratory
MS J580
P.O. Box 1663
Los Alamos, NM 87545
USA
Phone: +1 505 665 0216
Fax: +1 505 665 7740
E-mail: Daney@lanl.gov

Däumling, Manfred
Technical University of Denmark
Dept. of Electric Power Engineering
Building 325
DK-2800, Lyngby
DENMARK
Phone: +45 45 25 3001
Fax: +45 45 88 6111
E-mail: md@eltek.dtu.dk

Dhallé, Marc
Université de Geneve
Departement de Physique de
la Matiere Condensée
24 Quai Ernest-Ansermet
CH-1211 Geneve 4
SWITZERLAND
Phone: +41 22 702 65076
Fax: +41 22 702 6869
E-mail: marc.dhalle@physics.unige.ch

Dolez, Patricia
University of Sherbrooke
Physics Department
2500 Bd Université
J1K 2R2 Sherbrooke,
Quebec, CANADA
Phone: +1 819 821 8000, x3040
Fax: +1 819 821 8046
E-mail: Patricia.dolez@physique.usherb.ca

Dolgosheev, P.I.
JSC
VNIIKP
5 Shosse Entuziastov St.
Moscow 111112
RUSSIA
Phone: +7 095 137 9489, +7 095 271 1320
Fax: +7 095 361 1259, +7 096 757 4843
E-mail: Vsytn@podolsk.ru

Dresner, Lawrence
111 Stanton Lane
Oak Ridge, TN 37830-8408
USA
Phone:
Fax:
E-mail: Ldresner@aol.com

Dutoit, Bertrand
EPFL
DE-CIRC
CH-1015
Lausanne, SWITZERLAND
Phone: +41 21 693 4689
Fax: +41 21 693 6700
E-mail: Bertrand.dutoit@epfl.ch

Eckelmann, Hubert
Forschungszentrum Karlsruhe
Institut für Technische Physik
P.O. Box 3640
D-76126 Karlsruhe
GERMANY
Phone: +49 72 4782 5341
Fax: +49 72 4782 5398
E-mail: hubert.eckelmann@fzk.itp.de

Egorov, Serguei A.
STC, "Sintez," Efremov Institute
Institute of Electrophysical Apparatus
Sovetskij pr., 1 Metallostroj
St. Petersburg 189631
RUSSIA
Phone: +7 812 464 4611
Fax: +7 812 464 4623
E-mail: egorov@niiefa.spb.su

Fleshler, Steven
American Superconductor Corporation
Two Technology Drive
Westborough, MA 01581
USA
Phone: +1 508 836 4200
Fax: +1 508 836 4248
E-mail: sfleshl@asc.mhs.compuserve.com

Foitl, Michael
Technical University Vienna
Institute for Experimental Physics
Wiedner Hauptstr. 8-10/131
A-1040 Wien
AUSTRIA
Phone: +43 1 58801 5794
Fax: +43 1 586 3191
E-mail: foitl@xphys.tuwien.ac.at

Friedman, Alex
Bar-Ilan University
Department of Physics
Ramat-Gan 52900
ISRAEL
Phone: +972 3 531 8607
Fax: +972 3 535 3298
E-mail: Friedman@PHYSNET.PH.BIU.AC.IL

Friend, Chris M.
BICC Cables Ltd.
Wrexham Technology Centre
Wrexham LL13 9XP
UNITED KINGDOM
Phone: +44 1978 66 2612
Fax: +44 1978 66 2464
E-mail: Cfriend@bicc.co.uk

Fukui, Satoshi
Niigata University
Faculty of Engineering
8050 Ikarashi Nino-cho
Niigata, 950-2181
JAPAN
Phone: +81 25 262 6731
Fax: +81 25 262 6731
E-mail: fukui@eng.niigata-u.ac.jp

Funaki, Kazuo
Kyushu University
Faculty of Engineering
6-10-1 Hakozaki, Higashiku
Fukuoka 812-81
JAPAN
Phone: +81 92 642 4016
Fax: +81 92 632 2438
E-mail: funaki@sc.kyushu-u.ac.jp

Ghosh, Arup K.
Brookhaven National Laboratory
Bldg. 902-A
Upton, NY 11973-5000
USA
Phone: 516-282-3974
Fax: 516-282-2190
E-mail: Ghosh@bnl.gov

Gislon, Paola
ENEA-CRE-Frascati
Sezione Superconduttivita
P.O. Box 65
00044 Frascati (Roma)
ITALY
Phone: +39 6 9400 5396
Fax: +39 6 9400 5734
E-mail: gislon@frascati.enea.it

Godeke, Arno
University of Twente
Low Temperature Division
P.O. Box 217
7500 AE Enschede
THE NETHERLANDS
Phone: +31 53 489 3889
Fax: +31 53 489 1099
E-mail: a.godeke@tn.utwente.nl

Goldacker, Wilfried
Forschungzentrum Karlsruhe
Institut für Technische Physik
P.O. Box 3640
D-76021 Karlsruhe
GERMANY
Phone: +49 724 782 4179
Fax: +49 724 782 2849
E-mail: Wilfried.goldacker@itp.fzk.de

Gömöry, Fedor
Pirelli Cavi SpA
Department 2714
Viale Sarca 222
I-20126 Milano, ITALY
Phone: +39 2 6442 9408
Fax: +39 2 6442 9431
E-mail: fedor.gomory@pirelli.com

Haken, Bennie ten
University of Twente
Low Temperature Division
P.O. Box 217
7500 AE Enschede
THE NETHERLANDS
Phone: +31 53 489 3190
Fax: +31 53 489 1099
E-mail: b.tenhaken@tn.utwente.nl

Hassel, Angelique van
Nederlandse Kabel Fabrieken
Postbus 26
2600 MC Delft
THE NETHERLANDS
Phone: 015 260 5691
Fax: 015 260 5664
E-mail: a.hassel@dlf2.nkf.nl

Huang, Yingkai
University of Twente
Low Temperature Division
P.O. Box 217
7500 AE Enschede
THE NETHERLANDS
Phone: +31 53 489 3140
Fax: +31 53 489 1099
E-mail: y.huang@tn.utwente.nl

Ishii, Sadato
Yokohama National Univ./Fac. of Eng.
Division of Electrical and Computer Eng.
79-5 Tokiwadai, Hodogaya-ku
Yokohama, 240-850
JAPAN
Phone: +81 45 339 4121
Fax: +81 45 338 1157
E-mail: osami@tsukalab.dnj.ynu.ac.jp

Ishiyama, Atsushi
Waseda University
Dept. of Electrical Engineering
3-4-1 Ohkubo
Shinjuku-ku
Tokyo 169-8555
JAPAN
Phone: +81 3 5286 3376
Fax: +81 3 3208 9337
E-mail: Atsushi@mn.waseda.ac.jp

Iwakuma, Masataka
Kyushu University
Faculty of Engineering
6-10-1 Hakozaki, Higashiku
Fukuoka 812-8581
JAPAN
Phone: +81 92 642 4017
Fax: +81 92 632 2438
E-mail: Iwakuma@ees.kyushuu.ac.jp

Kasztler, Andrea
Technical University Vienna
Institute for Experimental Physics
Wiedner Hauptstr. 8-10/131
A-1040 Wien
AUSTRIA
Phone: +43 1 58801 5794
Fax: +43 1 586 3191
E-mail: kasztler@xphys.tuwien.ac.at

Kate, Herman H.J. ten
University of Twente
Low Temperature Division
P.O. Box 217
7500 AE Enschede
THE NETHERLANDS
Phone: +31 53 489 3190
Fax: +31 53 489 1099
E-mail: h.h.j.tenkate@tn.utwente.nl

Kim, Seog-Whan
CERN LHC-MMS
Division LHC-MMS
CH 1211
Geneva, 23
SWITZERLAND
Phone: 41.22.767.9776
Fax: 41.22.767.6300
E-mail: Seog-whan.kim@cern.ch

Kirchmayr, Hans
Technical University Vienna
Institute for Experimental Physics
Wiedner Hauptstr. 8-10
A-1040 Wien
AUSTRIA
Phone: +43 1 58801 5700
Fax: +43 1 586 3191
E-mail: exphys@xphy.tuwien.ac.at

Kiss, Takanobu
Kyushu University
Information Science and Electrical
Engineering (ISEE)
6-10-1 Hakozaki, Higashiku
812-81 Fukuoka
JAPAN
Phone: +81 92 642 3910
Fax: +81 92 642 3963
E-mail: kiss@wwwsc.ees.kyushuu.ac.jp

Klein Zeggelink, William F.A.
University of Twente
Low Temperature Division
P.O. Box 217
7500 AE Enschede
THE NETHERLANDS
Phone: +31 53 489 3889
Fax: +31 53 489 1099
E-mail: w.f.a.kleinzeggelink@tn.utwente.nl

Knoopers, Hennie J.
University of Twente
Low Temperature Division
P.O.Box 217
7500 AE Enschede
THE NETHERLANDS
Phone: +31 53 489 3190
Fax: +31 53 489 1099
E-mail: h.g.knoopers@tn.utwente.nl

Kordyuk, Alexander A.
Institute of Metal Physics
Solid State Spectroscopy
36 Vernadskogo str.
252680 KIEV
UKRAINE
Phone: +380 44 444 9538
Fax: +380 44 444 2561
E-mail: kord@imp.kiev.ua

Krooshoop, Eric
University of Twente
Low Temperature Division
P.O. Box 217
7500 AE Enschede
THE NETHERLANDS
Phone: 31 53 489 3889
Fax: +31 53 489 1099
E-mail: h.j.g.krooshoop@tn.utwente.nl

Kühle, Anders
Technical University of Denmark
Dept. of Electric Power Engineering
Building 325
DK-2800, Lyngby
DENMARK
Phone: +45 45 25 3516
Fax: +45 45 88 6111
E-mail: Anders.kyhle@eltek.dtu.dk

Kummeth, Peter
Siemens AG
Corporate Technology,
Paul-Gossen-Strasse 100
P.O. Box 3220
D-91050 Erlangen
GERMANY
Phone: +49 9131 734254
Fax: +49 9131 733323
E-mail: Peter.kummeth@erls.siemens.de

La Cascia, Piero
c/o Pier Luigi Ribani
University of Bologna
Dept. of Electrical Engineering
Viale Risorgimento 2
I-40136 Bologna
ITALY
Phone: +39 51 644 3581
Fax: +39 51 644 3588
E-mail: pierluigi.ribani@mail.ing.unibo.it

Leghissa, Martino
Siemens AG
Corporate Technology
P.O. Box 3220
D-91050 Erlangen
GERMANY
Phone: +49 9131 732634
Fax: +49 9131 733323
E-mail: martino.leghissa@erls.siemens.de

Lehtonen, Jorma
Tampere University of Technology
Lab. of Electricity and Magnetism
P.O. Box 692
FIN-33101 Tampere
FINLAND
Phone: +358 3 365 2730
Fax: +358 3 365 2160
E-mail: jlehtone@cc.tut.fi

Majoros, Milan
Superconductivity Research Centre
University of Cambridge
Cavendish Laboratory
Madingley Road
Cambridge CB3 OHE
UNITED KINGDOM
Phone: +44 1223 337441
Fax: +44 1223 337074
E-mail: Mm293@cus.cam.ac.uk

Martinez, E.
University of Southampton
Dept. of Mechanical Engineering
SO17 1BJ
Southampton, Hampshire
UNITED KINGDOM
Phone: +44 1703 594760
Fax: +44 1703 593230
E-mail: emr@soton.ac.uk

Miyagi, Daisuke
Yokohama National Univ./
Fac. of Eng.
Division of Electrical and
Computer Eng.
79-5 Tokiwadai, Hodogaya-ku
Yokohama, 240-850
JAPAN
Phone: +81 45 339 4121
Fax: +81 45 338 1157
E-mail: osami@tsukalab.dnj.ynu.ac.jp

Mocaër, Philippe
GEC Alsthom, DEA/Fil-Bat. 52
Groupes Machines Electriques
3 Avenue des Trois Chenes
90018 Belfort Cedex
FRANCE
Phone: +33 384 55 13 45
Fax: +33 384 55 70 93
E-mail: Christian-eric.bruzek@wanadoo.fr

Navarro, Rafael
University of Zaragossa
Maria de Luna 3
50015 Zaragossa
SPAIN
Phone: +34 976 76 1958
Fax: +34 976 76 1957
E-mail: Rnavarro@posta.unizar.es

Nibbio, Nadia
EPFL
DE-CIRC
CH-1015
Lausanne
SWITZERLAND
Phone: +41 21 6932703
Fax: +41 21 6936700
E-mail: nadia.nibbio@circ.de.epfl.ch

Nijhuis, Arend
University of Twente
Low Temperature Division
P.O. Box 217
7500 AE Enschede
THE NETHERLANDS
Phone: +31 53 4893889
Fax: +31 53 4891099
E-mail: a.nijhuis@tn.utwente.nl

Noordman, Niels
University of Twente
Low Temperature Division
P.O. Box 217
7500 AE Enschede
THE NETHERLANDS
Phone: +31 53 4893889
Fax: +31 53 4891099
E-mail: n.h.w.noorman@tn.utwente.nl

Oomen, Marijn P.
Siemens AG
Corporate Technology
P.O. Box 3220
D-91050 Erlangen
GERMANY
Phone: +49 91317 34889
Fax: +49 91317 33323
E-mail: Student2.zten4@erls.siemens.de

Ouden, Andries den
University of Twente
Low Temperature Division
P.O. Box 217
7500 AE Enschede
THE NETHERLANDS
Phone: +31 53 4894578
Fax: +31 53 4891099
E-mail: a.denouden@tn.utwente.nl

Passi, Jaakko A.J.
Tampere University of Technology
Lab. of Electricity and Magnetism
P.O. Box 692
FIN-33101 Tampere
FINLAND
Phone: +358 3365 2009
Fax: +358 3365 2160
E-mail: paasi@cc.tut.fi

Pantsyrnyi, Victor I.
A.A. Bochvar's All Russia Scientific &
Research Inst. of Inorganic Materials
5 Rogova Street
123060 Moscow
RUSSIA
Phone: : +7 095 190 82 50
Fax: : +7 095 196 66 71
E-mail: : vor@bochvar.ru

Polcari, Albino
University of Geneva
24, quai Ernest Ansermet
CH-1211
Geneve 4
SWITZERLAND
Phone: +41 22 7026 578
Fax: +41 22 7026 869
E-mail: polcari@sc2a.unige.ch

Rabbers, Jan Jaap
University of Twente
Low Temperature Division
P.O. Box 217
7500 AE Enschede
THE NETHERLANDS
Phone: +31 53 4893889
Fax: +31 53 4891099
E-mail: j.j.rabbers@tn.utwente.nl

Rhyner, Jakob
ABB Corporate Research Ltd.
CH-5405
Baden
Dattwill
SWITZERLAND
Phone: +41 56 486 8217
Fax: +41 56 493 71 47
E-mail: Jacob.rhyner@chcrc.abb.ch

Ribani, Pier Luigi
University of Bologna
Dept. of Electrical Engineering
Viale Risorgimento 2
I-40136 Bologna
ITALY
Phone: +39 51 644 3581
Fax: +39 51 644 3588
E-mail: pierluigi.ribani.@mail.ing.unibo.it

Ricci, M.
ENEA-CRE-Frascati
ERG-FUS-SUPERC
P.O. Box 65
00044 Frascati (Roma)
ITALY
Phone: +39 6 9400 5224
Fax: +39 6 9400 5734
E-mail: mricci@frascati.enea.it

Rieger, Juergen
Siemens AG
Corporate Technology
P.O. Box 3220
D-91050 Erlangen
GERMANY
Phone: +49 9131 7 34889
Fax: +49 9131 7 33323
E-mail: Juergen.rieger@erls.siemens.de

Ries, Günter
Siemens AG
ZT EN 4
P.O. Box 3220
D-91050 Erlangen
GERMANY
Phone: +49 9131 731614
Fax: +49 9131 721339
E-mail: guenter.ries@erls.siemens.de

Romanovskii, V.R.
Russian Research Center
'Kurchatov Institute'
Superconducting and Solid State Institute
1 Kurchatov Square
123182 Moscow
RUSSIA
Phone: +7 095 196 9600
Fax: +7 095 196 5973
E-mail: rvr@kev.kiae.su

Schild, Thierry
Tore Supra, Assoc Euratom-CEA
Department de Recherche
sur la Fusion Control
CE Cadarache,
DRFC/STID, Bt 513
F-13108, Saint Paul les Durance
FRANCE
Phone: 33.442.25.64.93
Fax: 33.442.25.49.90
E-mail: tschild@cea.fr

Schmidt, Curt
Inst. für Technische Physik
Kernforschungszentrum Karlsruhe
P.O. Box 3640
D-76021 Karlsruhe
GERMANY
Phone: +49 7247 82 4008
Fax: +49 7247 82 2849
E-mail: curt.schmidt@itp.fzk.de

Seo, Kazutaka
Mitsubishi Electric Corp.
8-1-1 Tsukaguchi-Honmachi
Amagasaki City
Hyogo Pref., 661
JAPAN
Phone: +81 6 497 7127
Fax: +81 6 497 7288
E-mail: Seo@ele.crl.melco.co.jp

Shevchenko, Oleg
University of Twente
Low Temperature Division
P.O. Box 217
7500 AE Enschede
THE NETHERLANDS
Phone: +31 53 4893889
Fax: +31 53 4891099
E-mail: o.a.shevchenko@tn.utwente.nl

Sjöström, Må rten
EPFL
DE-CIRC
CH-1015
Lausanne
SWITZERLAND
Phone: +41 21 693 2703
Fax: +41 21 693 6700
E-mail:

Staines, Michael
New Zealand Inst. for Industrial R&D
Gracefield Research Centre,
Gracefield Road
P.O. Box 31-310
Lower Hutt
NEW ZEALAND
Phone: +64 4 5690291
Fax: +64 4 5690117
E-mail: m.staines.@irl.cri.nz

Stavrev, Svetlomir
EPFL
DE-CIRC
CH-1015
Lausanne
SWITZERLAND
Phone: +41 21 693 2703
Fax: +41 21 693 6700
E-mail:

Sumption, Mike D.
Ohio State University
Dept. of Materials Science
and Engineering
2041 College Ave.
477 Watts Hall
Columbus, OH 43201-1179
USA
Phone: 614 688 3684
Fax: 614 688 3677
E-mail: mdsimption+@osu.edu

Sytnikov, Victor E
JCS "VNIIKP"
Superconducting Wire & Cable
5, Shosse Entuziastov
111024 Moscow
RUSSIA
Phone: +7 095 137 9489/+7 095 271 1320
Fax: +7 095 361 1259/+7 096 757 4843
E-mail: vsytn@poololsk.ru

Takács, Silvester
Slovak Academy of Sciences
Institute of Electrical Engineering, Applied Superconductivity
Dúbravská cesta 9
842 39 Bratislava
SLOVAK REPUBLIC
Phone: +421 7 3782003
Fax: +421 7 375816
E-mail: elektaka@savba.sk

Takao, Tomoaki
Sophia University
Dept. of Electrical Engineering
7-1, Kioi-Cho, Chiyoda-Ku
Tokyo, 102
JAPAN
Phone: +81 3 3238 3327
Fax: +81 3 3238 3321
E-mail: Takao@toshi.ee.sophia.ac.jp

Takeo, Masakatsu
Kyushu University
Faculty of Engineering
6-10-1 Hakozaki, Higashi-ku
Fukuoka 812-81
JAPAN
Phone: +92 642 4024
Fax: +92 632 2438
E-mail: Takeo@ees.kyushu-u.ac.jp

Tønnesen, Ole
Technical University of Denmark
Dept. of Electric Power Engineering
DTU, Building 325
DK-2800, Lyngby
DENMARK
Phone: +45 45 25 3511
Fax: +45 45 88 6111
E-mail: ot@eltek.dtu.dk

Traeholt, Chresten
Technical University of Denmark
Dept. of Electric Power Engineering
DTU, Building 325
DK-2800, Lyngby
DENMARK
Phone:+45 45 25 3501
Fax: +45 45 88 6111
E-mail: ct@eltek.dtu.dk

Tsukamoto, Osami
Yokohama Natl. Univ./Fac. of Eng.
Division of Electrical and Computer Eng.
79-5 Tokiwadai, Hodogaya-ku
Yokohama, 240-850
JAPAN
Phone: +81 45 339 4121
Fax: +81 45 338 1157
E-mail: osami@tsukalab.dnj.ynu.ac.jp

Vase, Per
NKT Research Center a/s
Nordic Superc. Techn. A/S
Priorparken 878
DK-2605 Brøndby
DENMARK
Phone: +45 4348 3592
Fax: +45 4348 2501
E-mail: p.vase@nkt-rc.dk

Verweij, Arjan P.
CERN LHC-MMS
Division LHC-MMC
CH 1211
Geneva, 23
SWITZERLAND
Phone: 41.22.767.9432
Fax: 41.22.767.6300
E-mail: Arjan.verweij@cern.ch

Vysotskii. V.V.
Institute for Metal Physics
Nat. Acad. Sci. of Ukraine
36 Vernadsky St.
252142 Kiev
UKRAINE
Phone: +380 44 444 1031
Fax: +380 44 444 1031
E-mail: pan@d09imp.kiev.ua

Wessel, Sander
University of Twente
Low Temperature Division
P.O. Box 217
7500 AE Enschede
THE NETHERLANDS
Phone: +31 53 4893896
Fax: +31 53 4891099
E-mail: w.a.j.wessel@tn.utwente.nl

Wilson, Martin N.
Oxford Instruments
Tubney Wood
Abingdon
OX 13 5QX
UNITED KINGDOM
Phone: +44 1865 882855
Fax: +44 1865 881944
E-mail: martin.wilson@oxinst.co.uk

Yang, Yifeng
University of Southampton
Institute of Cryogenics
Dept. of Mechanical Engineering
Highfield, SO17 1BJ
Southampton, Hampshire
UNITED KINGDOM
Phone: +44 1703 59 3204
Fax: +44 1703 59 3230
E-mail: yifeng@soton.ac.uk

Yazawa, Takashi
University of Twente
Low Temperature Division
P.O. Box 217
7500 AE Enschede
THE NETHERLANDS
Phone: +31 53 4893889
Fax: +31 53 4891099
E-mail: ywa@tn.utwente.nl

Zapretilina, Elena R.
ITER EDA
Naka Joint Work Site
801-1 Mukouyama, Nakamachi
Naka-gun, Ibaraki-ken, 311-0193
JAPAN
Phone: +81 292 70 7773
Fax: +81 292 70 7606
E-mail: Zaprete@itergps.naka.jaeri.go.jp

IV. DISCUSSION OF TODAY'S NEEDS AND TODAY'S PERFORMANCE

As discussed in Section II, HTS must offer distinct economic and technical benefits to find wide use. Since an important technical benefit is the reduction of AC losses, it is important to establish some standard of comparison with present practice. To avoid confusion, it is also necessary to understand what is in the expert literature.

IV.1 FIGURES OF MERIT

A few authors have sought to establish figures of merit. Indeed, Ries et al. have laid out their reasoning with admirable clarity.[1] Here we recall their line of thought and explain why we differ with their conclusion. The figure of merit adopted by Ries et al. is to achieve losses of one-quarter that of copper at 300 K. To quantify this requirement, they use the effective current density, J_{EFF}, and resistivity, r, of copper at 300 K:

$$J_{EFF} = 250\ A/cm^2; \qquad r = 1.8 \times 10^{-6}\ W \cdot cm \qquad \text{(IV.1.1)}$$

Recalling that $E = rJ$, the electric field along a bulk sample is

$$E = 45 mW / Am, \qquad \text{(IV.1.2)}$$

To convert this to a value at 77 K, some estimate of cryogenic efficiency is needed. They assume that it takes 15 W to remove 1 W @ 77 K to 300 K. The maximum allowed dissipation at 77 K to equal copper is then the value in Eq. IV.1.2 divided by 15, or 3.46 *mW/A*×*m*. If J_{EFF} is half of J_c, the value of 3.46 *mW/A*×*m* must be divided by 2, and if the HTS is to be four times as good as copper, the result must be divided by 4. This gives a final value of 0.43 *W/kA*×*m*, which is the goal put forth by Ries et al. This result and the line of thought leading to it are not dissimilar to the discussion presented in Section II.1.2. After presenting their goal, Ries et al. discuss a cable and conclude by noting that Siemens constructed a 10-m, 2-kA cable with an AC loss of 0.8 *W/m* or roughly 0.4 *W/kA-m*.

The emphasis of this report is different, and the goals discussed in Sections II.1.3.2 and II.1.4.3 are more ambitious, for several reasons. First, we recall that AC loss is only one among several contributions to a cable's refrigeration load (see Section II.1.3.1), so there is no unique value to be established without explicitly considering the other contributing factors. Second, we expect the market for underground transmission cable to be smaller than the market for transformers,[2] and thus meeting the requirements for transformers will have greater impact than meeting what may be the more modest requirements for other applications. Third, some interested utilities prefer self-contained refrigeration, with which performance is 30:1, worse than the 15:1 assumed by Ries et al. Finally, and most important, goals must reflect the capital as well as operating cost; only the latter is reflected in the 15:1 ratio or any other measure of

[1] G. Ries et al., *Physica C* **310**: 283 (1998).

[2] A single 30-MVA transformer would have about 5,000–8,500 kA-m of conductor. On the other hand, between 1996 and 1998, the total increase in underground transmission or subtransmission (41-132 kV) cable miles within all of the United States was 1,000 miles (1,600 km). (The increase in length of underground cable below 40 kV was much greater. We suggest that a niche be sought there.)

efficiency. Thus, we are led to suggest more ambitious technical goals for reducing AC losses, as is discussed in Section II.1.4. There is an indissoluble link between the cost of refrigeration and technical goals for AC losses.

IV.2 AC LOSS THRESHOLD LEVEL AND MAGNETIC FIELD REQUIREMENTS FOR VARIOUS DEVICES

The magnetic field requirements for various electrical devices are given in Table IV.2.1 below.

Table IV.2.1. Magnetic Field Environment for Various Electrical Devices

Magnetic Field	Electrical Device
> 1 T	Motors, Generators, SMES, Inductive Fault Current Limiters
0.1 – 0.5 T	Transformers
< 0.1 T	Cables

Source: B. Riley, *Approaches to Very Large Jc Improvements in BSCCO*, 1999 DOE Wire Workshop, Cocoa Beach, Fla., Jan. 12-13, 1999.

How close are existing tapes to achieving these requirements? As can be seen in Figure IV.2.1, if the peak field amplitude does not exceed 0.1 T, the multifilament conductors, available in 1997-1998, are near Ries et al.'s loss threshold of 0.43 *mW/A*x*m* when the field is parallel to the tape.

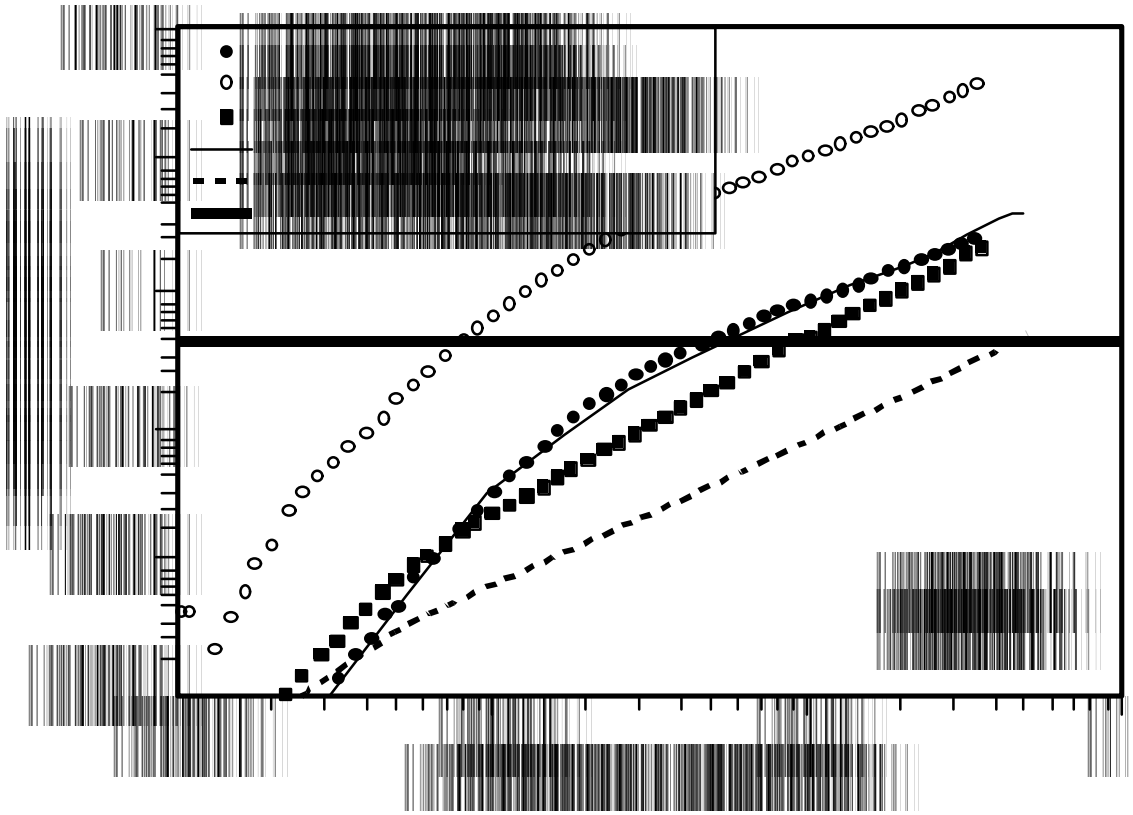

Figure IV.2.1. Sample measurements for Bi-2223 tape with Ag or AgPd-matrix. Source: G. Ries et al., *Physica C* **310**:283 (1998).

Pirelli states that in its development program with EdF (for a 225-kV–1-GVA system), the AC losses measured on a conductor prototype were 0.34 W/m at 2 kA(rms).[3] Recently, further progress has been reported from PSI and the University of Genève.[4] A modest extrapolation from measured data suggests that these groups' Bi-2223 tape would have an AC loss of 1,000 J/m^3 per cycle at 50 Hz and 77 K in a magnetic field of 0.1 Tesla, *perpendicular* to the plane of the tape. If this tape could be mass-produced with that performance and an engineering current density of 10^4 A/cm^2, one would have tape with an AC loss of 0.5 *W/kA*×*m* in the worst case, which occurs when the magnetic field is perpendicular to the plane of the tape.[5] One expects that such tape would have much smaller losses when the field is parallel to the plane of the tape. The authors are not aware of comparable work with Bi-2212.[6]

Hoechst has fabricated tubes of melt-cast Bi-2212 for use as shielding material. A group at Tel Aviv University has investigated its possible use in a fault-current limiter. The group summarizes some of its data in a curve showing losses (0 to 20 W/kg) vs. magnetic field (from 0 to 1,600 Oe).[7] Data were taken for 50 Hz and 77 K.

IV.2.1 Comparison with Copper: Physical Design Trade-Offs for Wire

This report found that hysteresis losses are likely to be larger than eddy current loss in the best of today's tapes. Ries et al. assumed it was reasonable to have equal eddy current and hysteresis loss contributions of 0.225 *mW/A*×*m* for a total of 0.45 *mW/A*×*m*, and they calculated the limits for the relevant conductor parameters of filament diameter and twist length (discussed in Section VI.2.3). The results are shown in the table below.

State-of-the-art HTS tapes with a superconducting filament diameter of 200 *mm* meet the AC loss limit requirement for cables even when the filaments are untwisted and fully coupled. Ries et al.'s basic conclusion is that "economically feasible cables and HTSC-transformers are within reach. Resistive matrix material [discussed in Section VI.2.1] and new concepts with nonmetallic barriers [discussed in Section VI.2.2] promise a breakthrough to lower matrix losses." As already noted, their conclusion refers implicitly to operating costs, not capital cost.

---

[3]Personal communication from M. Nassi to A.M. Wolsky (April 3, 2000).

[4]K. Kwasnitza, S. Clerc, R. Flükiger, and Y. Huang. *Reduction of alternating magnetic field losses in high-Tc multifilament Bi(2223)/Ag tapes by high resistive barriers*, Cryogenics **39**(10):829-841 (Oct. 1999).

[5](1,000 J/m^3 per cycle x 50 Hz x 10^{-4} m^2/cm^2) / (10^4 A/cm^2) = 0.5 *W/kA*×*m*.

[6]AC losses with transport current in Bi-2212 tape were reported by M.N. Pitsakis et al., *Appl. Phys. Lett.* **67**:1772 (1995).

[7] H. Castro, A.Gerber, and A. Milner, "Calorimetric study of ac-field losses in superconducting BSCCO tubes," *Physica* C **331**:141-149 (2000).

Table IV.2.2.1 Calculated Conductor Parameters for 50-Hz Applications.

Temperature	4.2 K (*l* He)	20 K (*l* H_2)	77 K (*l* N_2)
Cryogenic efficiency	1:700	1:70	1:15
Filament diameter $\perp$ *B in* μm			
AC cable ($B = 0.02\ T_{RMS}$)	5	50	220
Transformer ($B = 0.15\ T_{RMS}$)	0.3	3	15
Generator / motor ($B = 1.5\ T_{RMS}$)	0.03	0.3	1.5
Twist length in mm: circular, alloy-matrix, effective matrix resistance $r = 10\ W\text{-}m$			
Cable	7	25	45
Transformer	1	3	6
Generator, motor	0.1	0.3	0.6
Twist length in mm: tape $3.5 \times 0.25\ mm^2$, *Ag-matrix,* $r = 3 \times 10^{-9}\ W\ m$, $B \parallel$ *tape*			
Cable	15	60	120
Transformer	2	7	15
Generator, motor	Not applicable, B $\parallel$ and $\perp$ tape		

With equal contributions from hysteretic loss and matrix loss of *0.225 mW/A•m.*
[G. Ries et al., *Physica C* **310**:283 (1998)].

IV.2.2 Trade-Offs between AC Losses, Type of Conductor, and Cooling

Because of the difficulty in fabricating practical wire from YBaCuO, it is not yet possible to make prototype HTS equipment with YBaCuO conductor. Today, Bi-2212 and Bi-2223 are used for high-amperage conductors and YBaCuO for flywheel bearings and (by Siemens) for fault current limiters. On the other hand, substantial effort is now being devoted to exploring ways to make high-amperage conductor from YBaCuO conductor.

Trade-offs between the types of superconductor are interesting because of their different properties. YBaCuO has better performance in high magnetic fields than does BSCCO in the temperature range of 30-77 K, but cryocooler costs with BSCCO are comparable in this range for DC applications[8]. That is, BSCCO has adequate field dependence at 30 K. In addition, high engineering current densities require thick YBaCuO films and ultra thin substrates, which are limited by stress and handling issues.

One can then expect trade-offs between BSCCO fabricated into round wire, filamentary tapes, or surface-coated tapes. Another trade-off is associated with the type of BSCCO, Bi 2212, or Bi 2223. The performance of each of these can be improved by cryopumping, at the cost of decreased cryogenic efficiency for removing heat due to AC losses.

[8] L.G. Fritzemeier, *HTS Wire at Commercial Performance Levels*, Wire Development Workshop, Cocoa Beach, Fla., Jan. 12-13, 1999.

V. DIFFICULTIES TO BE SURMOUNTED

V.1 POWDER-IN-TUBE TECHNOLOGY

The biggest impediment to using powder-in-tube (PIT) conductor incorporating Bi-2223 or Bi-2212 is the price, now approximately $300/kA-m and $100/kA-m, respectively. One way to reduce these prices is to get more performance from the same material and fabrication processes.

Chief among the desired performance improvements is increased engineering current density — most likely to be achieved by boosting the critical current density of the superconductor. Currently, the sum of the strongly and weakly linked areas comprises about 2–10% of the filament area. Thus, the room for improvement is a factor of between 10 and 50. Increasing the critical current always reduces AC losses. However, increasing the strongly linked fraction alone (rather than the sum of the weakly and strongly linked areas) would only be expected to increase critical currents by up to 50%.

The superconducting film on surface-coated tapes has a high aspect ratio (ratio of the width of the coating to its thickness), exacerbating the anisotropic magnetic loss properties of the material; the ratio of the hysteretic losses in a perpendicular magnetic field, to those in a parallel field, is proportional to the aspect ratio of the superconductor. Interestingly enough, *self-field* hysteretic losses in BSCCO multifilamentary tape decrease with increasing aspect ratio.[1]

Both for Bi-2223 PIT and Bi-2212 surface-coated conductors, the critical current increases with increases in *c*-axis texture (having the *c*-axis of the superconducting crystal grains better aligned perpendicular to the silver substrate). The critical current is found to be highest at the superconductor-silver interface, where the superconductor microstructure has the greatest homogeneity.[2] This suggests that the superconducting filaments should be made as fine as possible, and the interfaces be made with great uniformity. An outstanding question (raised in Reference 3) is why Bi-2212 coated conductor has about a factor of two greater critical currents than Bi-2212 PIT. Will understanding this difference lead to improvements in Bi-2223?

The second desired performance improvement is to decrease the sensitivity of the current density to magnetic field strength and orientation, known in shorthand as “increase flux pinning.” Proton irradiation shows great promise for introducing columnar defects perpendicular to the copper oxide planes that are capable of pinning flux, but no economic process is currently known.

---

[1] A. Polcari et al., *Physica C* **310**:177 (1998).

[2] B. Riley, *Approaches for Very Large J_c Improvements in BSCCO*, 1999 DOE Wire Workshop, Cocoa Beach, Fla., Jan. 12-13, 1999.

Increases in critical current density have also been achieved by optimizing the homogeneity of the precursor powders used in the conventional powder-in-tube method of fabricating BSCCO wires, as well as by using modified PIT techniques.[3]

As shown in Figures II.1.4.3 b and c, even if the cost of conductor were reduced by a factor of 10 or 30, it would still be important to reduce AC losses.

AC losses are generated by three mechanisms: (a) hysteresis in the superconductor; (b) ohmic loss in the metal matrix when current flows from one superconducting filament to another, often called coupling loss; and (c) ohmic loss in the metal matrix that is generated by induced eddy currents that flow even when there are no superconducting filaments. Section VI discusses various strategies for reducing AC losses in BSCCO tapes. Among these is the fabrication of thin twisted superconducting filaments. The use of barriers to reduce coupling losses may allow for longer twist pitch, thereby reducing twisted tape fabrication difficulties. Finally, increased resistance in the metal matrix would reduce eddy currents.

V.2 COATED CONDUCTOR

As mentioned in Section II.2.2, YBaCuO has until recently been very difficult to fabricate into practical conductor because deposition techniques are generally very slow and expensive. To achieve practical YBaCuO conductor at a reasonable cost, this limitation (which is not unexpected during the developmental phase) must be overcome. The processing of YBCO tapes by the Ion-Beam-Assisted Deposition (IBAD) and Rolling-Assisted Biaxially Textured Substrates (RABiTS) techniques shows great promise; these techniques have yielded coated conductors that have achieved engineering critical current densities exceeding 10^8 A/m^2. Processing times have been dramatically decreased in the IBAD technique by using MgO for a buffer layer, rather than yttria-stabilized zirconia (YSZ). CeO_2 has also been used as a buffer material. Production of a one-meter length of substrate-coated tape (which, to date, has only been demonstrated with the IBAD process[4]) takes about twenty hours with YSZ and on the order of minutes if MgO is used (less than a minute for a 10-*nm* layer over the entire meter[5]).

In addition to strong pinning with an external magnetic field parallel to the *a,b*-planes, there is also strong pinning with the field aligned along the *c*-axis. This means that the critical current is not so dependent as it is in BSCCO on the angle between the field and the tape (this should not be confused with AC losses which could be strongly dependent on field direction).

Given the importance of these "second generation" conductors, we describe these developments in some additional detail.[6] Coated YBaCuO tapes are fabricated by depositing a

---

[3]B. Fischer et al., *Fabrication and Properties of Bi-2223 Tapes*, presented at the Applied Superconductivity Conference, Palm Desert, Calif., Sept. 13-18, 1998; G. Grasso et al., *J. Supercond.* **11**:489 (1998).

[4]D. E. Peterson, Los Alamos National Laboratory, private communication, Jan. 27, 2000.

[5]Ibid.

[6]X. D. Wu et al., *Appl. Phys. Lett.* **65**:1961 (1994); P. N. Arendt et al., *Appl. Supercond*. **4**:429 (1996); X. F. Zhang et al., *J. Mater. Res.* **14**:1204 (1999); S. R. Foltyn et al., to appear in *IEEE Trans. on Appl. Supercond*.; also the review and assessment given by D. K. Finnemore et al., *Physica C* **320**:1 (1999) and, most recently, A.P. Malozemoff et al. *Supercond. Sci. Technol.* **13**:1-4 (2000).

relatively thick film (1-5 μm) of YBaCuO on a textured substrate or a textured layer deposited on a polycrystalline substrate. The buffer layer serves both to chemically isolate the superconductor from the metal tape and, in the case of RABiTS, to transmit the texture of the metal to the superconductor.

The powder-in-tube process used for BSCCO tapes produces good uniaxial texturing, but to eliminate the current barriers due to weak links it is necessary to produce a biaxial texture. The ideal substrate material for YBCO is a polished single-crystal oxide material with a lattice matching the superconductor basal plane. The biaxial texture is achieved in the IBAD technique by means of a secondary ion gun, which orients an oxide film buffer layer (YSZ or MgO) that is being deposited on a polycrystalline metallic substrate, usually a nickel alloy. The resulting buffer layer approximates a single-crystal oxide substrate. The biaxial texture is achieved in the RABiTS process by mechanically rolling a face-centered cubic metal (usually nickel), followed by heat treatment.

Optimal texture for the YSZ compound used in the IBAD process requires deposition of a buffer film of thickness ~1 μm. The same degree of texturing is achieved with MgO with a thickness of only 10 *nm*, hence the shorter processing time with MgO. The process by which a biaxial texture develops with MgO deposition is not understood.

The critical current of YBCO films depends on the deposition rate used during their manufacture, dropping linearly from over $2 \times 10^6 A/cm^2$ at 75 K, in a self-field and a deposition rate of 2*Å /s*, to 10^6 *A/cm*^{2} at 240 *Å /s* .[7] However, annealing the high-rate films at 790°C for as little as 20 minutes improved the critical current density (as well as the critical temperature, resistivity, and critical current density in an external magnetic field) to within 20% of the low-deposition-rate values.

IBAD deposition of YSZ or MgO on alloy tapes has yielded superconducting layers with a grain-to-grain alignment within 3 to 5 degrees. (Similar results have been achieved by using the RABiTS process with a variety of oxide layers on textured nickel tapes.) Research lengths of prototype wires in strong magnetic fields at 65 K have already achieved performance levels that exceed those of NbTi and Nb_3Sn in liquid helium.

Values of critical current density consistently greater than 10^6 *A/cm*^{2} in self-field at 77 K are obtainable with RABiTS, and values in excess of $2 \times 10^6 A/cm^2$ have been obtained on both YSZ and MgO substrates. A nonmagnetic tape (Ni-13%Cr) using the RABiTS process has given a critical current greater than $1.5 \times 10^6 A/cm^2$.[8]

Matsumoto et al. have reported the fabrication of YBCO films on textured nickel tapes buffered with epitaxial NiO, using the surface-oxidation epitaxy method. To enhance the superconducting properties of the final YBCO films, the authors subsequently deposited thin

---

[7]S. R. Foltyn et al., *J. Mater. Res*. **12**:2941 (1997).

[8]Preprint by R.A. Hawsey et al., *Development of Biaxially Textured $YBa_2Cu_3O_7$ Coated Conductors in the U.S.*, to be published in Advances in Supercond. XII: Proc. of the 12th Int. Symp. On Superconductivity (ISS '99), Morioka, Japan, Oct. 17-19, 1999. As reported in High T_c Update, Vol. 14, No. 1, Jan. 1, 2000.

oxide cap layers, such as YSZ, CeO_2, and MgO, on the NiO buffer layer. These oxide cap layers, grown epitaxially on the NiO, provided the template for epitaxial growth of the YBCO film. Using a MgO cap layer of 50 nm thickness, the authors obtained tapes with the following results: T_c = 88 K; $J_c = 3 \times 10^5 A/cm^2$ (77 K, 0 T); and 10^4 A/cm^2 (77 K, 4 T, $\boldsymbol{H} \parallel c$).[9]

[9]K. Matsumoto et al., *High Critical Current Density $YBa_2Cu_3O_{7-d}$ Tapes Prepared by Surface-Oxidation Epitaxy Method*, to appear in *Physica C*. As reported in High T_C Update, Vol. 14, No. 2, Jan. 15, 2000.

At the time of this writing, six United States companies (3M, American Superconductor Corp., ERUS Technologies, Intermagnetics General Corporation, MicroCoating Technologies, and Oxford Superconducting Technology) plan to try to produce YBCO coated conductors for power and physics applications. Important work is under way in Göttingen at the Georg-August-Universität Institut für Metallphysik and with its collaborators. Likewise, Hitachi (which worked on IBAD for many years) and Furukawa are pressing ahead.

To date, most work has been on nickel substrates. Nickel offers one improvement over silver: nickel's resistivity is twice that of silver in the range 60–80 K. However, nickel is a ferromagnet, and so it may be the seat of a new hysteresis loss. The IBAD technique typically uses 1-*cm*-wide strips of 100-μ*m*-thick Hastelloy (a nickel-based alloy) or Inconel 625, which exhibit essentially no hysteresis losses. The AC loss properties, in relevant magnetic fields, of the YBaCuO coated nickel tapes are not, however, currently available.

VI. TODAY'S STRATEGIES FOR LOSS REDUCTION

AC losses are generated by three mechanisms: (a) hysteresis in the superconductor; (b) ohmic loss in the metal matrix when current flows from one superconducting filament to another, often called coupling loss; and (c) ohmic loss in the metal matrix that is generated by induced eddy currents, which flow even when there is no transport current in the superconducting filaments.

VI.1 HYSTERESIS

Recall that in a superconductor, current flows in a surface layer, the thickness of which depends on the critical current. In the case of a filament, when the transport current or shielding current due to an external magnetic field is large enough, the current sheath reaches the center of the filament, and this corresponds to full penetration. For fields greater than would be needed for full penetration, hysteresis losses are proportional to the thickness of the filament (see Appendix 1, Fig. A1.1.4). There are two strategies for reducing hysteresis losses in multifilamentary composites: increase the critical current and decrease the filament diameter.

VI.1.1 Increased Critical Current

A number of approaches are available for increasing the critical current in BSSCO. Perhaps the two most important are increasing the strongly and weakly linked area of the superconducting material (currently 2–10% of filament area) and using irradiation to increase flux pinning. The first of these approaches involves changes in processing techniques to achieve phase purity and better *c*-axis alignment, while the second introduces columnar defects perpendicular to the copper oxide planes (i.e., along the *c*-axis) within the BSCCO material. A ten-fold increase in critical current (at about 0.6 T, with the field aligned *along* the *c*-axis) has been achieved by means of proton irradiation of an 85-filament Bi-2223/Ag tape at 75 K.[1] Unfortunately, silver, the matrix material, becomes activated under irradiation; its half life is about one year.

Increases in critical current density have been achieved by optimizing the homogeneity of the precursor powders used in the conventional powder-in-tube (PIT) method of fabricating BSCCO wires. As the Bi-2212 phase is converted to the Bi-2223 phase, the degree of texturing (the area occupied by a given phase) of the Bi-2212 phase is transferred to the Bi-2223 phase.[2] The goal is to maximize the Bi-2223 phase by optimizing the processing. The degree of texturing of the Bi-2212 phase can be enhanced by the cold working process and the previous annealing steps.

VI.1.2 Decreased Filament Diameter

---

[1]B. Riley, *Approaches for Very Large J_c Improvements in BSCCO*, 1999 DOE Wire Workshop, Cocoa Beach, Fla., Jan. 12-13, 1999.

[2]B. Fischer et al., *Fabrication and Properties of Bi-2223 Tapes*, presented at the Applied Superconductivity Conference, Palm Desert, Calif., Sept. 13-18, 1998.

Where the field is greater than would be needed for full penetration, the hysteresis loss density is proportional to the thickness of the superconductor perpendicular to the field. This proportionality provides the incentive for reducing the diameter of the superconductor and, to obtain adequate current-carrying capacity, for making multifilament wires. With superconducting tapes, it is the thickness of the superconductor in the direction perpendicular to the tape surface that is important. In tapes where the filaments are not twisted, the coupling currents can become large enough to saturate the filaments. At that point, the multifilamentary core behaves as one large filament with large hysteresis losses. Therefore, for the strategy of employing multiple filaments to be effective, it is important that full coupling be avoided. Twisting the filaments with a short twist pitch can help (see Section VI.2.3).

VI.2 OHMIC LOSSES IN THE NORMAL MATRIX

There are three basic approaches to reducing eddy or coupling current losses; increasing the effective resistivity of the matrix, introducing interfilamentary barriers to achieve the same end, and twisting the filaments. While the first two approaches are conceptually easy to understand, the same cannot be said for the last. For this reason, the calculation of losses in twisted filamentary composites is treated in some detail.

VI.2.1 Silver Alloy Tubes for BSCCO

From the history of multifilament, low-temperature superconductors, it is known that in addition to twisting the filaments, coupling current losses may be reduced by increasing the resistivity of the matrix between the filaments. In HTS, this approach offers limited promise because changes in the matrix material (the alloys of choice are AgMg, AgMgZr, AgPd, and AgAu, the last two of which increase the cost of materials) affect the formation of oriented Bi-2223 crystals during wire fabrication and treatment. Because of this effect, typical matrix resistivity enhancement is limited to a factor of five to eight at 77 K, and at best to an order of magnitude.[3] Losses for various matrix materials are shown in Fig. VI.2.1.1.[4]

A recent study of AC losses in tapes, using different matrix materials (Ag, Ag alloys, and ceramic barriers), has been published by Oomen et al.[5] With a combination of short twist pitch length and ceramic barriers, they observed the first indications of filament decoupling in magnetic fields perpendicular to the tape (parallel to the *c*-axis of the BSCCO crystals), resulting in a reduction in AC losses in low perpendicular fields.

---

[3]W. Goldacker et al., *Physica C* **310**:182 (1998).

[4]J. Yoo, J. Ko, H. Kim, and H. Chung, "Fabrication of Twisted Multifilamentary BSCCO2223 Tapes by Using High Resistive Sheath for AC Application," *IEEE Transactions on Applied Superconductivity*, **9**(2):2163-2166 (June 1999).

[5]M. P. Oomen et al., *IEEE Trans. on Appl. Superconductivity* **9**:821 (1999).

Sumpton and Collings[6] have found a surprisingly high effective transverse resistivity in filamentary tapes. They attribute this anomalously high value to an aspect ratio dependence of the transverse resistivity (i.e., the influence of the flattened filament array on the transverse current paths).

[6]M. D. Sumpton and E. W. Collings, *Aspect Ratio Dependence of Effective Transverse Matrix Resistivity in Multifilamentary HTSC/Ag Strands*, 11th International Symposium on Superconductivity, Fukuoka, Japan, Nov. 16-19, 1998.

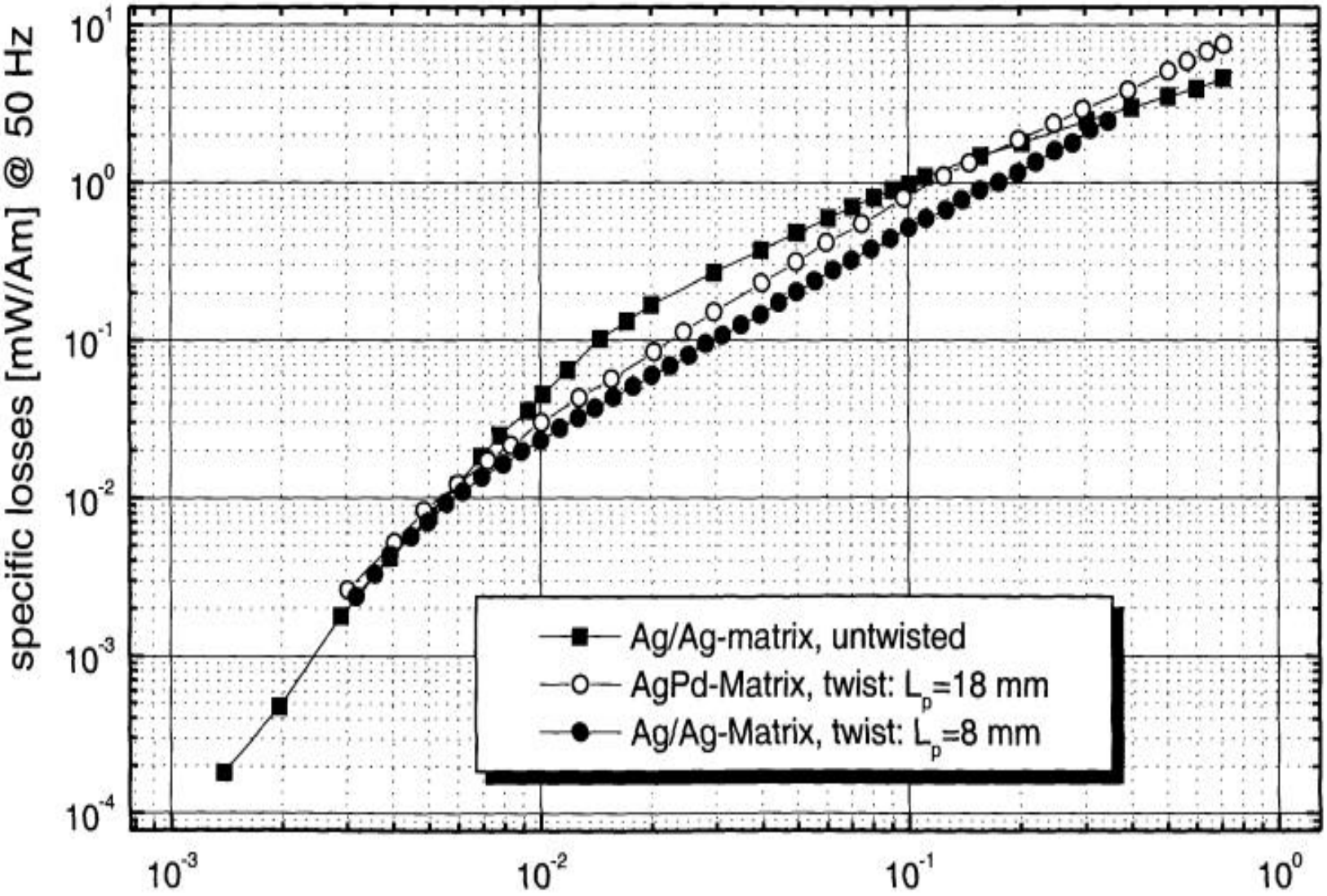

Figure VI.2.1.1. Specific losses at 50 Hz for different matrix material. Source: Presentation at Vacuumschmelze, April 23, 1999.

Blank for figure VI.2.1.1

VI.2.2 Interfilamentary Resistive Barriers

Another approach to reducing coupling current losses is to introduce insulating barriers in the matrix between the filaments. The first successfully applied barrier material was $BaZrO_3$.[7] More recent work has been done with strontium carbonate ($SrCO_3$).[8] Thus far, the focus has been on the successful fabrication of tapes using resistive barriers, although it is clear that the approach has utility in reducing coupling losses.

Two basic approaches have been developed: the Dip-Coated Barrier (DCB) technique, where the hexagonal monocores are dip-coated in a paste of $SrCo_3$ and ethanol prior to bundling; and the Wire-in-Tube Barrier (WITB) technique, where the ring-like spacing between the Ag-sheathed monocore and a surrounding Ag tube is filled with barrier material, followed by

---

[7]Y. B. Huang and R. Flükiger, *Physica C* **294**:71 (1998); Y. B. Huang et al., *IEEE Trans. on Appl. Superconductivity* **9**:1173 (1999).

Y.B. Huang, M. Dhallé, G. Witz, et al., "Development of Bi(2223) multifilamentary tapes with low ac losses," *J. Supercond*. **11**(5):495-505 (Oct. 1998).

M. Dhallé, A. Polcari, F. Marti, et al., "Reduced filament coupling in Bi(2223)/BaZrO3/Ag composite tapes," *Physica* C **310**(1-4):127-131 (Dec. 1998).

K. Kwasnitza, S. Clerc, R. Flükiger, et al, "Alternating magnetic field losses in high-Tc superconducting multifilament tapes with a mixed matrix of Ag and BaZrO3," Physica C **299**(1-2):113-124 (April 10, 1998).

K. Kwasnitza, S. Clerc, R. Flükiger, et al., "Reduction of alternating magnetic field losses in high-Tc multifilament Bi(2223)/Ag tapes by high resistive barriers," *Cryogenics* **39**(10:)829-841 (Oct. 1999).

M. Dhallé, L. Porcar, M. Ivancevic, et al., "Current transfer lengths in multifilamentary superconductors with composite sheath materials," *IEEE Trans. on Appl. Supercon*. **9**(2):1093-1096, Part 1 (June 1999).

Y.B. Huang, M. Dhallé, F. Marti, et al., "Oxide barriers and their effect on AC losses of Bi,Pb(2223) multifilamentary tapes," *IEEE Trans. on Appl. Supercon*. **9**(2):1173-1176, Part 1 (June 1999).

[8]H. Eckelmann et al., *Physica C* **310**:122 (1998); W. Goldacker et al., *Physica C* **310**:182 (1998); W. Goldacker et al., *Novel Resistive Interfilamentary Carbonate Barriers in Multifilamentary Low AC Loss Tapes*, ASC 98, Palm Springs, Calif. [Talk MMA-05), published version in *IEEE Trans. on Appl. Superconductivity* **9**:2155 (1999]; H. Eckelmann et al., *AC Losses in Multifilamentary Low AC Loss Bi(2223) Tapes with Novel Interfilamentary Resistive Carbonate Barriers*, ASC 98, Palm Springs, Calif. (Poster LLB-02), published version in *IEEE Trans. on Appl. Superconductivity* **9**:762 (1999).
H. Eckelmann, M. Quilitz, C. Schmidt, et al., "AC losses in multifilamentary low AC loss Bi(2223) tapes with novel interfilamentary resistive carbonate barriers," *IEEE Trans. on Appl. Supercon*. **9**(2):762-765, Part 1 (June 1999).

W. Goldacker, M. Quilitz, B. Obst, et al. "Novel resistive interfilamentary carbonate barriers in multifilamentary low AC loss Bi(2223)-tapes," *IEEE Trans. on Appl. Supercon*. **9**(2):2155-2158, Part 2 (June 1999).

H. Eckelmann, M. Quilitz, M. Oomen, et al., "AC losses in multifilamentary Bi(2223) tapes with an interfilamentary resistive carbonate barriers," *Physica* C **310**(1-4):122-126 (Dec. 1998).

swaging and drawing.[9] The main difference between the resulting tapes is that DCB tapes have a continuous, fully connected barrier net around the monocores, whereas in WITB tapes there is a ring-like separated barrier geometry about each monocore. DCB tapes have a higher superconductor content compared with conventional tapes, and WITB tapes have a more homogeneous barrier layer, which may minimize defects. As of this writing, the DCB approach has not yielded wires of reasonable length that have current-carrying capacity exceeding that of the BSCCO powder-in-tube method.[10]

R. Flükiger has recently reported to the authors of this report better results with strontium zirconate ($SrZrO_3$). His group made 50 m of tape, which was then cut into 2-m lengths and tested. The best results for AC losses are in the range of 0.33 *W/kA-m*, with average critical currents of 10^8 A/m^2. AC loss measurements with $BaZrO_3$ barriers have been reported by Dhallé et al.[11] and Kwasnitza et al[12]. The uncoupling of filaments by using magnesium oxide (MgO), without significantly degrading tape performance, has been observed by Lennikov et al.[13] The group at Sumitomo under K. Sato is also working on barriers made from MgO, but performance figures are not known to the authors.

VI.2.3 Twisted Filaments

The existence of coupling losses led to the strategy of twisting the filaments. It should be understood that only filaments transverse to the field are uncoupled by twisting; filaments stacked along the field are uncoupled even if the filaments are untwisted.

A simple example that demonstrates how twisting can cancel the induced field is given by the case of two parallel superconducting filaments in a resistive silver matrix in the form of a plate with the magnetic field perpendicular to the plane of the silver. A changing magnetic field induces a current that flows along the filaments and through the matrix, where it dissipates energy. If the filaments are made to cross over each other with equal matrix areas in the regions where they are still parallel, the current cancels and the loss vanishes. This is shown in Figure VI.2.3.1.

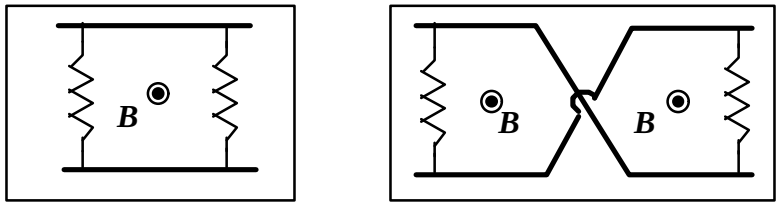

(*a*) (*b*)

[9]W. Goldacker, M. Quilitz, B. Obst, et al., "Reduction of AC losses applying novel resistive interfilamentary carbonate barriers in multifilamentary Bi(2223) tapes" *Physica* C **310**(1-4):182-186 (Dec. 1998).

[10]B. ten Haken and M. Oomen, private communication, Feb. 8, 2000.

[11] M. Dhallé et al., *Physica* C **310**:127 (1998).

[12] K. Kwasnitza et al., *Physica* C **299**:113 (1998).

[13]V. Lennikov et al., *IEEE Trans. on Appl. Superconductivity* **9**:2553 (1999).

Figure VI.2.3.1. In (*a*), the changing magnetic field generates a current that flows through the superconducting filaments and dissipates energy in the Ag matrix; in (*b*), the twist cancels the current to first order and the loss vanishes.

A somewhat more sophisticated example, one that allows the calculation of the critical length, is given in FigureVI.2.3.2, where $I(x)$ is the current *per unit distance* in the *z*-direction.

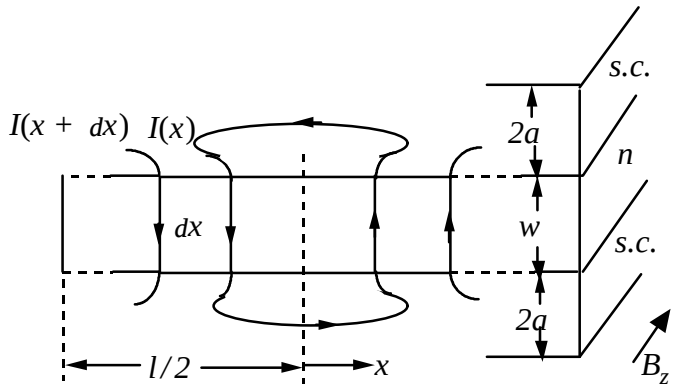

Figure VI.2.3.2. Screening currents in a composite of superconducting (*s.c.*) and normal (*n*) materials in slab geometry. $\dot{B}$ is assumed to be position-independent.

The screening currents cause a voltage to appear across the normal region, and currents through this region produce a resistive loss. The induced voltage is

$$\mathrm{E} = -\frac{\mathrm{d}f}{\mathrm{d}t} = -\dot{B}\,\{\textit{Area of the loop}\} = -2\dot{B}(wx). \qquad \text{(VI.2.3.1)}$$

From the figure, it is clear that $I(x + dx) - I(x) = dI(x)$, and therefore by Ohm's law

$$dI(x) = -\frac{2\dot{B}\,wx\,dx}{rw}, \qquad \text{(VI.2.3.2)}$$

where r is the resistivity.[14] If one solves the differential equation

$$\frac{\mathrm{d}I(x)}{\mathrm{d}x} = -2\frac{\dot{B}}{r}x \qquad \text{(VI.2.3.3)}$$

resulting from Eq. VI.2.3.2,

$$I(x) = -\frac{\dot{B}}{r}x^2 + C\,. \qquad \text{(VI.2.3.4)}$$

[14]It should be noted that the presentation here follows that of Wilson [M.N. Wilson, *Superconducting Magnets* (Clarendon Press, Oxford, 1986)] but differs in that some minor errors have been corrected. (He has a sign error and is missing a factor of two. His plus sign would lead to an imaginary "critical distance." The factor of two leads to a final result that differs from Wilson's by a factor of $\sqrt{2}$).

Imposing the boundary condition that the induced field (opposite to B_z shown in the figure) vanish at the surface $x = l/2$ by setting $I(l/2) = 0$, which means that the constant of integration in Eq. VI.2.3.4 is $C = \frac{\dot{B}}{r}\frac{l^2}{4}$, gives the result

$$I(x) = \frac{\dot{B}}{\rho}\left(\frac{l^2}{4} - x^2\right) . \qquad \text{(VI.2.3.5)}$$

The maximum current is at $I(0)$ and will fill the cross section when the critical current is reached: i.e., when $I(0) = 2aJ_c$. This condition, substituted into the above equation, defines the *critical length* l_c as

$$l_c = 2\left(\frac{2\alpha\rho J_c}{\dot{B}}\right)^{1/2} \qquad \text{(VI.2.3.6)}$$

The conclusion is that composite wires should be twisted with a pitch much less than l_c if eddy current losses in the normal material are to be minimized.

In untwisted tapes, the induced coupling currents flow in a plane perpendicular to the magnetic field direction. In twisted tapes, the current flows through the matrix material in a direction parallel to the field (see Section VI.2.3.1) so long as the outer ring of filaments is not saturated. This is illustrated in Figure VI.2.3.3.

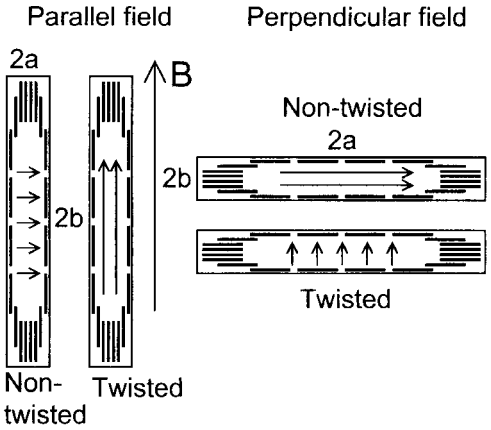

Figure VI.2.3.3. Direction of the interfilamentary coupling currents below saturation (only the outer filaments are shown). Source: M. P. Oomen et al., *Physica C* **310**:137 (1998).

The outer ring of filaments will to some extent shield the interior of the tape.

Twisting the superconducting filaments does not come without a cost. The losses in untwisted tape for magnetic fields that are less than that required for penetration are *less* than

those for twisted filament tape, while the losses are *more* than those in twisted tape for fields exceeding the value needed for full filament penetration.[15] This can be seen in Figure VI.2.3.4.

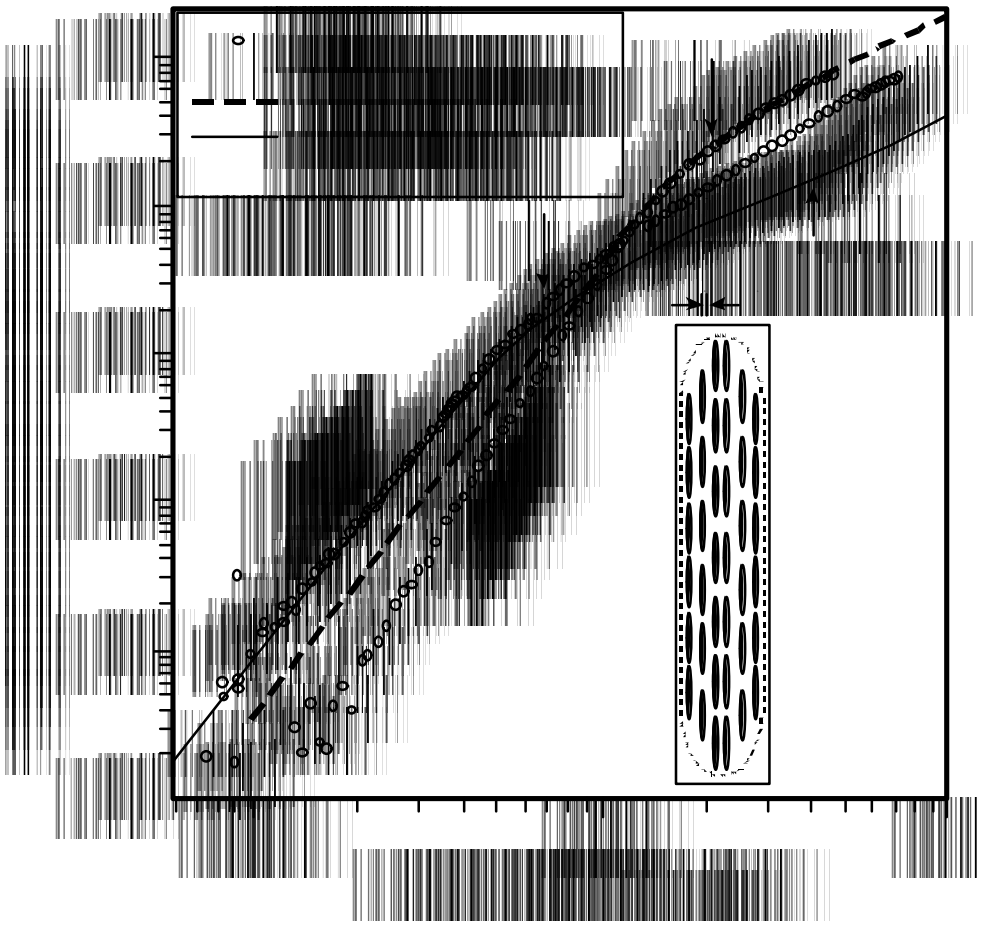

Figure VI.2.3.4. Loss per cycle per meter of 37-filament tape. The twist pitch is 10 *mm* and the critical current density is about 2×10^8 A/m^2. lt is the effective thickness of the silver matrix perpendicular to the field, which is parallel to the tape (vertical in the figure). The penetration fields, B_p, for twisted and untwisted tape are indicated. Source: Y. Yang et al., *Physica C* **310**:147 (1998).

In FigureVI.2.3.4, the total loss is the sum of the superconductor loss and the coupling loss. Q_C is the critical coupling field. Twisting offers an advantage, since one generally wants to operate the tape in the high field region.

The twist pitch of the tape used to obtain the data shown in the figure above was 10 *mm*, but twist pitches as small as 3.5 *mm* in alloy tape have been produced[16] with a J_c of about $2 \times 10^8 A/m^2$ and a J_e of greater than $5.5 \times 10^7 A/m^2$. The difference in losses as a function of

[15]See also Y. Yang et al., *IEEE Trans. on Appl. Superconductivity* **9**:1177 (1999).

[16]F. Darmann et al., *Techniques for lowering eddy current losses in Bi-2223 tapes and devices*, EPRI-sponsored Workshop on AC Losses, Palo Alto, Calif., April 8-9, 1999.

pitch length can be clearly seen in Figure VI.2.3.5. Note also the large difference in losses between parallel and perpendicular magnetic fields.

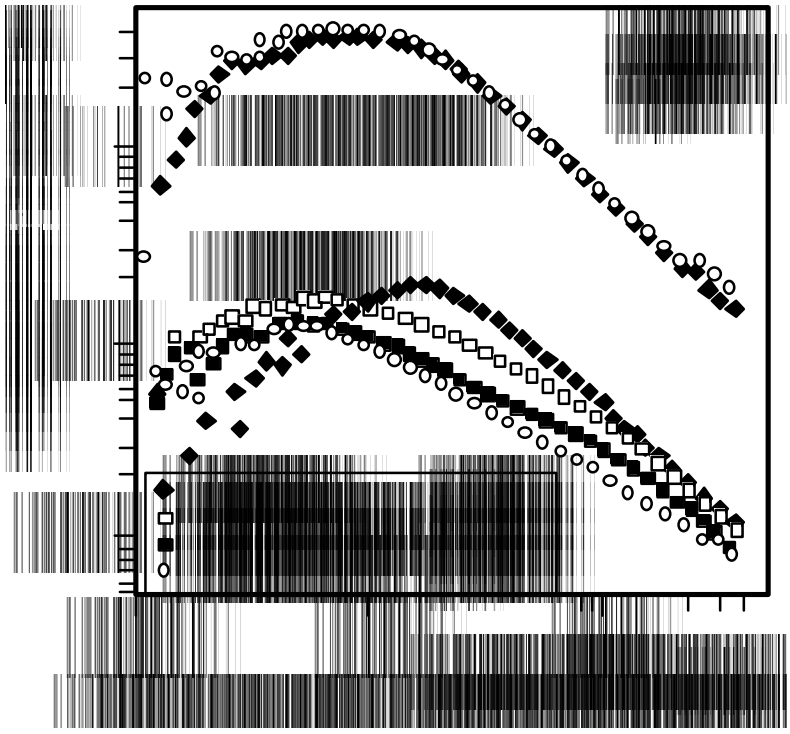

Figure VI.2.3.5. AC losses measured in Ag-matrix tapes with various twist pitches. Note the loss normalization. Source: Oomen et al., *Physica C* **310**:137 (1998).

VI.3 STABILITY AND HTSC

As was discussed earlier, two of the strategies for reducing coupling or eddy current losses are to increase the resistivity of the normal matrix or put resistive barriers around the superconducting filaments. However, higher resistivity means reduced thermal conductivity and the possibility of decreased stability. The key factors in instability are shown in Figure VI.3.1.[17]

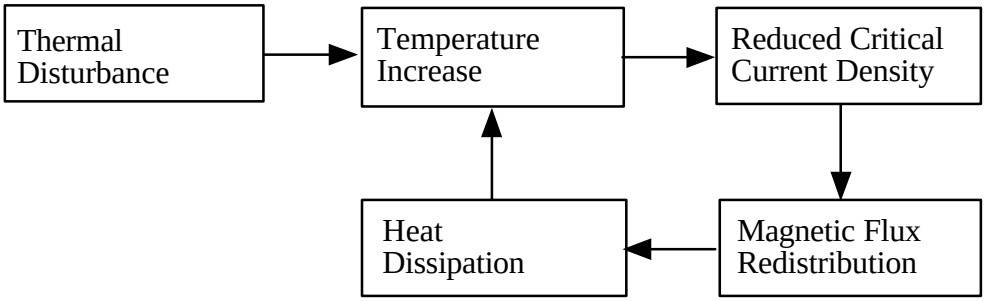

Figure VI.3.1. Instability is both an electromagnetic and a thermal

[17]A. J. M. Roovers, *An Experimental Study of AC Losses in Superconducting Wires and Cables* (CIP-Gegevens Koninklijke Bibliotheek, Den Haag, 1989).

problem.

A thermal disturbance might be generated by flux jumping or by mechanical motion to relieve stresses. Both heat and magnetic fields move through a superconductor by diffusion, so when the magnetic diffusion coefficient is significantly less than the thermal diffusion coefficient, heat cannot be conducted away and the dissipated energy raises the superconductor's temperature.

Much of the concern about stability grew out of experience with low-temperature superconductors, such as NbTi, where stability requirements led to significant design constraints. For example, the heat generated per unit length during the quenching of a superconducting filament depends on its diameter. Given that the diffusion coefficients are fixed, stability requirements set a maximum filament diameter, typically 50-100 μm in LTS materials.

In HTS tapes, the far greater heat capacity of HTS guarantees stability at much larger filament diameters. In addition, the thermal conductivity of HTS is about an order of magnitude greater at 77 K than at 4 K.[18] In any case, the filament thickness for HTS along the *c*-axis is ~25 μm, and material properties and cooling are such that any quench is unlikely to propagate.

The normal-to-superconducting transition in HTS is also less abrupt (lower *n*-value) than in LTS, because of thermally activated flux creep and macroscopic inhomogeneities.[19] This means that heat can be generated at subcritical currents, a factor that must be taken into account when designing practical devices. However, even at 30 K, while stability cannot be ignored, its requirements do not drive design.

Thus, stability is not a problem for single tapes, although layers of tapes with poor cooling could raise stability questions.

VI.4 ORDER-OF-MAGNITUDE COSTS

At this time, the cost of pursuing any of the approaches to reduced AC losses in Bi-2223 is unclear. No new fabrication method to increase the critical current density or decrease the filament size is discussed in the open literature. The only way known to the authors to increase critical current density is to operate at even lower temperatures. By dropping from 77 K to 4.2 K, one picks up a factor of 5.5 for Bi-2223 and perhaps a factor of 45 for Bi-2212. As was discussed in Section II, this change reduces annual cost. Here, we note that a precise estimate of the best operating temperature and the benefit of operating there must also take account of (1) the increase in ohmic losses in the normal metal matrix that would result from its decrease in resistivity as its temperature falls and (2) the increase in cost of removing heat that flowed from the environment to the cold region, something that is very important to cable developers.

The cost of twisting filaments is likely to be negligible, unless twisting increases the reject rate of the conductor at the manufacturer. The cost of interfilamentary barriers is not

[18]T.P. Sheahen, *Introduction to High-Temperature Superconductivity* (Plenum, New York, 1994), Section 17.4; see also J. Lehtonen et al., *Physica C* **310**:340 (1998).

[19]J. Lehtonen, R. Mikkonen, and J. Paasi, *Physica C* **310**:340 (1998).

known, but we expect that conductor manufacturers will pursue this approach when they supply the demonstration transformer planned by EdF and the U.S. transformer project being led by ABB.

Before ending this section, we describe the room for improvement between today's published price, \$300/kA-m, for Bi-2223 tape and the cost of materials that go into that tape. The cost of silver is often discussed, but the commodity price of silver is \$134/kg or \$1.34/g, which should be compared with \$0.50/g from BSCCO powder. With today's performance, the volume of 1 kA-m at 77 K of tape is 7.8 cm^3 and the cost of materials is about \$20/kA-m. Significantly reducing the future price of Bi-2223 tape is not ruled out by the cost of silver. Of course, learning how to use less silver would help, as shown by one manufacturer who presented the following graph.

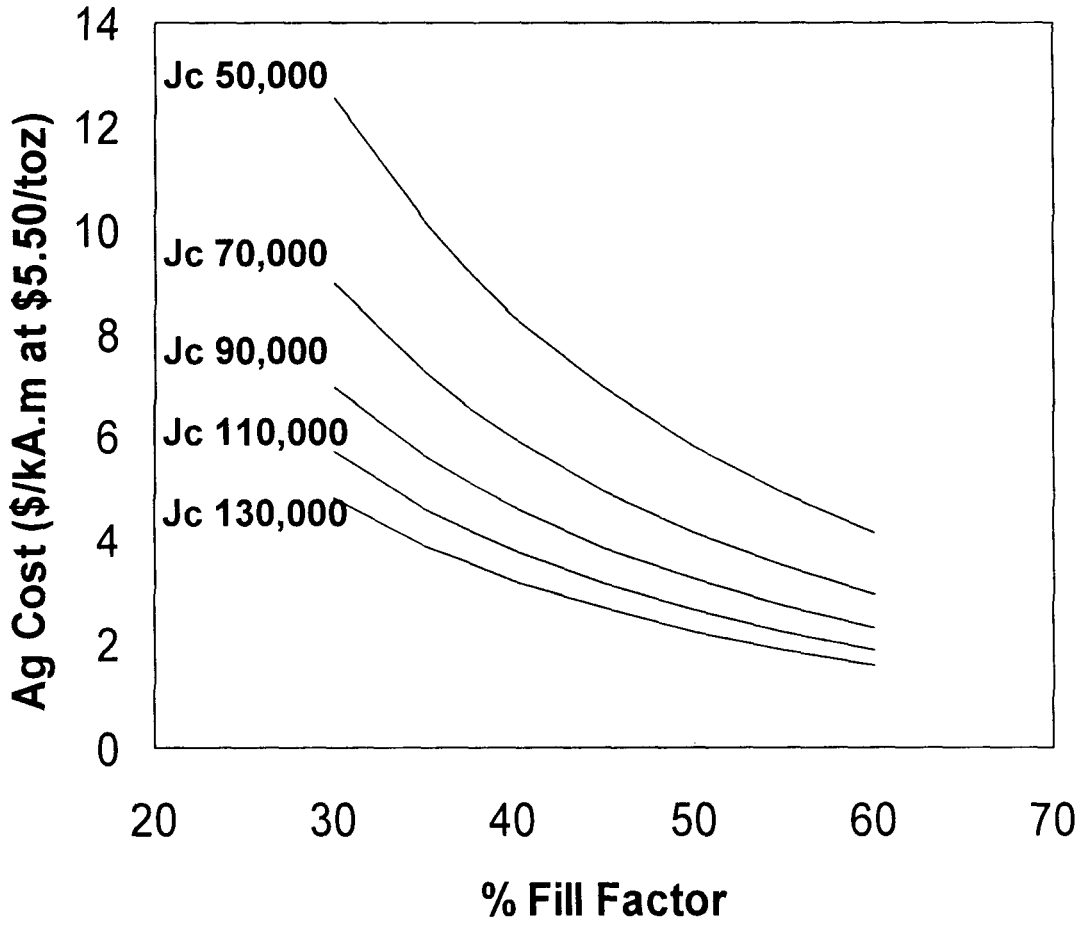

Figure VI.4.1. Silver cost (\$/troy oz)[20] as a function of fill factor with the critical current as a parameter. Source: L. G. Fritzemeier et al., *HTS Wire at Commercial Performance Levels*, presented at the Wire Development Workshop in Cocoa Beach, Fla., Jan. 12-13, 1999.

[20] 1 troy oz $= \frac{1}{12} lb = \frac{1}{12 \times 2.2} Kg \approx 38\ g.$

VI.5 THE PROMISE OF YBaCuO "COATED CONDUCTOR"

During the past 10 years, Bi-2223 has received the most attention from wire developers. The result is conductor that has served the need created by the development of prototype devices incorporating ceramic superconductor. A manufacturing process has been developed that provides long lengths of robust tape that has 5-micron-thin filaments and critical current densities of 35,000 A/cm^2. The aspect ratio of the filaments is roughly 4:1, and the aspect ratio of the tape is in the range 10:1 – 15:1. Typically, two thirds of the volume of the tape is composed of silver alloy and the remainder is Bi-2223. Today's price is $300/kA-m.

As discussed in Sections II.2.3 and V.2, during the past five years, attention has been given to the possibility of making high-amperage conductor by laying a film of YBaCuO on a suitably prepared substrate of nickel. This interest derives from the wish to make less expensive ceramic superconductor with better current density in magnetic fields and less anisotropy. Film thicknesses of 1-2 microns are usually made. Critical current densities in the range 0.5 - 2.0 $\times$ 10^6 A/cm^2 have been reported by many groups. (To date, critical current density declines as film thickness increases; no one knows why.) Such conductor is made slowly, in lengths on the order of meters.

It is not too early to speculate about the possible reduction in AC losses that might result from successful development. We will do so here, using a simple intuitive approach that is compatible with the more systematic developments reviewed in other sections of this report.

We consider two superconductors that have different critical current densities. Call the one with higher critical current density "Y" and the one with lower critical current density "B". These two superconductors can be made from different materials or from the same material but at different operating temperatures. For the sake of definiteness, suppose the "B" type has a critical current density of 33,000 A/cm^2 and the critical current density of the "Y" type is 500,000 A/cm^2. We assume each type can be described by the phenomenological theory reviewed in the Appendix, and each has a high enough n-value to allow the London-Bean Model to provide an order-of-magnitude approximation. In that case, the energy of the magnetic field that penetrates the conductor is irreversibly dissipated with each cycle. (In other cases, only a fraction of the energy might be dissipated.) The energy density is proportional to B^2 in the superconductor. The superconductor can be fabricated no thicker than needed, and the volume of 1 kA-m of superconductor equals $(I / J_C \times 1\ m)$. The energy dissipated per cycle per kiloampere-meter would be as shown below:

> Energy dissipated per cycle per kiloampere-meter equals the fraction of energy density lost to irreversible processes times the average energy density in HTS times the volume of penetrated HTS.

Energy dissipated per cycle per kiloampere-meter

$$= (\text{constant}) \times B^2 \times ((I / J_c) \times 1\ m)$$

Now we consider the ratio of loss per cycle in the two superconductors when they carry the same current in the same field.

(Energy dissipated in "B") / (Energy dissipated in "Y")

$$= (J_{c\,"Y"} / J_{c\,"B"}) = 500/33 = 15$$

One sees the reduction of AC loss with increased critical current density, if this ratio has semi-quantitative reliability. In our example, the losses would be 15 times smaller in the "Y" type than in the "B" type. In fact, Pirelli has called attention to the inverse relation between current density and AC losses in discussing future desires for cable.[21] Furthermore, it appears possible to make thin enough YBaCuO films that one can avoid having to pay for "idle superconductor."

The possibility of obtaining high current density and thin film together raise the reasonable hope that YBaCuO coated conductor can very substantially reduce AC losses.

VI.6 TODAY'S EXPERIMENTAL SITUATION WITH YBaCuO "COATED CONDUCTOR"

It is expected that coated conductor will soon be available in 10-m lengths. Today, it is made in "meter lengths." Today's measurements of AC loss can only be done on single tapes. This leaves unanswerable two important questions, the resolution of which may have to wait until more tape is available.

First, the magnetic field arising from transport current within a single tape will have a non-negligible component perpendicular to the tape. This is true for DC, as well as for AC. This perpendicular component suppresses the critical current density and so increases losses. While it is possible to think of ways to try to disentangle these "orientation losses" from "AC losses," experimentalists have not yet had the sustained opportunity to do so. In fact, one group is said to have tried this by laying three Bi-2223 tapes side by side and connecting them in parallel – thus reducing the relative importance of the perpendicular component compared with the tangential component. The result was an apparent increase in critical current density, which rose from 35,000 A/cm^2 to almost 65,000 A/cm^2.

Second, the substrates that have been most widely used are made of nickel. Nickel is a ferromagnet and it displays hysteresis, which causes the dissipation of electrical energy and the generation of heat. To our knowledge, no experiments have been performed in which coated conductor on a nickel substrate was subjected to 50-60 Hz magnetic fields in the range of 0.1–0.5 T. Such tests would be desirable, as would tests on the promising nonmagnetic nickel-13% chrome alloys now being investigated by ORNL.

[21] M. Nassi, *2000 Wire Development Workshop Proceedings* (forthcoming), U.S. Department of Energy Workshop, held in St. Petersburg, Fla, Feb. 2000.

VII. WHAT IS TO BE DONE

Here, we recall the central conclusions of this report and suggest some topics worthy of future investigation or increased future investigation.

VII.1 EFFECTS OF AC LOSSES ON DEVICE COST AND PERFORMANCE

The importance of reducing AC losses is indissolubly related to the cost and performance of the cryogenics that would be part of the equipment that incorporates ceramic superconductors. The worse the performance and the higher the cost of the cryogenics are, the more important the reduction of AC losses becomes. Some authors with technical backgrounds assume that the ratio of input shaft power to output cooling power is 15:1, and they do not dwell on the capital cost of the cryogenics. Some utilities prefer self-contained refrigeration. The performance of such refrigeration is approximately 25:1 at 77 K and declines as temperature falls; furthermore, its capital cost is not negligible. If such cryogenics are necessary, then reducing AC losses becomes even more important and AC loss performance goals should be more ambitious than otherwise.

Among the devices now under development, AC losses will have their greatest impact on the economics of transformers. Although a near-term goal for AC losses of 0.25 W/kA-m is sometimes proposed, we find good reason to aim for lower losses, if today's cryogenics must be employed. Transformers likely offer the largest potential market for ceramic superconductors. A single 30-MVA transformer embodies 5,000–8,500 kA-m.

Improved cost and performance for cryogenics would be desirable. They could be achieved if the electrical infrastructure included "superconducting substations" at which many HTS transformers (and other HTS equipment) were located. Such a station could be served by a common cryogenic facility. Improved cryogenic performance could also be obtained if utilities chose to supply their facilities with coolant delivered by truck or, if circumstances permit, by pipeline.

AC losses also contribute to the refrigeration load of cable. However, the large surface-to-volume ratio of cable permits more heat to flow from the environment to the cold region than is generated by AC loss in the superconductor. Thus, even if the superconductor's AC loss is reduced to zero, a substantial refrigeration load will remain. Stated goals for AC loss in cables should not be separated from these other considerations.

VII.2 PERFORMANCE GOALS FOR AC LOSSES

W suggest that the technical community focus on the long-term goal of reducing AC loss until it falls in the range of 0.08–0.25 W/kA-m at 50–60 Hz, in magnetic fields from 0.1–0.5 T, at the desired operating temperature. We believe this goal is second in importance only to the goal of reducing the capital cost of conductor.

VII.3 ACTIVITIES BEARING UPON AC LOSSES THAT DESERVE INCREASED CONSIDERATION

We suggest the following activities deserve increased attention, which may provide the basis for increased effort and support.

VII.3.1 Relationship between Cost-Performance Goals for AC Losses and for Cryogenics

As discussed earlier, the significance of the cost and performance of cryogenics and AC losses are interrelated. It would be helpful to formulate and clarify the requirements that each places on the other, particularly in the case of transformers.

VII.3.2 Computer Modeling and Simulation of Coils

In the long run, numerical work can reduce the cost of development. However, ceramic superconductors are anisotropic, and so one cannot simply use most of the codes that are already written to anticipate future performance and assist in the design of windings. We suggest that pertinent existing codes and the imperfections in them be identified and the technical requirements for new codes or additions to existing codes be established.

VII.3.3 Localization of AC Losses

Promising work to reduce AC losses in Bi-2223 tape has been reported in recent years. The improvements are likely due to changed construction of the tape. However, little work to observe the localized flow of current has been done; with one exception, only measurements of spatial averages are reported. Two possibilities are open: (a) observe the spatially resolved flow of direct current (e.g., magneto-optical imaging, micro-Hall probes) in conductor architectures designed for AC and (b) observe the spatially resolved flow of alternating current. For the next several years, only BSCCO tape will be available for prototype devices.

VII.3.4 AC Losses in Coated Conductor

Hope for low-cost, high-amperage conductors is focused on the development of "coated conductor," by which we mean films of YBaCuO (or REBaCuO) that are deposited on a suitable substrate, currently nickel or a nickel alloy. It is not too early to consider how to reduce the AC losses in these conductors. (Figures II.1.4.3b and II.1.4.3c show the effect of AC losses on the economics of hypothetical conductors under several capital assumptions.) Several paths are open for investigation.

VII.3.4.1 Measurement of AC Losses in Today's Coated Conductor

To date, no one has reported measurements of AC loss in the range 0.1-0.5 T and 50-60 Hz. These measurements (all orientations) and others (in a wider range of frequencies) could suggest the scope of the problem and its roots. Temperatures in the range 40-77 K are likely to be relevant.

VII.3.4.2 Effect of Coated Conductor Substrate on Losses

To date, most work has been done on nickel. As is well known, pure nickel is a ferromagnet; its electrical resistivity is less than twice that of pure silver. Some investigators have sought suitable nonmagnetic alloys. This goal will remain important, unless results from measurements of the type described in Section VII.3.3.1 show otherwise. Investigators working on PIT fabrication have sought silver alloys with increased electrical resistivity. Similar attention to nonmagnetic nickel alloys with increased electrical resistivity may be worthwhile. Finally, the resistivity of the substrate must also be considered in light of its potential role as a conductor when the device is subject to an inrush of power caused by a fault elsewhere in the system. [The buffer layers are ceramics and so are electrical and thermal insulators; however, their thickness (on the order of micrometers) may not cause problems.]

VII.3.4.3 Effect of Induced Currents in the Coated Superconductor

To date, most discussion of coated conductor has been about its fabrication as a film of superconductor on a normal substrate. Substantial currents can be induced in a sheet of excellent conductor. Some consideration might be given to the desired width of the coated conductor and to how two adjacent superconductors could or should be "insulated" from each other. (In today's tape, each BSCCO filament might be $2mm \times 5mm$, and each filament is supposed to be separated from its neighbors by a silver alloy.) Promising work has suggested how to reduce AC losses in Bi-2223 tape by including insulating sheaths or jackets between filaments. The relevance of this work (or approaches suggested by it) to coated conductor should be considered.

VII.3.5 Precompetitive Cooperation to Reduce AC Losses

The issues broached above are technically demanding and unlikely to be resolved in the near term. Experts on AC loss are active in Asia, Europe, and the United States. Many of these experts have met each other. It may be feasible and cost-effective to address the need to reduce AC losses by fostering precompetitive, inter-institutional collaborations, including international collaborations. It would also be helpful to standardize testing and calibration procedures for AC coils and cables.

APPENDIX 1: A CRITICAL STATE MODEL

This appendix recalls standard results of the critical state model that describes NbTi and Nb_3Sn. Some comments are made with regard to high-temperature superconductors (HTS) to highlight key differences.

As mentioned in Section II.4.1.1, it is assumed in the critical state model[1] that the critical current density J_c flows in any current-carrying portion of a superconductor. If there is no flux line pinning, the magnetization curve for a LTS is similar to that shown in Figure A1.1.1 below. When H_a is decreased from H_{c2} to zero, the magnetization return path closely follows the path described by the magnetization during the increase of H_a. The critical current for such a superconductor rapidly decreases with increasing applied magnetic field.

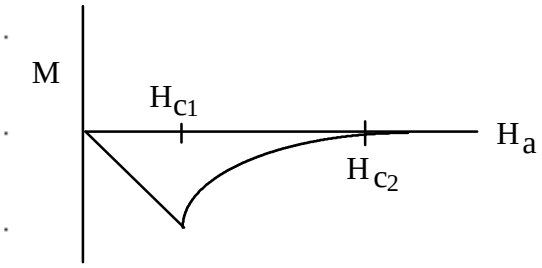

Figure A1.1.1. Magnetization vs. applied magnetic intensity for a reversible Type II superconductor.

For $H_a < H_{c1}$, $M = -H_a$, and the superconductor exhibits perfect diamagnetism with only a Meissner surface current flowing to the penetration depth l so as to shield the interior.

For H_a just above H_{c1}, a bulk current density, set equal to J_c in the critical state model, begins to flow in addition to the surface current. Since $J = J_c$, the depth of penetration of the bulk current is fixed by the magnitude of the field. The current distribution depends on the geometry (e.g., a sine distribution for an applied field perpendicular to a round wire). Such a distribution shields the interior of the wire by producing a uniform internal field, equal and opposite to the applied field.

In the region $H_{c1} < H_a < H_{c2}$, vortices enter the superconducting material because such penetration leads to a reduction in Gibbs free energy, and equilibrium is due to the mutual repulsion of the vortices. The increment in Gibbs free energy is $dG = -\mu_0 M\, dH_a$, so that

$$G(H_a) - G(0) = -\mu_0 H_a \int_0^{H_a} M\, dH_a. \qquad \text{(A1.1.1)}$$

In the region $H_a > H_{c2}$, the magnetization M vanishes and the flux density is $\mu_0 H_a$.

[1] C. P. Bean, *Phys. Rev. Lett.* **8**:250 (1962); *Rev. Mod. Phys.* **36**:31 (1964).

There are various types of lattice imperfections that help inhibit flux line motion (pinning). These could be lattice dislocations, the phenomenon of "twinning," where the *a* and *b* axes of the HTS are interchanged in the unit cells comprising the crystal lattice so as to create twin boundaries, which are important for YBCO, or oxygen vacancies in BSCCO. Because of these imperfections, LTS and HTS will both typically have magnetization curves that look like those in Figure A.1.1.2.

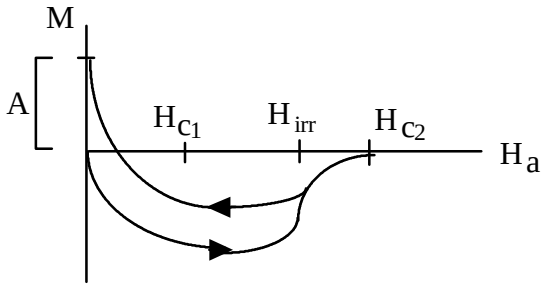

Figure A1.1.2. Typical magnetization curve. The region A corresponds to flux trapping by pinning.

The irreversibility field, H_{irr}, is the point where M vs. H_a is no longer double-valued. M vs. H_a curves are a function of the temperature T, and $H_{irr}(T)$ plotted against T gives the irreversibility line, above which flux lines move freely and the superconductor dissipates energy. One must therefore operate at a value of $H_a < H_{irr} < H_{c2}$. For LTS, $H_{irr} \sim H_{c2}$, but this is not true for HTS, where thermal activation becomes significant and allows easier flux line motion between H_{irr} and H_{c2}. The superconductor is termed "soft" between H_{irr} and H_{c2} and "hard" below H_{irr}. In LTS or HTS at a temperature of 0 K, the electric field due to flux flow resistance rises steeply above J_c with $E = r\,(J\text{-}J_c)$, but for HTS the resistivity is a nonlinear function of current (rather than a constant) due to thermally activated flux motion.

In a 1-T field, the resistivity of $YBa_2Cu_3O_7$ (YBCO) drops below that of copper between 80 K and 90 K; at 12 T, the resistivity falls below that of copper just below 70 K, both curves having rather sharp drop-offs. The resistivity of $Bi_{2.2}Sr_2Ca_{0.8}Cu_2O_{8+d}$ (BSCCO) in a 1-T field falls below that of copper just above 30 K; and in a 12-T field, just below 20 K, the drop-off being far less sharp than that of YBCO. In both cases, the resistivity remains above that of copper at temperatures well below the nominal T_c. While YBCO would appear to be far more useful than BSCCO in high magnetic fields, thus far one can make long lengths of prototype wire only for BSCCO.

AC Losses in the Critical State Model

In the critical state model, since the critical current flows in any current-carrying portion of a superconductor, the power generated *per unit volume* is $\boldsymbol{E}\cdot\boldsymbol{J}_c$. At the frequencies of interest, the loss per cycle is independent of the frequency; such losses are termed "hysteresis losses." In composite superconductors, in addition to hysteresis losses in the superconducting portion of the

wire, there are eddy current losses generated in the normal metal part of the composite. The total energy loss per second is then

$$W = f(\text{hysteresis loss/cycle}) + f^2(\text{eddy current loss/cycle}). \qquad \text{(A.1.1.2)}$$

The frequency is squared in the second term on the right-hand side, since for eddy losses $P = IE \propto E^2 \propto \dot{B}^2 f^2$.

AC Losses per Cycle in Slab Geometry

To a large extent, the presentation in this appendix follows that of M. N. Wilson.[2] The situation relevant to the following discussion is shown in Figure A1.1.3.

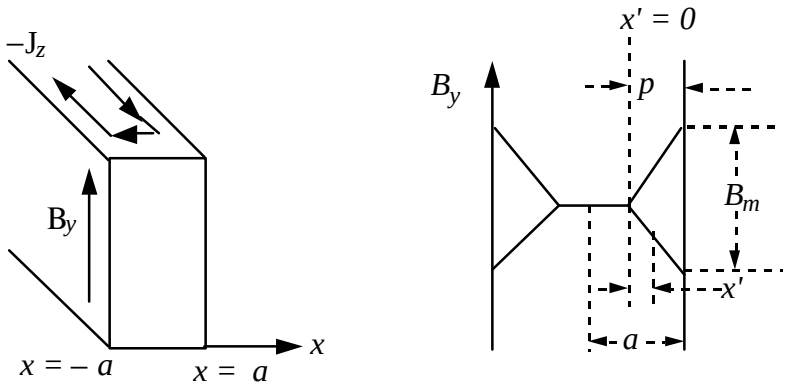

Figure A1.1.3. Field profiles in slab geometry. The screening current $-J_z$ reduces the field B_y as the slab is penetrated. B_m is the peak-to-peak amplitude (1/2 cycle).

The power generated in a thin slab dx' at a distance x' from the penetration depth p is $J_c E = J_c \frac{df}{dt}$, which implies that the loss *per unit volume per half cycle*, q, is $J_c \Delta f(x')$ integrated over the slab and divided by the volume. Now in the slab geometry shown above, $\nabla \times \boldsymbol{B} = \mu_0 \boldsymbol{J}$ implies that $\frac{dB}{dx'} = \mu_0 J_c$ so that $B = \mu_0 J_c x'$ and $\Delta f(x') = (\mu_0 J_c x')x'$. (The x' on the far right-hand side of the latter expression represents the area, since the calculations are per unit volume and y = z = 1. Similarly, $1/a$ corresponds to dividing by the volume.) The loss per unit volume per half cycle, q, is then

[2]M. N. Wilson, *Superconducting Magnets* (Clarendon Press, Oxford,1986).

$$q = \frac{1}{a}\int_0^p J_c \Delta f(x')\,dx' = \frac{1}{a}\int_0^p J_c(m_0 J_c x')x'\,dx' \qquad \text{(A1.1.3)}$$

$$= \frac{m_0}{a}\int_0^p J_c^2 x'^2\,dx' = \frac{m_0 J_c^2 p^3}{3a}$$

Using $B = m_0 J_c x'$, and remembering that B_m is the peak-to-peak field,[3] the penetration depth in terms of B_m is $p = B_m/2m_0 J_c$. Define B_p as the peak-to-peak amplitude of the field which just penetrates to the center ($p = a$), so that $B_p = 2m_0 J_c a$, and further define $b = B_m/B_p$. Then

$$q = \frac{\mu^0 J_c^2}{3a}\left(\frac{B_m}{2\mu_0 J_c}\right)^3 = \frac{1}{4\mu_0} B_m^2 \frac{\beta}{3} \qquad \text{(A1.1.4)}$$

The total loss per cycle, Q, is $2q$ because one must add in the region $-a \quad x \quad 0$. The final result, for $b < 1$, is

$$Q = 2q = \frac{B_m^2}{2m_0}\frac{b}{3} = \frac{B_m^2}{2m_0} G(b), \qquad b < 1. \qquad \text{(A1.1.5)}$$

For $b > 1$, B_m is greater than B_p, and one uses Eq. A1.1.3 with $p = a$ and an additional loss per half cycle $q_2 = J_c \Delta f = J_c(B_m - B_p)a$, as shown in Figure A1.1.4. The factor a in the expression for q_2 again corresponds to an area.

Using the fact that now $B_p = 2m_0 J_c a$, the loss per cycle is

$$Q = 2(q_1 + q_2) = 2\left[\frac{1}{12m_0}\frac{B_m^2}{b^2} + J_c(B_m - B_p)a\right] = \frac{B_m^2}{2m_0}\left[\frac{1}{b} - \frac{2}{3b^2}\right]. \qquad \text{(A1.1.6)}$$

This can be written in terms of the "loss factor" G(b) and the "normalized field change" b as

$$Q = \frac{B_m^2}{2m_0}\Gamma(b), \qquad b > 1, \qquad \text{(A1.1.7)}$$

where now

$$\Gamma(b) = \left[\frac{1}{b} - \frac{2}{3b^2}\right]. \qquad \text{(A1.1.8)}$$

---

[3]The reader is cautioned that Wilson uses slightly unusual nomenclature. He uses the field change $B_m = 2\,B_0$, where $B = B_0 \sin wt$, while the peak field B_0 is often used instead. Similarly, his $B_p = 2m_0 J_c a$, while $B_p = m_0 J_c a$ is often used.

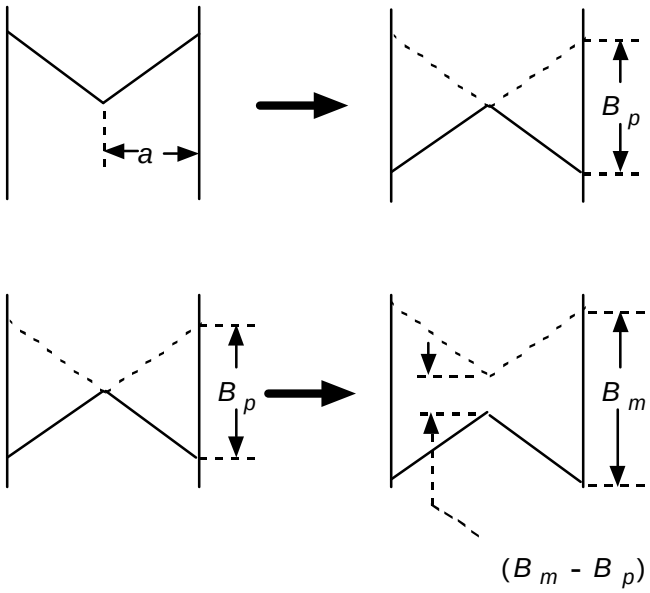

{Use Eq. (A1.1.3) with $p = a$.}

$q_2 = J_c \Delta f = J_c(B_m - B_p)a$

Figure A1.1.4. Field profiles for calculating loss factors q_1 and q_2 for $b > 1$.

This can be written in terms of the "loss factor" G(b) and the "normalized field change" b as

$$Q = \frac{B_m^2}{2\mu_0}\Gamma(b), \qquad b > 1, \tag{A1.1.7}$$

where now

$$\Gamma(b) = \left[\frac{1}{b} - \frac{2}{3b^2}\right]. \tag{A1.1.8}$$

G(b) depends on the geometry, and if one plots G(b) vs. b for the slab, and the cylinder is oriented parallel and perpendicular to the field, it becomes apparent that the maximum losses occur for $b \sim 1$. Ideally, the operating point should be chosen so that $b >> 1$ or $b << 1$.

Hysteresis Loss with a DC Transport Current

In the case of no transport current, J_t, we had $B_p = 2\mu_0 J_c a$. With a transport current, define B_p as

$$B_p' = 2\mu_0 J_c a - 2\mu_0 J_t a = 2\mu_0 J_c a\left(1 - \frac{J_t}{J_c}\right). \tag{A1.1.9}$$

Defining $J_t/J_c = I_t/I_c = i$,

$$B_p' = 2\mu_0 J_c a(1 - i) = B_p(1 - i). \tag{A1.1.10}$$

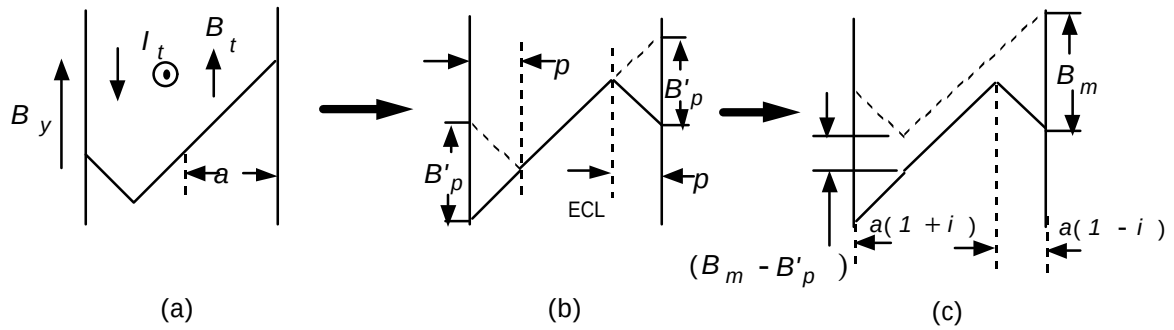

Figure A1.1.5. Field profiles for calculating loss factors when a transport current I_t is present. In (a), note the displacement of the profile as a result of the field B_t due to the transport current being subtracted from the external field B_y on the left and added on the right. This results in a displacement of the Electrical Center Line (ECL) as shown in (b), along with the definition of B_p' as the peak-to-peak amplitude that just penetrates to the center line. When $B_m > B_p'$, as in (c), the losses on either side of the ECL must be calculated separately.

The loss, q_1, in going from (a) to (b) in the figure above (that is, in going from the maximum field in the +y-direction to "penetration") is given by Eq. A1.1.3 with $p = a(1 - i)$ and $B_p' = 2\mu_0 J_c a(1 - i)$. Note that $B_m > B_p'$ implies that $b > (1 - i)$:

$$q_1 = \frac{\mu_0 J_c^2 p^3}{3a} = \frac{B_p'^2}{4\mu_0}\frac{(1-i)}{3} \qquad \text{(A1.1.11)}$$

The loss, q_2, in going from penetration to the maximum reverse field B_m [i.e., in going from (b) to (c) in the figure above] is

$$q_2 = \frac{1}{2a}\left\{\int_0^{a(1-i)} J_c \Delta f\, dx + \int_0^{a(1+i)} J_c \Delta f\, dx\right\}, \qquad \text{(A1.1.12)}$$

where $\Delta f = (B_m - B_p')x$, the factor $1/2a$ corresponds to volume normalization, and x has been set equal to zero at the ECL for convenience.

The total loss for $B_m > B_p'$, or $b > (1 - i)$, is then

$$Q = 2(q_1 + q_2) = \frac{B_p'^2}{2\mu_0}\frac{(1-i)}{3} + \frac{J_c a}{2}(B_m - B_p')\left[(1-i)^2 + (1+i)^2\right]. \qquad \text{(A1.1.13)}$$

Using the definitions of B_p' and b, B_p' can be written as $B_p' = \frac{B_m}{b}(1 - i)$, and substitution into the above equation yields

$$Q = \frac{B_m^2}{2m_0}\left(\frac{(1+i^2)}{b} - \frac{2}{3}\frac{(1-i^3)}{b^2}\right). \qquad \text{(A1.1.14)}$$

For $b >> (1 - i)$, or $B_m >> B_p'$, Q is approximately

$$Q = \frac{B_m^2}{2m_0}\frac{(1+i^2)}{b}, \qquad \text{(A1.1.15)}$$

and for $b < (1 - i)$, one uses Eq. A1.1.4:

$$Q = \frac{B_m^2}{2m_0}\frac{b}{3}. \qquad \text{(A1.1.16)}$$

One uses both Eqs. A1.1.15 and A1.1.16 for a typical loss vs. b curve. When $i = J_t/J_c > 0.5$, the peak loss is very close to $b = (1 - i)$, with the loss decreasing extremely rapidly to the value given by Eq. A1.1.16 for $b < (1 - i)$. This type of behavior should be expected, since for $B_m = B_p'$, $b = (1 - i)$.

A1.2 Eddy Current Loss in Twisted Filamentary Composites: Transverse Field

As mentioned in Section II.4.2, eddy current losses are also know as "coupling losses" when part of the circuit is composed of superconducting filaments. The seminal paper in this area is by Morgan.[4] He makes the approximation that the interior superconducting filaments carry *no* induced current: only the surface filaments carry a current due to $\dot{B}$, which shields the interior. The current through any cross section perpendicular to the wire therefore has a cosine distribution. The discussion given here is meant for heuristic purposes and uses the example of a wire of circular cross section. A discussion of the problem for tapes is contained in Oomen et al.[5]

Understanding the flow of eddy currents in twisted filamentary composites is somewhat counter-intuitive since *current flows in the direction of the applied external field*. To understand the reason for this, consider Figure A1.2.1 below.

[4]G. H. Morgan, *J. Appl. Phys.* **41**:3673 (1970).

[5]M. P. Oomen et al., *Physica C* **310**:137 (1998).

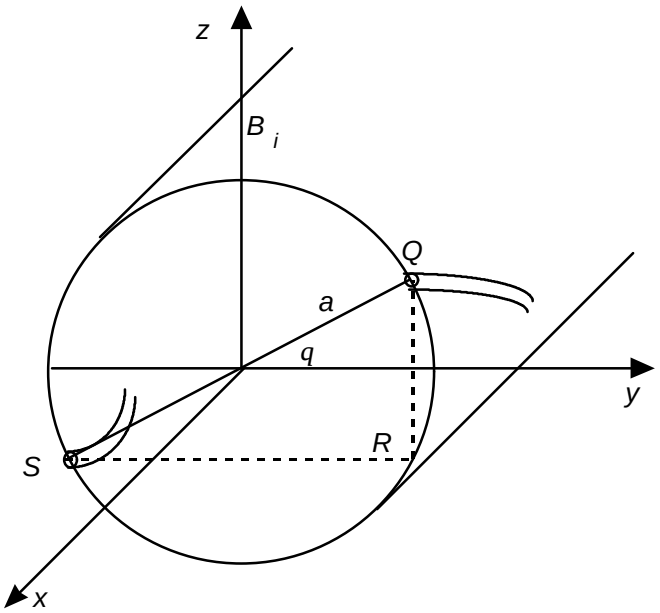

Figure A1.2.1. Circular Cross-Section Twisted Filamentary Composite. Two surface layer filaments are indicated in the figure at *S* and *Q*. B_i is the field inside the composite; *a* is the radius; and *B* and $\dot{B}$ are both in the *z*-direction.

There are a number of observations that are critical for determining the eddy current loss. First, paths like *RS* cannot have an electric field along them due to $\dot{B}$ because of symmetry (the electric fields due to $\dot{B}$ at adjacent points along *RS* cancel); in the *x*-direction, the current follows the superconducting filaments; an electric field, therefore, appears only along paths like *RQ* in the *z*-direction parallel to the applied magnetic field.

Following a superconducting filament, the change in *q* due to moving a distance d*x* in the *x*-direction is $\mathrm{d}q = \frac{2p}{L}\,\mathrm{d}x$, where *L* is the distance along *x* for *q* to turn through 2*p*. Ignoring the diameter of the filament, the change in flux produced by traveling a distance d*x* is

$$\mathrm{d}\Phi \;=\; 2aB_i \cos\left(\frac{2p}{L}x\right)\mathrm{d}x\,. \qquad \text{(A1.2.1)}$$

The voltage induced by the changing magnetic field $\dot{B}$ is then

$$V \;=\; -\frac{\mathrm{d}\Phi}{\mathrm{d}t} \;=\; -\frac{\partial}{\partial t}\int \frac{\mathrm{d}\Phi}{\mathrm{d}x}\,\mathrm{d}x \;=\; 2a\dot{B}_i \sin\left(\frac{2p}{L}x\right)\frac{L}{2p}. \qquad \text{(A1.2.2)}$$

Noting that $z = a\sin\left(\frac{2p}{L}x\right)$, the voltage induced along the path *QR* is

$$V = \int_Q^R E \, dy = 2\dot{B}_i \left(\frac{L}{2p}\right) z. \qquad \text{(A1.2.3)}$$

Different paths *RQ* have different values of *z*, but Eq. A1.2.3 always holds, implying that the electric field is uniform and equal to $E_z = \dot{B}_i \left(\frac{L}{2p}\right)$. (The factor of two does not appear because 2*z* is the path length.) The current density is then also uniform and given by

$$J_z = \dot{B}_i \left(\frac{L}{2p}\right) \frac{1}{r_t} \qquad \text{(A1.2.4)}$$

where r_t is the transverse resistivity, to be discussed shortly. The power dissipated *per unit volume* is then

$$P = \dot{B}_i^2 \left(\frac{L}{2p}\right)^2 \frac{1}{r_{et}}, \qquad \text{(A1.2.5)}$$

where r_{et} is the effective transverse resistivity, also discussed below.

The effective transverse resistivity, r_{et}, in Eq. A1.2.5 depends on manufacturing techniques. In addition, currents also flow in the normal peripheral layer outside the first layer of superconducting filaments. Screening eddy currents in this layer have the effect of reducing $B_{applied}$ to B_i. These combine to give

$$\frac{1}{r_{et}} = \frac{1}{r_t} + \frac{w}{a r_m} + \frac{aw}{r_m} \left(\frac{2p}{L}\right)^2, \qquad \text{(A1.2.6)}$$

where r_m is the matrix resistivity and r_t the transverse resistivity (each of these terms will be derived below). r_t depends on the contact between the filaments and the normal matrix, and Carr[6] finds that it falls between the two extremes,

$$r_m \frac{1 - l}{1 + l} \le r_t \le r_m \frac{1 + l}{1 - l}, \qquad \text{(A1.2.7)}$$

where *l* is the fraction of superconductor in the cross section. The left-hand limit corresponds to no contact resistance, while the right-hand limit is the usual case of high contact resistance. For very fine filaments, r_t can be greater than $r_m \frac{1 + l}{1 - l}$.

The way r_{et} is arrived at is as follows: J_z and J_r , in Fig. A1.2.2 below, are supplied by the induced $\dot{B}$ current J_F in the superconducting filaments. J_F is defined *per unit length perpendicular to the filament. It is important to keep this in mind for what follows.*

---

[6]W. J. Carr, Jr., *IEEE Trans. Mag.* **13**:192 (1977).

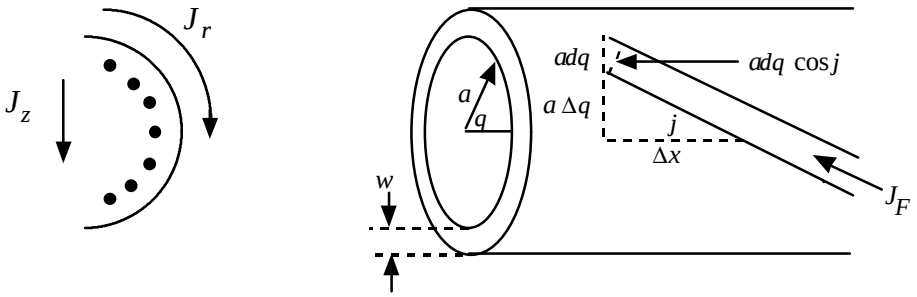

Figure A1.2.2. Geometry associated with induced $\dot{B}$ current. The width of the superconducting filament is exaggerated to define terms.

From Figure A1.2.2, the *current* in the filament band of width $a\,dq\cos j$ is $(\Delta J_F)a\,dq\cos j$; this current must supply the currents due to J_z and J_r. Using Eq. A1.2.4 for J_z, the current DI_z is

$$\Delta I_z = \dot{B}_i\left(\frac{L}{2p}\right)\frac{1}{r_t}\,a\,dq\,\frac{a\,\Delta q}{\tan j}\sin q\,, \qquad \text{(A1.2.8)}$$

where the fact that $\Delta x = \dfrac{a\,\Delta q}{\tan j}$ has been used to define the elemental area through which J_z passes (see Figure A1.2.3).

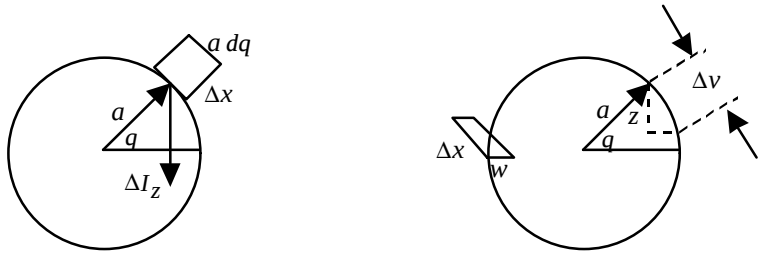

Figure A1.2.3. Geometry for finding DI_z and DI_r.

The voltage along z is $V = \dot{B}_i\left(\frac{L}{2p}\right)z$, so that $\Delta V = \dot{B}_i\left(\frac{L}{2p}\right)a\,dq\cos q$. But DV is also equal to $J_r a\,dq\,r_m$, yielding for $J_r(q)$

$$J_r(q) = \dot{B}_i\left(\frac{L}{2p}\right)\frac{1}{r_m}\cos q\,. \qquad \text{(A1.2.9)}$$

D I_r is then

$$\Delta I_r = \frac{\mathrm{d}J_r}{\mathrm{d}a}\,dq(\mathrm{w}\Delta x) = \frac{wa\,\Delta q}{\tan j}\,\dot{B}_i\left(\frac{L}{2p}\right)\frac{1}{r_m}\sin q\,dq\,. \qquad \text{(A1.2.10)}$$

Setting the sum of DI_r and DI_z equal to $\Delta J_F a\,dq\cos j$ results in

$$\frac{\Delta J_E}{\Delta a} = \dot{B}_i \left(\frac{L}{2p}\right) \frac{\sin q}{\cos j \tan j} \left[\frac{a}{r_t} + \frac{w}{r_m}\right]. \qquad \text{(A1.2.11)}$$

Integrating, setting the constant of integration equal to zero so as to satisfy the boundary condition that $J_F = 0$ at $q = p/2$, and remembering that $\tan j = (2p\,a)/L$,

$$(J_F)_x = \dot{B}_i \left(\frac{L}{2p}\right)^2 \cos q \left[\frac{1}{r_t} + \frac{w}{a\, r_m}\right], \qquad \text{(A1.2.12)}$$

where the z-component, $(J_F)_x$, is given by $J_F \cos j$.

The last term to be included is that due to eddy currents in the outer jacket of thickness w. The eddy current density is defined as $J_e = \dot{B}_i\, a \cos q / r_m$. Note that $J_e r_m$ is an electric field that, from the fact that $\dot{B}_i$ is multiplied by $a\cos a$, is in the y-direction. J_e must be converted to a current density per unit length, which is done by multiplying by the width w. This also makes sense from the perspective that the eddy current loss is proportional to w. If the total screening current (which produces a uniform field in the interior of the composite) is written in the form $\dot{B}_i \left(\frac{L}{2p}\right)^2 \frac{\cos q}{r_{et}}$, obtained by taking the limit of vanishing w in Eq. A1.2.12, one has the total screening current as the sum of Eq. A1.2.12 and the eddy current per unit length; i.e.,

$$J_x = \dot{B}_i \left(\frac{L}{2p}\right)^2 \frac{\cos q}{r_{et}} = \dot{B}_i \left(\frac{L}{2p}\right)^2 \cos q \left[\frac{1}{r_t} + \frac{w}{a\, r_m}\right] + \dot{B}_i \frac{a \cos q}{r_m}. \qquad \text{(A1.2.13)}$$

Solving for $1/r_{et}$

$$\frac{1}{r_{et}} = \frac{1}{r_t} + \frac{w}{a\, r_m} + \frac{a}{r_m}\left(\frac{2p}{L}\right)^2. \qquad \text{(A1.2.14)}$$

The internal field B_i produced by the J_x cosine distribution will be uniform if the external applied field, B_a, is uniform. The magnitude of the field is

$$B_i = B_a - \frac{1}{2}\, m_0 J_x \Big|_{q=0} = B_a - \frac{1}{2}\, m_0 \dot{B}_i \left(\frac{L}{2p}\right)^2 \frac{1}{r_{et}} = B_a - \dot{B}_i\, t, \qquad \text{(A1.2.15)}$$

where

$$t = \frac{m_0}{2 r_{et}} \left(\frac{L}{2p}\right)^2. \qquad \text{(A1.2.16)}$$

If B_a is given a particular form (e.g., exponential or sinusoidal), $B_i = B_a - \dot{B}_i\, t$ can be solved for B_i and the loss calculated from Eq. A1.2.5,

$$P = \dot{B}_i^2 \left(\frac{L}{2p}\right)^2 \frac{1}{r_{et}} = \frac{2\dot{B}_i^2}{m_0}\, t\,. \qquad \text{(A1.2.17)}$$

Here t is the time constant associated with the decay of the screening currents and is similar to the diffusion time. For frequencies of the applied field greater than $1/t$, the interior of the conductor is shielded. Dimensionally, this can be turned into the thickness of the saturation region by multiplying by $2wH_a/J_c$, which gives the depth of saturation

$$d_{sat} = \frac{2wH_a}{J_c} t \cong \frac{wH_a}{J_c} \frac{m_0}{r_{et}} \left(\frac{L}{2p}\right)^2. \qquad \text{(A1.2.18)}$$

Penetration Loss

In deriving screening currents above, it is assumed that current flows through a thin current sheet at radius a. But it actually flows within a saturated region, as shown below.

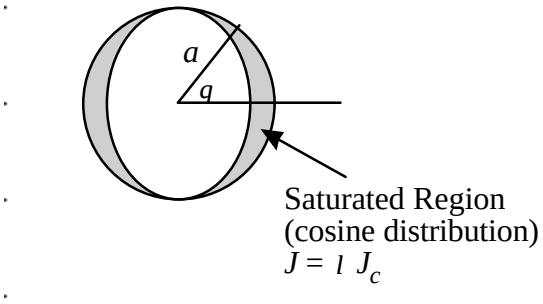

Figure A1.2.4. Penetration loss, where l is the fraction of superconductor in the cross section.

The loss in the saturated region should be included. Penetration loss in a twisted filamentary composite can be approximated as hysteresis loss in a solid wire of the same diameter with current density lJ_c and a difference between internal and external fields B_a - B_i given by Eq. A1.2.15, with a specified time dependence.

Transport Current (Transverse Field)

A transport current increases the total loss by a factor of $(1 + i^2)$ for high rates of change of the field, with more complicated behavior for low rates of change. This includes the loss due to the phenomenon of dynamic resistance.

If a superconductor carrying a DC transport current is placed in an oscillating external field strong enough to fully penetrate the superconductor, the transport current produces additional flux motion (from one side of the conductor to the other), which generates a current opposing the transport current. This appears as a magnetic-field-dependent resistance known as the dynamic resistance.[7] This can be understood by noting that the transport current produces an azimuthal flux about the superconducting wire, which adds to the external field on one side of the wire and subtracts on the other. The sides reverse as the external field reverses direction.

[7]B. Taquet, *J. Appl. Phys.* **36**:3250 (1965); W. J. Carr, Jr., *AC Loss and Macroscopic Theory of Superconductors* (Gordon and Breach, New York, 1983).

A1.3 Eddy Current Loss in Twisted Filamentary Composites: Longitudinal Field

Generally, the case most often encountered is that of a filamentary composite in a transverse field. However, when the windings of a coil in a given piece of electrical machinery have a complicated shape, one may find substantial components of the field parallel to the conductor. In cables, for example, one often twists the conductors, making up different layers of the cable with a different pitch so as to equalize the current flowing through each layer. Such twisting produces an axial magnetic field. For this reason, and for completeness, the authors consider it worthwhile to include this section.

For a single filament, the loss is similar to that for a slab, as computed previously. The geometry is shown in Figure A1.3.1.

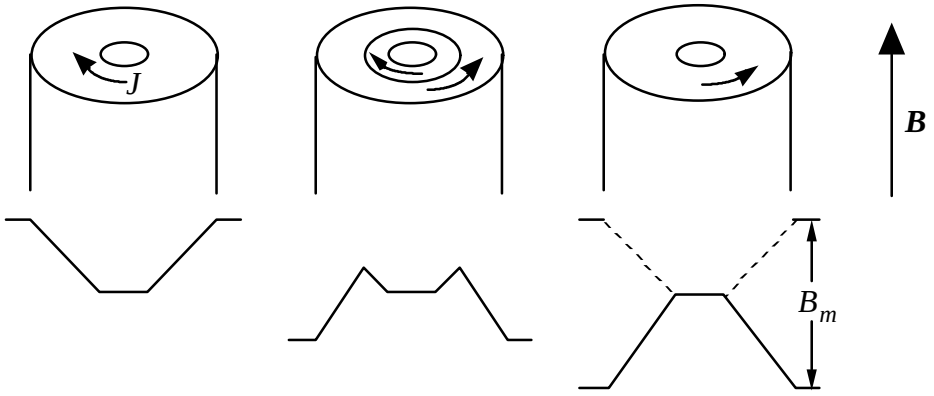

Figure A1.3.1. Single filament in a longitudinal field. The field profiles are shown below the filament cross section, where the induced currents change direction as the external longitudinal field changes from maximum to minimum.

The loss per cycle is given by:

$$Q = \begin{cases} \dfrac{B_m^2}{2\mu_0}\left[\dfrac{2b}{3} - \dfrac{b^2}{3}\right] & b < 1 \\ \dfrac{B_m^2}{2\mu_0}\left[\dfrac{2}{3b} - \dfrac{1}{3b^2}\right] & b > 1 \end{cases} \qquad \text{(A1.3.1)}$$

The case of a twisted filamentary composite conductor in a longitudinal magnetic field is shown in Figure A1.3.2. Note that since the total current upward must equal the total downward, the magnetic field in the center, B_z, must be equal to the external field. As the external field, B_e, increases, the return current increases, and the boundary between inner and outer zones moves *inward*.

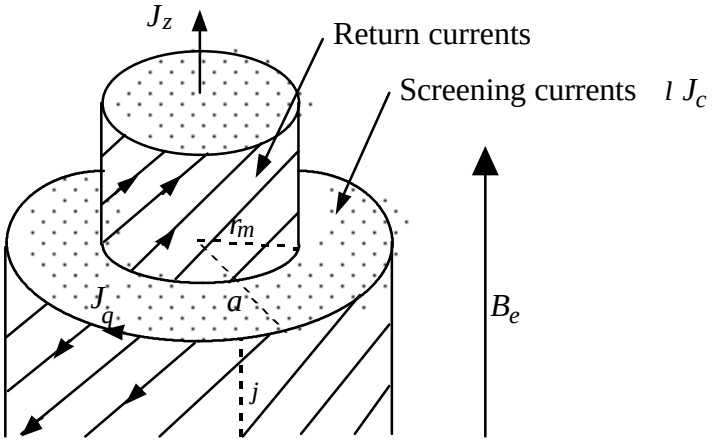

Figure A1.3.2. Filamentary composite in a longitudinal magnetic field. For small $\dot{B}_e$, the interior region will be subcritical so that E must vanish along the center lines of the filaments, implying that the electric field is parallel to the filaments.

As B_e continues to increase, a value of the external field is finally reached where the inner zone also reaches critical density; i.e., $J_z = l\,J_c$ in both regions. The radius at which this occurs is where $p r^2 = p a^2 - p r^2$, or $r = a/\sqrt{2}$. This point, where the critical current density is reached for both the inner and outer regions, is called *full penetration*, and the external field change needed to go from full penetration in one direction to full penetration in the other is defined as H_{pl}.

The magnitude of the field H_{pl} can be determined as follows: from the geometry in the figure, one has that

$$\frac{B_q}{B_z} = \tan j = \left(\frac{2p r}{L}\right). \qquad \text{(A1.3.2)}$$

It is also true that

$$\int_{q=0}^{2p} B_q\, r\, dq = m_0 I. \qquad \text{(A1.3.3)}$$

But $I = p r^2 J_z$ so

$$B_q = \frac{m_0 J_z r}{2}. \qquad \text{(A1.3.4)}$$

Using Eq. A1.3.2, and remembering that in the central region $B_z = B_e$,

$$J_z = \frac{4p B_e}{m_0 L}. \qquad \text{(A1.3.5)}$$

Now at penetration $J_z = l J_c$ and $B_e = m_0 H_{pl}$, so

$$H_{pl} = \frac{l J_c L}{2p}, \qquad \text{(A1.3.6)}$$

where the extra factor of two on the right-hand side comes from the fact that the field must change from full penetration in one direction to full penetration in the other.

To obtain the losses, one finds the magnetization per unit volume — or, in this case, the magnetization per unit length — which is of the form $\frac{m_0}{A}\int I_q(r)A(r)\,dr$. Remembering that $J_a = l J_c \tan j$ for $r > r_m$ and $J_a = J_z \tan j$ for $r < r_m$, the magnetization per unit volume, M_m, is

$$M_m = \frac{m_0}{p a^2}\left[\int_0^{r_m} -p r^2 J_z \tan j \; dr + \int_{r_m}^{a} p r^2 l J_c \tan j \; dr\right]. \qquad \text{(A1.3.7)}$$

The radius r_m is determined from the condition that the net longitudinal current vanish; i.e., $J_z p r_m^2 = l J_c p a^2 - l J_c p r_m^2$. Solving for r_m^2,

$$r_m^2 = \frac{l J_c a^2}{J_z + l J_c} = \frac{a^2}{1 + \frac{J_z}{l J_c}}. \qquad \text{(A1.3.8)}$$

Using Eqs. A1.3.5 and A1.3.6 for J_z and lJ_c, one obtains $\frac{J_z}{l J_c} = \frac{2B_e}{B_{pl}} = b$ since $2B_e = B_m$ and $b = \frac{B_m}{B_{pl}}$ by definition. Therefore,

$$r_m = \frac{a}{(1+b)^{1/2}}. \qquad \text{(A1.3.9)}$$

Equation A1.3.7 then becomes

$$M_m = \frac{m_0}{p a^2}\left[\int_0^{r_m} -p r^2\left(\frac{4pB_e}{m_0 L}\right)\left(\frac{2pr}{L}\right) dr + \int_{r_m}^{a} p r^2\left(\frac{2pH_{pl}}{L}\right)\left(\frac{2pr}{L}\right) dr\right] \qquad \text{(A1.3.10)}$$

$$= \frac{m_0 2p^2}{a^2 L^2} H_{pl}\left[\int_0^{r_m} -2br^3 \; dr + \int_{r_m}^{a} 2r^3 \; dr\right].$$

Using Eq. A1.3.9 to evaluate the integrals,

$$M_m = \frac{\mu_0 p^2 a^2}{L^2} H_{pl} \frac{b}{(1+b)}. \qquad \text{(A1.3.11)}$$

The extreme values of the magnetization are $\pm M_m$. To get the hysteresis loops, $M(H)$, one needs to add to the extreme the change as a function of H. Consider the following series of current profiles in the composite superconductor (Figure A1.3.3):

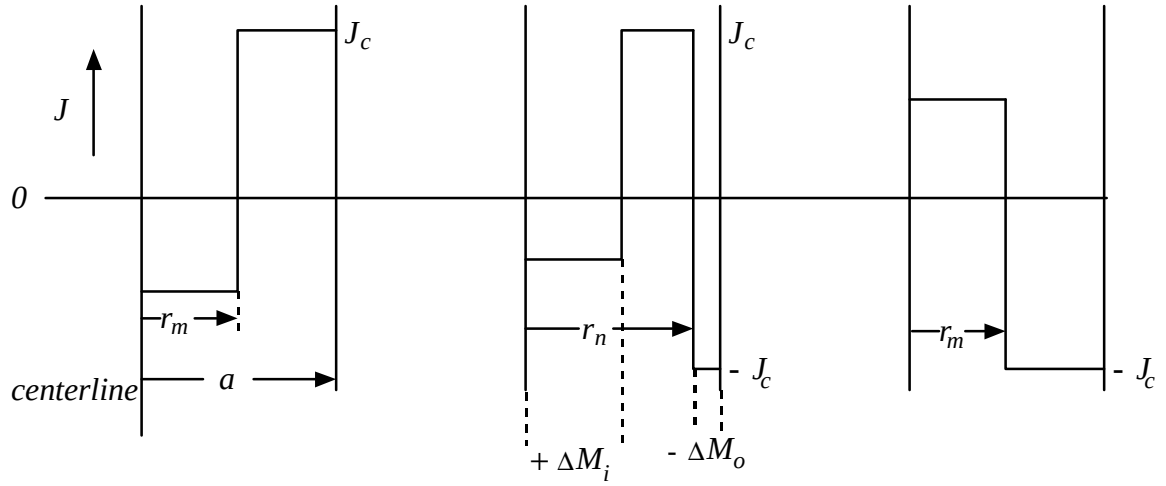

Figure A1.3.3. Current profiles in a twisted filamentary composite as a longitudinal magnetic field is lowered from its maximum value to its minimum value.

Once ΔM_i and ΔM_o are determined, the loss can be obtained by integrating $\int M(H)\, dH$ over a full cycle. ΔM_i is determined from the first integral on the right-hand side of Eq. A1.3.7 by using Eq. A1.3.5 with ΔB_e identified with $\mu_0 \Delta H$,

$$\Delta M_i = \frac{\mu_0}{p a^2} \int_0^{r_m} -p r^2 \Delta J_z \tan\varphi \, dr = \frac{\mu_0 2 p^2 a^2}{L^2} \frac{\Delta H}{(1+b^2)}. \qquad \text{(A1.3.12)}$$

The radius r_n is determined by using the condition that the total axial current vanish; i.e., $\lambda 2 J_c (a^2 - r_n^2) = \Delta J_z r_m^2$, where the factor of two comes from the fact that in the region $r_n < r < a$ the current changes from $+J_z$ to $-J_z$. Solving for r_n and again using Eq. A1.3.5 with ΔB_e identified with $\mu_0 \Delta H$ and the fact that $L \lambda J_c = 2p H_{pl}$,

$$r_n = \left[1 - \frac{\Delta H}{H_{pl}} \frac{1}{(1+b)}\right]^{1/2}. \qquad \text{(A1.3.13)}$$

ΔM_o is the change in the outer sheath $r > r_n$, or

$$\Delta M_o = \frac{\mu_0}{\pi a^2}\int_{r_n}^{a} \pi r^2 2\lambda J_z \tan\varphi \, dr = \frac{2\mu_0 H_{pl}\pi^2}{a^2 L^2}\left(a^4 - r_n^4\right)$$

$$= \frac{2\mu_0 H_{pl}\pi^2 a^2}{L^2}\left\{1 - \left(1 - \frac{\Delta H}{H_{pl}(1+\beta)}\right)^2\right\}. \qquad \text{(A1.3.14)}$$

The magnetization at a given moment during the cycle is then given by the sum $M = M_m + \Delta M_i - \Delta M_o$, or

$$M = \frac{\mu_0 \pi^2 a^2}{L^2(1+\beta)^2}\left\{H_{pl}\beta(1+\beta) - 2\Delta H(1+2\beta) + \frac{2(\Delta H)^2}{H_{pl}}\right\}. \qquad \text{(A1.3.15)}$$

If this is integrated over the hysteresis loop in the M, H-plane, the loss per cycle is

$$Q = \frac{B_m^2 4\pi^2 a^2}{2\mu_0 L^2}\left(\frac{\beta}{3(1+\beta)^2}\right) \qquad \textit{for} \qquad \beta = \frac{2\pi B_m}{\mu_0 \lambda J_c L} < 1 \qquad \text{(A1.3.16)}$$

and

$$Q = \frac{B_m^2 4\pi^2 a^2}{2\mu_0 L^2}\left(\frac{1}{2\beta} - \frac{5}{12\beta^2}\right) \qquad \textit{for} \qquad \beta = \frac{2\pi B_m}{\mu_0 \lambda J_c L} > 1. \qquad \text{(A1.3.17)}$$

APPENDIX 2: NONLINEAR CONDUCTOR MODEL

The critical state model used to calculate hysteresis losses in low-temperature superconductors assumes a discontinuous jump from zero resistivity to normal state resistivity at the critical current. In high-temperature superconductors, the resistive transition is typically very broad, violating this basic assumption. Why then do formulas based on the critical state model often give relatively accurate results when used to estimate AC losses?

Dresner[1] has answered this question by using a dimensional analysis approach and finds that "the exponents of the power-law dependences of the hysteresis loss on current (current-driven losses), magnetic field (field-driven losses), and AC frequency are rather insensitive to the *n*-value." He finds that the value of the time-averaged AC loss power per unit face area of tape conductor, *P*, depends on the following exponents (when J_c does not depend on an inverse power of the magnetic field):

DRIVER	PENETRATION	w	I_{max} or B_{max}
Current	Incomplete	$(n + 1)/(n + 2)$	$(3n + 4)/(n + 2)$
Current	Full	0	$(n + 2)$
Field	Incomplete	$(n + 1)/(n + 2)$	$(3n + 4)/(n + 2)$
Field	Full	$(n + 2)/(n + 1)$	$(n + 2)/(n + 1)$

The critical state model appears to work well because, for relatively small *n*, the value of these exponents is close to their values for *n* = .

Modeling a high-temperature superconductor having a power law current-voltage characteristic as a nonlinear conductor gives a theoretical basis for analytical calculations of AC losses that are in good agreement with Dresner's conclusions. In this model, $n = 1$ corresponds to the ohmic linear case and *n* = to the critical state model. It will be seen that for *n* values as small as $n = 8$, the nonlinear conductor model gives results very similar to the critical state model.

To engineering accuracy, the relation between the current density, $\boldsymbol{J}$, and the electric field, $\boldsymbol{E}$, follows a power law:

$$\boldsymbol{E} = E_0 \left(\frac{J}{J_0}\right)^{n-1} \frac{\boldsymbol{J}}{J_0}, \qquad \text{(A2.1)}$$

where, in general, J_0 depends on B and $J_0 = J_c$ in the critical state model (*n* =). When $n = 1$, the resistivity is given by $r = E_0/J_0$, and as $n \to \infty$ the expression in brackets causes an increasingly sharp rise in the electric field near J_o. The power law current-voltage characteristic interpolates between the ohmic linear case, where the skin effect is important, and the critical state case, where hysteresis effects dominate. While it is assumed here that the resistivity only

[1] L. Dresner, "Hysteresis Losses in Power-Law Superconductors," *Applied Superconductivity* **4**:167 (1996).

depends on the magnitude of the current density, in general it depends independently on the perpendicular and parallel components of both the magnetic field and current density. It should also be noted that, unlike the critical state model, when the resistive transition is wide the hysteresis losses may be frequency-dependent.[2]

In the nonlinear conductor model,[3] the electric field "diffuses" through the HTS in a nonlinear manner. To see this, one first derives the diffusion equation for the electric field from Maxwell's equations. Given the frequencies of interest, the displacement current can be ignored, so that

$$\nabla \times \boldsymbol{H} = \boldsymbol{J} = \frac{\boldsymbol{E}}{r}. \qquad \text{(A2.2)}$$

Taking the time derivative of this equation gives

$$\nabla \times \frac{\partial \boldsymbol{H}}{\partial t} = \frac{\partial(\boldsymbol{E}/r)}{\partial t}. \qquad \text{(A2.3)}$$

When this result is combined with the second of Maxwell's equations,

$$\nabla \times \boldsymbol{E} = -\mu_0 \frac{\partial \boldsymbol{H}}{\partial t}, \qquad \text{(A2.4)}$$

one obtains

$$-\frac{1}{\mu_0}\nabla \times \nabla \times \boldsymbol{E} = \frac{\partial(\boldsymbol{E}/r)}{\partial t}. \qquad \text{(A2.5)}$$

If the divergence of $\boldsymbol{E}$ vanishes, as it must since there are no free charges, the left-hand side of this equation simplifies to the diffusion equation

$$\frac{1}{\mu_0}\nabla^2 \boldsymbol{E} = \frac{\partial(\boldsymbol{E}/r)}{\partial t}. \qquad \text{(A2.6)}$$

The nonlinearity enters when the power law relation, Eq. A2.1, is used to substitute for the electric field in Eq. A2.6. Since $\boldsymbol{E} = r\boldsymbol{J}$, and

$$\boldsymbol{E} = \frac{E_0}{J_0}\left(\frac{J}{J_0}\right)^{n-1}\boldsymbol{J} = k\left(\frac{J}{J_0}\right)^{n-1}\boldsymbol{J}, \qquad \text{(A2.7)}$$

one has $r = k\left(\frac{J}{J_0}\right)^{n-1}$, where $k = E_0/J_0$. Substituting r and E, as given in Eq. A2.7, into Eq. A2.6 yields the nonlinear diffusion equation

---

[2]J. Paasi and M. Lahtinen, "AC Losses in Multifilamentary Bi-2223/Ag Superconducting Tapes," *IEEE Trans. on Magn*. **32**:2792 (1996).

[3]J. Rhyner, *Physica C* **212**:292 (1993).

$$\nabla^2\left[k\left(\frac{J}{J_0}\right)^{n-1}\left(\frac{\boldsymbol{J}}{J_0}\right)\right] = \mu_0\frac{\partial}{\partial t}\left(\frac{\boldsymbol{J}}{J_0}\right). \qquad \text{(A2.8)}$$

While this form of the diffusion equation is useful for showing how the nonlinearity arises, it is not the most useful form for what follows. Instead, write Eq. A2.2 as

$$\rho\,\nabla\times\boldsymbol{H} = \boldsymbol{E}\ , \qquad \text{(A2.9)}$$

and take the curl to obtain

$$\nabla\times\left(\rho\,\nabla\times\boldsymbol{H}\right) = \nabla\times\boldsymbol{E}\ . \qquad \text{(A2.10)}$$

Use this in Eq. A2.4 to substitute for $\nabla\times\boldsymbol{E}$ to obtain the diffusion equation in the form

$$\frac{\partial\boldsymbol{B}}{\partial t} = -\frac{1}{\mu_0}\nabla\times\left(\rho(\boldsymbol{J})\,\nabla\times\boldsymbol{B}\right). \qquad \text{(A2.11)}$$

It has been assumed in writing this equation that J_0 is insensitive to B, so that

$$\rho(\boldsymbol{J}) = \frac{E_0}{J_0}\left(\frac{\boldsymbol{J}}{J_0}\right)^{n-1}. \qquad \text{(A2.12)}$$

In fact, both the critical current and the exponent n depend strongly on the field.[4] At low fields, the critical current and n value are high, so the critical state model can be expected to apply, while at higher fields, the critical current is less sensitive to changes in B and the n value is low, so the nonlinear conductor model should be applicable. The assumption that J_0 is insensitive to B was made by Rhyner to obtain semi-analytic results and so that the limiting case of $n = \infty$ would correspond to the critical state model. This assumption did not affect the numerical calculations of field distributions and losses.

If one now assumes the superconductor is in the form of a tape with the magnetic field directed parallel to the surface of the tape, and that the magnitude of the external magnetic field is less than the penetration field, the geometry can be considered to be that of a superconducting half-space $z \geq 0$. If the field is directed along the y-axis, the external field $\boldsymbol{B}_{ext}$ may be written as $\boldsymbol{B}_{ext} = \boldsymbol{B}_0 \sin \omega t$, where $\boldsymbol{B}_0 = (0, B_0, 0)$. The field internal to the superconductor only has a component in the y-direction, and this component is only a function of z. Substituting Eq. A2.12 into A2.11 and calculating the curl in the assumed geometry gives

$$\frac{\partial B}{\partial t} = \frac{E_0}{(\mu_0 J_0)^n}\frac{\partial}{\partial z}\left[\mathrm{sign}\left(\frac{\partial B}{\partial z}\right)\left|\frac{\partial B}{\partial z}\right|^n\right], \qquad \text{(A2.13)}$$

where

[4] O.A. Shevchenko et al., *Physica C* **310**:106 (1998).

$$\text{sign}\left(\frac{\partial B}{\partial t}\right) = \pm 1 \,. \qquad \text{(A2.14)}$$

It is useful, for purposes of discussion, to introduce dimensionless variables. To that end, let $Y = B/B_0$, $t = wt$, and $x = z/z^*$. Equation A2.13 then becomes

$$\frac{\partial Y}{\partial t} = \frac{\partial}{\partial x}\left[\text{sign}\left(\frac{\partial Y}{\partial x}\right)\left|\frac{\partial Y}{\partial x}\right|^n\right], \qquad \text{(A2.15)}$$

where

$$z^* = \frac{B_0}{(m_0 J_0)}\left(\frac{m_0 J_0 E_0}{B_0^2 w}\right)^{\frac{1}{1+n}} . \qquad \text{(A2.16)}$$

Note that as $n \to \infty$, $z^* \to B_0/m_0 J_0$ which is the penetration depth in the critical state model. Here, z^* measures the depth within which losses occur in a power law superconductor. On the other hand, when $n = 1$, one obtains the usual skin depth

$$z^* = \left(\frac{E_0}{m_0 J_0 w}\right)^{1/2} = \left(\frac{r}{m_0 w}\right)^{1/2} \cong d = \left(\frac{2r}{m_0 w}\right)^{1/2}, \qquad n = 1. \qquad \text{(A2.17)}$$

The relation between the critical state model and the nonlinear diffusion model as a function of n can also be illuminated by rewriting Eq. A2.16 for z^* as

$$z^* = \underbrace{\left(\frac{B_0}{m_0 J_0}\right)}_{\text{Critical State}} \underbrace{\left[\frac{(E_0/wB_0)}{(B_0/m_0 J_0)}\right]^{1/1+n}}_{\text{Finite}n\text{ Correction.}} \qquad \text{(A2.18)}$$

The second term in square brackets on the right-hand side of the equation is the ratio of two lengths. It is interesting to determine the value of J_0 needed to obtain the critical state model for given values of B_0, independent of n; i.e., when the quantity in square brackets is ~1. One finds that

$$B_0 = 1T \quad \Rightarrow \quad J_0 = 2.5 \times 10^{12}\, A/m^2$$

$$B_0 = 0.5T \quad \Rightarrow \quad J_0 = 6.25 \times 10^{11}\, A/m^2,$$

where 1 T corresponds to the magnitude of the magnetic field associated with motors, generators, and SMES, while 0.1 - 0.5 T is the field associated with transformers. These values of J_0 should be compared with the typical observed value of $J_0 \approx 10^8\, A/m^2$.

The answer to the question of when the critical state model is appropriate to use is obtained by plotting the solutions to Eq. A2.15 for various values of n. The result is shown in Figure A2.1. The critical state model can be seen to be well justified for $n > 8$.

AC losses per cycle per unit area may also be computed in the nonlinear conductor model from

$$\frac{Q}{A} = \int_0^{2p/w} dt \int_0^{\infty} dz\, \boldsymbol{J}\cdot\boldsymbol{E} = \int_0^{2p/w} dt \int_0^{\infty} dz\, \frac{E_0}{J_0}\left(\frac{J}{J_0}\right)^{n-1}|\boldsymbol{J}|^2, \qquad \text{(A2.19)}$$

w being $2pf$, and substituting for $\boldsymbol{J}$ and $\boldsymbol{B}$ the expressions

$$J = \left|\frac{\nabla\times\boldsymbol{B}}{m_0}\right| \quad \text{and} \quad \boldsymbol{B} = (0, B(z), 0)$$

to obtain

$$\frac{Q}{A} = \int_0^{2p} dt \int_0^{\infty} dz\, \frac{E_0}{(m_0 J_0)^n}\left(\frac{1}{m_0}\right)\left|\frac{\partial B}{\partial z}\right|^{n+1}. \qquad \text{(A2.20)}$$

In terms of the dimensionless variables $Y = B/B_0$, $t = wt$, and $x = z/z^*$ this becomes

$$\frac{Q}{A} = \left(\frac{B_0^2}{2m_0}\right) z^* \left\{ 2\int_0^{2p} dt \int_0^{\infty} dx \left|\frac{\partial Y}{\partial x}\right|^{n+1}. \right\} \qquad \text{(A2.21)}$$

Let the expression in curly brackets, which is a function of n, be called $J(n)$. It may be approximated by $J(n) \cong 1.33 + 3.11\, n^{-0.55}$ and, as can be seen in Figure A2.1, is of the order of unity.

PAGE BREAK FOR FIGURE A2.1

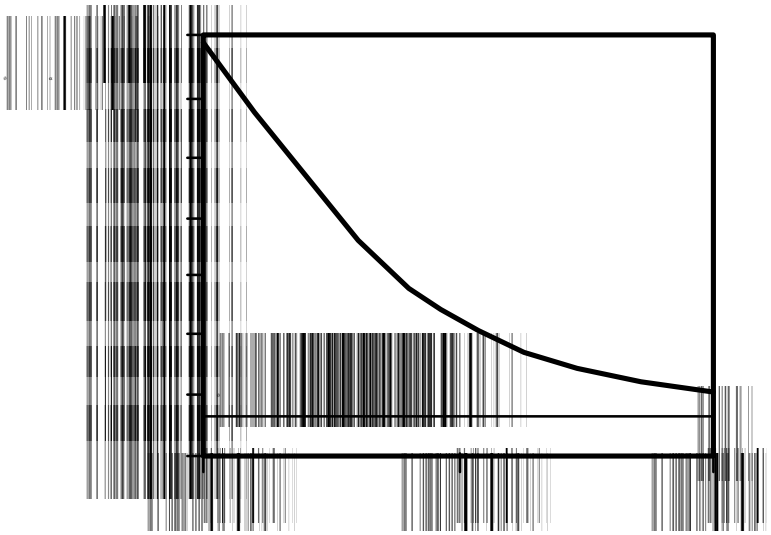

Figure A2.2. The form factor $J(n)$.

The dependence of the AC losses as a function of the applied field amplitude B_0 and the frequency w may be obtained by substituting Eq. A2.16 for z^* into Eq. A2.21. The result is

$$\frac{Q}{A} \sim B_0^{l} w^{n-1}, \qquad l = \frac{1+3n}{1+n}, \quad n = \frac{n}{1+n}, \tag{A2.22}$$

which in the limits of n takes the values

$$\frac{Q}{A} = \begin{cases} B_0^2 w^{-1/2} & \text{for } n = 1 \text{ (normal skin effect)} \\ B_0^3 & \text{for } n = \infty \text{ (critical state model)} \end{cases}. \tag{A2.23}$$

The assumption that the amplitude of the external field, B_0, is smaller than the penetration field allowed the superconductor to be approximated by a semi-infinite half-space and resulted in the analytic solutions described above. When this is not the case, the approach given above is still valid, but there are different boundary conditions and one must rely on numerical solutions of the equations.

APPENDIX 3: HYSTERESIS LOSSES RELATED TO THE IMAGINARY PART OF THE COMPLEX PERMEABILITY

This appendix is based on a 1979 report by Clem.[1] The power dissipated in a volume V averaged over one period is given by

$$P = T^{-1} \int_0^T \mathrm{d}t \int_V \boldsymbol{J} \cdot \boldsymbol{E} \, \mathrm{d}V. \qquad \text{(A3.1)}$$

The energy loss per cycle is then $W = PT$. Defining the power per unit volume and per unit area as $P_V = P/V$ and $P_A = P/A$, respectively, the energy loss per unit volume per cycle is $W_V = W/V = P_V T$, and the energy loss per unit area per cycle is $W_A = W/A = P_A T$. In terms of the area of the hysteresis loop, A_H, the energy loss per unit volume per cycle is $W_V = A_H/\mu_0$. Clem defined the area of the hysteresis loop as the area bounded by the trajectory of $\overline{B}$ vs. B_a, where B_a is the time-dependent magnetic induction applied longitudinally to a long solid cylinder of radius a, and $\overline{B}$ is the magnetic induction inside the specimen averaged over the volume.

The losses depend on the screening currents, which determine how much flux sweeps in and out of the specimen and if $\overline{B}$ is out of equilibrium with B_a. For very small or very large screening currents, the losses are small: in the first case $\overline{B}$ and B_a are in equilibrium, while in the second, little flux enters the specimen.

[1] J.R. Chem, *AC Losses in Type II-Superconductors*, unpublished proceedings of the Autumn School on Metal Physics, Nov. 26-Dec. 1, 1979, Piecowice, Poland (IS-M-280, 1980); and in *Magnetic Susceptibility of Superconductors and Other Spin Systems*, R.A. Hein, T.L. Francavilla, and D.H. Liebenberg, Eds., (Plenum, New York, 1992), pp. 177-211.

Figure A3.1. The voltage V induced by a time-dependent internal field $\bar{B}$. B_a is the external longitudinal field.

Let B_a be defined as

$$B_a = B_0 + b_0 \cos wt = B_0 + \mathrm{Re}\left(b_0 e^{-iwt}\right). \tag{A3.2}$$

The induced voltage V is given by

$$V = -\frac{\check{z}\Phi}{\check{z}t} = -\frac{\mathrm{d}}{\mathrm{d}t}\left(pa^2\overline{B}\right), \tag{A3.3}$$

and in the absence of a specimen $\overline{B} = B_a$ so that

$$V = -\frac{\mathrm{d}}{\mathrm{d}t}\left[pa^2(B_0 + b_0 \cos wt)\right] = V_0 \sin wt, \tag{A3.4}$$

where $V_0 = pa^2 b_0 w$.

In the presence of the specimen, one must find an expression for $\overline{B}$. Clem writes $\overline{B}$ in terms of its time average $\langle\overline{B}\rangle$, which does not enter into the losses, and the deviation $\bar{b}$ from the time average; i.e., $\overline{B} = \langle\overline{B}\rangle + \bar{b}$. He then expresses $\bar{b}$ in a Fourier series:

$$\bar{b} = \sum_{n=1}^{\infty}\left(m_n' \cos nwt + m_n'' \sin nwt\right) b_0, \tag{A3.5}$$

where

$$m_n' = \frac{w}{pb_0}\int_0^T \bar{b}\cos nwt\,\mathrm{d}t, \qquad m_n'' = \frac{w}{pb_0}\int_0^T \bar{b}\sin nwt\,\mathrm{d}t\,. \tag{A3.6}$$

Therefore,

$$V = -pa^2\frac{\mathrm{d}\bar{b}}{\mathrm{d}t} = pa^2 b_0 \sum_{n=1}^{\infty}\left(m_n' \sin nwt - m_n'' \cos nwt\right) nw \tag{A3.7}$$

$$= V_0 \sum_{n=1}^{\infty} n\left(m_n' \sin nwt - m_n'' \cos nwt\right).$$

If one only looks at the component of V varying as w, that is, $V = V_{n=1} = V_1$, then

$$V_1 = V_0\left(\mu_1' \sin wt - \mu_1'' \cos wt\right) = V_0\,\mathrm{Re}\left(i\mu e^{-iwt}\right), \qquad \text{(A3.8)}$$

where $\mu = \mu_1' + i\mu_1''$. In Eq. A3.8, consider V_1: μ_1'' corresponds to the component that is in phase with B_a, and there represents the resistive losses, while μ_1' corresponds to the out-of-phase or inductive component. One has that:

Normal metal at low frequency: $\mu' \sim \mu,\ \mu'' \sim 0 \Rightarrow V_1 \sim \mu V_0 \sin wt$;

Meissner superconductor: $\mu' \sim 0,\ \mu'' \sim 0 \Rightarrow V_1 \sim 0$.

Connection between μ'' and A_H, the Hysteresis Loop Area

The area of the hysteresis loop is given by

$$A_H = \oint B_a \mathrm{d}\overline{B} = \int_0^T (B_0 + b_0 \cos wt)\frac{\mathrm{d}\overline{B}}{\mathrm{d}t}\,\mathrm{d}t\,. \qquad \text{(A3.9)}$$

Since

$$\frac{\mathrm{d}\overline{B}}{\mathrm{d}t} = \frac{\mathrm{d}\overline{b}}{\mathrm{d}t} = nwb_0 \sum_{n=1}^{\infty}\left(\mu_n'' \cos nwt - \mu_n' \sin nwt\right), \qquad \text{(A3.10)}$$

one has that

$$A_H = \int_0^T \mathrm{d}t \left\{ \begin{array}{l} nwb_0 B_0 \displaystyle\sum_{n=1}^{\infty}\left(\mu_n'' \cos nwt - \mu_n' \sin nwt\right) \\ \\ + nwb_0^2 \cos wt \displaystyle\sum_{n=1}^{\infty}\left(\mu_n'' \cos nwt - \mu_n' \sin nwt\right) \end{array} \right\}. \qquad \text{(A3.11)}$$

Now the first term vanishes over a period, and the second vanishes unless $n = 1$. When that is the case, only the first term under the second summation contributes, and one is left with only $\int_0^{2p} \cos^2 wt\,\mathrm{d}t = p$. One therefore has the final result that

$$A_H = m'' p b_0^2 \,. \qquad \text{(A3.12)}$$

Note that this is misprinted in Clem's report, and that m''_1 was replaced with m'', since the terms in the expression for A_H involving m''_n all vanish for $n \neq 1$. The loss per unit volume per cycle is then

$$W_V = \frac{A_H}{m_0} = \frac{p b_0^2}{m_0} m'' \,. \qquad \text{(A3.13)}$$

APPENDIX 4: MEASUREMENT OF TRANSPORT LOSS AND LEAD CONFIGURATION

As mentioned in the main text of this report, when measuring transport current loss the configuration of the measurement leads is important. This is because changing external magnetic fields may couple to the leads and induce an error voltage. One simple way to reduce coupling is to induce equal and opposite currents in the lead configuration.[1] This is shown in Figure A4.1.

[1] Y. Yang et al., *Physica C* **256**:378 (1996); J. J. Rabbers et al., *Physica C* **310**:101 (1998).

Figure A4.1. The voltage induced in areas *A* and *B* by a changing external magnetic field is equal and opposite if the areas are equal.

Another rather elegant solution has been used by Tsukamoto and colleagues.2 This approach uses a spiral lead configuration, as shown below in Figure A4.2. The angular difference between taps is $2p$, and the number of turns in the spiral must be an integer. It will be shown below that the flux through the surface determined by the axis of the spiral and the spiral itself vanishes, and that the measured power dissipated is independent of the spiral radius. The spiral is described on the surface of a circular cylinder.

The theory behind this technique can be understood as follows: First, introduce a rectangular coordinate system at the front of the spiral in Figure A4.2, with the *z*-axis corresponding to the axis of the spiral. The position vector of the spiral *surface* defined by the *z*-axis and the spiral is given by

$$\boldsymbol{r} = (x\cos q, -x\sin q, aq). \qquad \text{(A4.1)}$$

The pitch of the left-handed helix is a so that the helix makes one turn in a distance along z equal to $2pa$. As x varies, q = constant gives the generators of the surface, and x = constant gives circular helices.

2S. Fukui et al., Paper presented at ICMC 1997, Portland, Ore., USA; an example of the application of this technique is given in O. Tsukamoto et al., *IEEE Trans. on Appl. Supercon.* **9**:1181 (1999).

Figure A4.2. Spiral lead arrangement for measuring transport current loss. Note: The spiral must be described on the surface of a circular cylinder (see Eq. A4.1); the elliptical cross section of the drawing is due to the projection.

The normal to the surface is

$$\hat{\boldsymbol{n}} = \frac{\frac{d\boldsymbol{r}}{dx} \times \frac{d\boldsymbol{r}}{dq}}{\left|\frac{d\boldsymbol{r}}{dx} \times \frac{d\boldsymbol{r}}{da}\right|}, \tag{A4.2}$$

where

$$\frac{d\boldsymbol{r}}{dx} = (\cos q, -\sin q, 0); \quad \frac{d\boldsymbol{r}}{da} = (-x \sin q, -x \cos q, a). \tag{A4.3}$$

Therefore,

$$\hat{\boldsymbol{n}} = \frac{\begin{vmatrix} \hat{\boldsymbol{i}} & \hat{\boldsymbol{j}} & \hat{\boldsymbol{k}} \\ \cos q & -\sin q & 0 \\ -x \sin q & -x \cos q & a \end{vmatrix}}{(a^2 + x^2)^{1/2}} = \frac{(-a \sin q, -a \cos q, -x)}{(a^2 + x^2)^{1/2}}. \tag{A4.4}$$

To compute $\boldsymbol{B} \cdot \hat{\boldsymbol{n}}\, dA$, one needs the element of surface area. This is given by

$$dA = H\, dx\, dq, \tag{A4.5}$$

where

$$H = (EG - F^2)^{1/2}, \tag{A4.6}$$

and where

$$E = \left(\frac{d\boldsymbol{r}}{dx}\right)^2 = 1; \qquad G = \left(\frac{d\boldsymbol{r}}{da}\right)^2 = x^2 + x^2; \qquad F = \frac{d\boldsymbol{r}}{dx} \cdot \frac{d\boldsymbol{r}}{da} = 0. \tag{A4.7}$$

H is then $(a^2 + x^2)^{1/2}$ and the element of area is this multiplied by $dx da$. The flux through the helicoid is then

$$\int \boldsymbol{B} \cdot \hat{\boldsymbol{n}}\, dA = \int\int_{x = 0,\ q = 0}^{x = R,\ q = 2p} -B_a a \sin q\, dx\, dq = 0. \tag{A4.8}$$

If the helical winding has more than one turn, the q upper limit of integration becomes $2np$, but the result (that the total flux through the helicoid vanishes) is the same.

The fact that the measured power dissipated is independent of the radius of the spiral is proven by constructing two spirals of radius R_A and R_B beginning at a given q and ending, for one turn, at $q + 2p$. The radii are chosen such that $R_B > R_A >$ the half-width of the tape. Now consider the closed circuits A and B consisting of each of the spirals, the radii connecting them to the axis, and the axis itself over the distance, l, corresponding to q and $q + 2p$. The voltage induced around each of these circuits is

$$V_A(t) = \oint_A E(t)\, ds; \qquad V_B(t) = \oint_B E(t)\, ds\,, \tag{A4.9}$$

where E is the electric field. The power dissipated per cycle in each of these loops is then

$$P_{\text{Spiral } A} = \frac{1}{T}\int_0^T I(t)V_A(t)\, dt; \qquad P_{\text{Spiral } B} = \frac{1}{T}\int_0^T I(t)V_B(t)\, dt\,, \tag{A4.10}$$

where T is the period of the AC current and I is the current.

The difference in the power generated in each circuit is

$$P_{\text{Spiral } A} - P_{\text{Spiral } B} = \frac{1}{T}\int_0^T I(t)\left[V_A(t) - V_B(t)\right] dt. \tag{A4.11}$$

But $\left[V_A(t) - V_B(t)\right]$ is $\dfrac{d(\Phi_B - \Phi_A)}{dt}$, where Φ_A and Φ_B are the fluxes in circuits A and B, respectively. The aim is to now compute $\Phi_B - \Phi_A$ so as to find $\dfrac{d(\Phi_B - \Phi_A)}{dt}$ and substitute for $\left[V_A(t) - V_B(t)\right]$ in Eq. A4.11. $\Phi_B - \Phi_A$ can be written as

$$\Phi_B - \Phi_A = \int_{R_A}^{R_B}\left[\int_0^{2p} B_q(r, q)\left(\frac{l}{2p}\right) dq\right] dr. \tag{A4.12}$$

But since $B_q(r, q)$ is the azimuthal component of the field, one can apply Ampere's law to obtain $\int_0^{2p} B_q(r, q)\, ds = \int_0^{2p} B_q r\, dq = \mu_0 I(t)$. $\Phi_B - \Phi_A$ is then

$$\Phi_B - \Phi_A = \mu_0 I(t)\left(\frac{l}{2p}\right)\int_{R_A}^{R_B}\frac{1}{r}\, dr = \mu_0 I(t)\left(\frac{l}{2p}\right)\ln\left(\frac{R_B}{R_A}\right). \tag{A4.13}$$

Therefore,

$$\frac{\mathrm{d}(\Phi_B - \Phi_A)}{\mathrm{d}t} = m_0 \left(\frac{l}{2p}\right) \ln\left(\frac{R_B}{R_A}\right) \frac{\mathrm{d}I(t)}{\mathrm{d}t}. \qquad \text{(A4.14)}$$

If $I(t)$ is proportional to coswt, then $\frac{\mathrm{d}I(t)}{\mathrm{d}t}$ is proportional to sinwt , and finally

$$P_{\text{Spiral } A} - P_{\text{Spiral } B} = \frac{1}{T}\int_0^T I(t)\frac{\mathrm{d}I(t)}{\mathrm{d}t}\,\mathrm{d}t \;\alpha\; \int_0^{2p} \cos u \sin u \,\mathrm{d}u = 0, \qquad \text{(A4.15)}$$

so that $P_{\text{Spiral } A} = P_{\text{Spiral } B}$.

APPENDIX 5: BENCHMARK PARAMETERS

When considering the state of the art, one must bear in mind both economics and the properties of available materials. We present the numerical values of some parameters of importance when considering AC loss in ceramic superconductors. Related and other information can be found in a recent book by R. Wesche, *High-Temperature Superconductors: Materials, Properties, and Applications* (Kluwer Academic Publishers, Boston, 1998).

A5.1 PROPERTIES OF MATERIALS

A5.1.1 Commercially Available Long Lengths of OPIT Bi-2223

Current density at 77 K in self-field, 1.0 microvolt per centimeter (1.0 μV/cm):

Critical current density in Bi-2223

$J_c = 35{,}000\ A/cm^2$

Engineering current density of tape

$J_e = 14{,}000\ A/cm^2$

Volume of a kiloampere-meter of tape at 77 K in self-field:

Volume per kA-m = (1 meter/1 meter) $(1 / J_e) = (10^{-4} / 14)\ (m^3 / kA\text{-}m) = 0.71 \times 10^{-5}\ m^3$

Volume fraction of superconductor	= 0.37
Volume fraction of Ag alloy matrix	= 0.63
Ratio of volumes	= 1.7 Ag-alloy / Bi-2223

A5.1.2 Electrical Resistivity of Materials at Ambient and Cryogenic Temperatures

N.B. The effective resistivity of Bi-2223 at critical current density is $2.8 \times 10^{-13}\ \Omega$–m
($2.8 \times 10^{-13}\ \Omega = 1\ \mu V/cm / 35{,}000\ A/cm^3$)

Electrical Resistivity ($10^{-8}\ \Omega$–m) *of Pure Metals, by Temperature*

Metal	298 K	80 K	60 K	40 K	20 K
Copper	1.7	0.215	0.097	0.024	0.003
Nickel	7.1	0.545	0.242	0.068	0.014
Silver	1.6	0.289	0.162	0.053	0.004

An alloy, Ag0.999Mg0.001, with a resistivity at 77 K of 0.62×10^{-8} Ω–m has been studied. Alloys of silver and gold have resistivities that are 10 times higher than that of pure silver.

A5.1.3 Temperature Dependence of Critical Current Density

The temperature dependence of the critical current density is often approximated by a linear equation. Another common (and more accurate) parametrization is given by

$$J_c(T)/J_c(T=0)=(1-T/T_c)^x.$$

Pertinent numerical values appear below.

Ag/Bi-2223:	T_c = 105-110 K	x = 1.4
Ag/Bi-2212:	T_c = 85-92 K	x = 1.8
Tl-1223 Film/YSZ	T_c = 107 K	x = 1.0
Y-123 RABiTS	T_c = 88 K	x = 1.2

For sufficiently small values of the ratio T / T_c, the temperature dependence shown above is nearly linear.

A5.1.4 Mass Densities at 298 K

Bi-2223	$\rho_{Bi\text{-}2223} = 6.4$ g/cm^3
Silver	$\rho_{Ag} = 10.5$ g/cm^3
Nickel	$\rho_{Ni} = 10.5$ g/cm^3
Copper	$\rho_{Cu} = 8.9$ g/cm^3
Iron	$\rho_{Fe} = 7.9$ g/cm^3

A5.1.5 Penetration Depth According to the Nonlinear Conductor Model

As described elsewhere in this report, ohmic conductors have a “skin depth,” and LTS superconductors that are well described by the Bean critical state model have a “Bean penetration depth.” In ohmic conductors, fields and current density decline exponentially with depth from the conductor-insulator interface. The “skin depth” is the distance over which the decline is 1/e or 0.27. In the critical state model, fields decline linearly and currents are constant, until they abruptly decline to zero. The “Bean penetration depth” is the minimum depth for which the fields and current are zero.

For engineering purposes, ceramic superconductors are well described as "nonlinear conductors." As described in other appendices to this report, the "nonlinear conductor model"[1] interpolates between the two extremes described above. According to this model, the penetration depth, z^*, in slab geometry is as follows:

$$z^* \equiv (B / \mu_0 J_c) ((e_0 \mu_0 J_c) / (\omega B^2))^{1/(1+n)} \qquad \text{where} \qquad E = e_0 (J / J_c)^n$$

For $B = 0.1$ T $\omega = 2$ 50 Hz $J_c = 3.5 \times 10^8$ A/ m^2 $= 3.5 \times 10^4$ A/ cm^2 $e_0 = 10^{-4}$ volt/m

$$z^* = (2.27 \times 10^{-2} \text{ cm}) \times (1.4 \times 10^{-2})^{1/(1+n)}$$
$$z^* = (2.27 \times 10^{-2} \text{ cm}) \times (0.4 \text{ for } n = 4;\ 0.6 \text{ for } n = 8;\ 0.7 \text{ for } n = 12)$$

This depth is much greater than 5 μm, the thickness of a superconducting filament or film.

A5.1.6 Hysteresis Loss According to the Nonlinear Conductor Model

As described elsewhere in this report, an externally driven oscillating magnetic field induces currents within a conductor. These currents dissipate electrical energy and generate heat. The nonlinear conductor model provides an expression for this. When the conductor is much deeper than the penetration depth and the geometry is "slab," that expression is

$$d/dt\ Q / A = (\omega / 2\pi) (B^2 / 2\mu_0) z^* f[n]$$

where f[n] is well approximated by $(1.33 + 3.11\ n^{-0.55})$, according to J. Rhyner, so we write

$$d/dt\ Q / A \approx (\omega / 2\pi) (B^2 / 2\mu_0) z^* (1.33 + 3.11\ n^{-0.55})$$

$$d/dt\ Q / A \approx (\omega / 2\pi) (B^2 / 2\mu_0) (B / \mu_0 J_c) ((e_0 \mu_0 J_c) / (\omega B^2))^{1/(1+n)} (1.33 + 3.11\ n^{-0.55})$$

We calculate the magnitude of the hysteresis for some values of the parameters pertinent to the power sector:

$B = 0.1$ T, $\omega = 2\pi$ 50 Hz $J_c = 3.5 \times 10^8$ A/m^2 $= 3.5 \times 10^4$ A/cm^2 $e_0 = 10^{-4}$ V/m

$$d/dt\ Q / A \approx 45 \text{ W/m}^2 \times (1.2 \text{ for } n = 4;\ 1.4 \text{ for } n = 8;\ 1.5 \text{ for } n = 12)$$

As noted above, in Section A5.1.5, most often, the conductor is thinner than the penetration depth. A more complex expression must then be used to calculate the answer.[2]

---

[1] J. Rhyner, "Magnetic properties and AC loss of superconductors with power law current voltage characteristics," *Physica* C **212**:292-300 (1993).

[2] J. Rhyner, "Magnetic properties and AC loss of superconductors with power law current voltage characteristics." *Physica* C **212**:292-300 (1993).

A5.2 Prices of Materials and Self-Contained Refrigeration

A5.2.1 Currency Exchange Rates

To the accuracy appropriate to engineering economics in this report, we suggest

1 Euro ≈ $1 ≈ 100 ¥ ,

which is approximately true at the time of this report's publication (April 2000).

A5.2.2 Price of Metals

Where indicated, the following are annual average commodity prices. Spot prices fluctuate, and delivered prices to the conductor manufacturer might be 50% higher than the commodity price.

Price of silver	$134.64/kg	(average commodity price, 1998)[3]
Price of nickel	$ 6.93/kg	(average commodity price, 1998)[4]
Price of copper	$ 1.76/kg	(average commodity price, 1998)[5]
Price of "electrical steel"	$ 1.25/kg	(estimate based on vendor quote)

A5.2.3 Today's Approximate "Cost of Materials" for Bi-2223 Tape

Today, ASC offers Bi-2223 tape for $300/kA-m. This price must cover the needed return to capital, cost of rejects, cost of labor, and cost of materials. Here we estimate the cost of materials, assuming BSCCO powder costs $0.50/g. (The price of powder is often a transfer price—what one part of a business charges another part of the same business — and so it is not firm. Indeed, were there a large market for powder, we would expect its price to fall, but not to fall below $0.30/g.) Our estimate of the Cost of Materials, CoM, is based on the values for current density, volume, density, and price that appear in this appendix.

CoM = (% volume HTS × density of Bi-2223 × powder price + % volume Ag × density × price) × volume of 1 kA-m of tape

---

[3] $0.80/lb; see Table 1171, U.S. Statistical Abstract, 1999 available at URL: http://www.census.gov/prod/99pubs/99statab/sec24.pdf

[4] $6,931/metric ton; see Table 1170, U.S. Statistical Abstract, 1999, available at URL: http://www.census.gov/prod/99pubs/99statab/sec24.pdf

[5] $5.10/fine oz; see Table 1171, U.S. Statistical Abstract, 1999, available at URL: http://www.census.gov/prod/99pubs/99statab/sec24.pdf
[1 fine oz. = 1/12 lb = (1/12) x (1/2.2) kg = 37.9 g]

CoM = $(0.37 \times \$0.5/g \times 6.4\ g/cm^3 + 0.63 \times \$0.134/g \times 1.5 \times 10.5\ g/cm^3) \times (7.8\ cm^3/kA\text{-}m)$

CoM = $(1.18 + 0.88 \times 1.5) \times 7.8$ ($/kA-m) = $19.50/kA-m at 77 K, in self-field

Assuming mass production of Bi-2223 tape, some have said that the price might fall to $50/kA-m in five years.[6] The expected future minimum price of Bi-2223 tape is more than twice the direct cost (direct labor and materials); the latter "may ultimately achieve cost performance close to $10/kA-m."[7]

A5.2.4 Cost of Nickel for Substrate of YBaCuO Coated Conductor

This estimate is meant to establish an order of magnitude, rather than to predict future performance. As performance improves, the following values should be adjusted. For the sake of definiteness, we adopt values that are reasonable today.

> Suppose the YBaCuO film can be made 2 μm thick with critical current density of 0.75×10^6 A/cm^2. Also, suppose the nickel substrate is 25 μm thick. Then

the following volume of nickel is needed for a tape that is 25 μm thick, 1 cm wide, and 1 m long:

$$25\ \mu m \times 1\ cm \times 1\ m = 25 \times 10^{-6} \times 10^{-2} \times 1\ m^3 = 2.5 \times 10^{-7}\ m^3 = 0.25\ cm^3$$

which is required to support the YbaCuO, which conducts 150 A for 1 m. Thus, the volume of nickel required for 1 kA-m is

$$(0.25/0.15)\ cm^3/kA\text{-}m = 1.70\ cm^3/kA\text{-}m$$

Recalling the density and commodity price of nickel, one finds that the contribution of commodity nickel to the cost of materials for our nominal tape is

$$1.70\ cm^3/kA\text{-}m \times 10.50 g/cm^3 \times \$6.93/kg = \$0.10/kA\text{-}m$$

We conclude that the price of commodity nickel would make a negligible contribution to the cost of materials, and thus to the cost of coated conductor. What the nickel supplier would charge for rolling the nickel into 25-μm tape is not included in the above considerations.

---

[6] L. Masur, E. Podtburg, D. Buczek, W. Carter, D. Daly, U. Kosasih, S.J. Long, K. Manwiller, D. Parker, P. Miles, M. Tanner, and J. Scudiere, "Long Length Manufacturing of BSCCO-2223 Wire for Motor and Cable Applications," 1999 CEC/ICMC, July 13-16, 1999 (Montreal, Canada).

[7] A.P. Malozemoff, S. Annavarapu, L. Fritzmeier, Q. Li, V. Prumier, M. Rupich, C. Thieme, W. Zhang, A. Goyal, M. Paranthaman, and D.F. Lee, "Low-Cost YBCO Coated Conductor Technology," *Supercond. Sci. Technol.*, **13**:1-4, (2000).

A5.2.5 Price and Performance of Self-Contained Refrigeration

As reported in the main text, one manufacturer, Cryomech, offers a cryocooler that can provide 300 W of cooling at 77 K and costs $27,400. The input is 7.4 kW. In the temperature range 40-80 K, the machine's performance is 7.3 times worse than that of a Carnot cryocooler. Expressing the same thing in another way, the ratio of the machine's input shaft power to the output cold power is $7.3 \times (298 - T_{cold})/T_{cold}$.

As reported in 1994,[8] one manufacturer, Carrier Corporation, built and tested a prototype, single-stage Stirling cryocooler that produced 250 W of cooling power at 77 K. The prototype's input was 3.7 kW, and its performance was approximately five times worse than that of a Carnot cryocooler. Expressing the same thing in another way, the ratio of the machine's input shaft power to the output cold power was approximately $5 \times (298 - T_{cold})/T_{cold}$. The machine was intended for the CMOS market, which did not materialize, and so the machine was not mass-produced. Carrier estimated that if sales totaled 1,000 machines per year, then the machine could be sold for approximately $20,000.

[8]R.F. Giese, *Refrigeration Options for High-Temperature-Superconducting Devices Operating between 20 and 80 K for Use in the Electric Power Sector*, for signatories of the IEA Implementing Agreement for a Co-Operative Programme for Assessing the Impacts of High-Temperature Superconductivity on the Electric Power Sector (Oct. 1994), 51 pages.